Viral and Cellular Determinants of HIV-1-Induced Innate Immune Activation

---

Inaugural-Dissertation

to obtain the academic degree

Doctor rerum naturalium

(Dr. rer. nat.)

submitted to the Department of

Biology, Chemistry, Pharmacy of

Freie Universität Berlin

by

Nicolas Dominik Arnow

from Berlin, Germany

Berlin, December 2023

This dissertation was written at the Robert Koch-Institute,

Unit 18: Sexually transmitted bacterial Pathogens (STI) and HIV in Berlin

in the period from March 2020 to December 2023.

1st reviewer: **Prof. Dr. Nobert Bannert** - Robert Koch-Institute, Berlin

2nd reviewer: **Prof. Dr. Andreas Diefenbach** - Freie Universität Berlin

Day of defense: 6 May 2024

Acknowledgements

After more than three years of work on my doctoral thesis project, I would like to express my gratitude to the people who have helped and supported me during this time. First and foremost, I would like to thank Prof. Dr. Norbert Bannert for informing me about the doctoral position and for having the confidence in me to undertake this work. He also accepted the position of first examiner, for which I am deeply grateful. Many thanks for this!

I would further like to thank Prof. Dr. Andreas Diefenbach for his support and guidance as the second examiner and for taking over the supervision on the part of the Freie Universität Berlin. His feedback during our meetings was invaluable and greatly appreciated.

I am also grateful to the Deutsche Forschungsgemeinschaft and the SPP1923 project, respectively, for providing the funding that enabled this work to be conducted.

Major thanks go to all members of Department 18 of the Robert Koch Institute for creating a pleasant working atmosphere and always engaging in constructive discussions. Special thanks go to Dr. Oliver Hohn and Dr. Uwe Fiebig for their professional support and willingness to listen when problems arose. Most of all, I will remember our many conversations outside of the lab and, of course, listening to music together. Coming to the lab every day was a joy knowing that you were there. Thank you so much!

I would like to extend my appreciation to my former colleague, Michelle Stuck, for always being willing to help me in the lab and for being a great company. It was a pleasure working with you. Thank you for the shared experiences!

However, my biggest thanks go to Ph.D. Oya Cingöz, who not only entrusted me with the doctoral position but also provided support whenever possible. Whether it was countless hours in the lab, literature questions, or personal concerns, she made my doctoral experience a special one through her dedication to science and her personal guidance. Thank you very much for this!

Lastly, I want to express my gratitude to my friends, parents, and partner who stood by me during difficult times throughout my doctoral thesis journey and supported me all the way. Thank you for always being there for me!

Declaration of Authorship

Herewith I certify that I,

Nicolas Dominik Arnow, have prepared and written my thesis independently and that I have not used any sources and aids other than those indicated by me. I also declare that I have not submitted the dissertation in this or any other form to any other institution as a dissertation.

Berlin, 2 December 2023

(date) (signature)

Table of Content

List of Figures

List of Tables

Abbreviations

Abbreviation	Meaning
+ssRNA	Positive-sense single-stranded RNA
AIDS	Acquired immunodeficiency syndrome
ANI	Asymptomatic neurocognitive impairment
APC	Antigen-presenting cell
APOBEC3	Apolipoprotein B mRNA-editing catalytic polypeptide-like
APS	Ammonium persulfate
B-cell	B lymphocyte
BSA	Bovine serum albumin
CA	Viral capsid
cART	Antiretroviral therapy
Cas9	CRISPR-associated 9
cDNA	Complementary double-stranded DNA
cGAMP	Cyclic GMP-AMP
cGAS	Cyclic GMP-AMP synthase
CLR	C-type lectin receptor
CNS	Central nervous system
cPPT	Central polypurine tract
CPSF6	Cleavage and polyadenylation specific factor 6
CRISPR	Clustered regularly interspaced short palindromic repeats
CRM-1	Chromosomal region maintenance 1
Ct	Cycle threshold
CXCL10	C-X-C motif chemokine ligand 10
DAMP	Danger-associated molecular pattern
DC	Dendritic cell
DCAF1	DDB1 and CUL4 associated factor 1
DMEM	Dulbecco's modified eagle medium
DMSO	Dimethyl sulfoxide
dNTP	Deoxyribonucleoside triphosphate
dsRNA	Double-stranded RNA
DTT	1,4-Dithiothreitol
EF-1α	Elongation factor-1α
ELISA	Enzyme-linked immunosorbent assay
Env / *Env*	Glycoprotein complex (gp41/ gp120) / envelope (gen)
FACS	Fluorescence-activated cell sorting
FBS	Fetal bovine serum
F-PERT	Fluorescent polymerase extension reaction
FVD	Fixable-viability dye
Gag / *gag*	Group-specific antigen
Gag/Pol	Gag/Pol precursor protein
GFP	Green fluorescent protein
GM-CSF	Granulocyte-macrophage colony-stimulating factor
GOI	Gene of interest
gp120, SU	Glycoprotein 120
gp41, TM	Glycoprotein 41
gRNA	Genomic RNA
HAART	Highly active antiretroviral therapy
HAD	HIV-associated dementia
HAND	HIV-associated neurocognitive disorders

HCl	Hydrochloric acid
HEPES	2-(4-(2-hydroxyethyl)-1-piperazinyl)-ethane sulfonic acid
HIV	Human immunodeficiency virus
HLA	Human leukocyte antigen
HRP	Horseradish peroxidase
IFIT1	Interferon induced protein with tetratricopeptide repeats 1
IFIT2	Interferon induced protein with tetratricopeptide repeats 2
IFN	Interferon
IFNAR	Interferon-alpha/beta receptor
IFNB1	Interferon-beta 1
IKKε	IκB kinase-ε
IN	Integrase
INI	Integrase inhibitor
IRF	Interferon regulatory factor
JAK	Janus kinase
kb	Kilo base
KO	Knockout
KPT-330	Selinexor
LAV	Lymphadenopathy associated virus
LPS	Lipopolysaccharide
MA	Matrix protein
MAVS	Mitochondrial antiviral signaling
MDA5	Melanoma differentiation-associated protein 5
MDM	Monocyte-derived macrophages
MHC	Major histocompatibility complex
MND	Mild neurocognitive disorders
MyD88	Myeloid differentiation factor 88
NC	Nucleocapsid protein
nef / *nef*	Negative factor
NF-κB	Nuclear factor κB
NK	Natural killer
$NL4.3_{GFP}$	VSV-G pseudotyped HIV-1-GFP reporter virus
$NL4.3_{Luc}$	VSV-G pseudotyped HIV-1-firefly luciferase reporter virus
NLR	NOD-like receptor
NNRTI	Non-nucleoside reverse transcriptase inhibitor
NOD	Nucleotide oligomerization domain
NRTI	Nucleoside reverse transcriptase inhibitor
NVP	Nevirapine
OMD	Oligonucleotide-directed mutagenesis
ORF	Open reading frames
p6	Link protein
p24	Capsid protein
PAMP	Pathogen-associated molecular pattern
PBMC	Peripheral blood mononuclear cell
PBS	Phosphate-buffered saline
PCR	Polymerase chain reaction
PEI	Polymer polyethylenimine
PI	Protease inhibitor
PIC	Pre-integration complex
PMA	Phorbol 12-myristate 13-acetate
pol	Viral polymerase gene
Pol II	RNA polymerase II
PR	Protease
$Pr55^{Gag}$	Gag precursor protein

PRR	Pattern recognition receptor
PVDF	Polyvinylidene difluoride
qPCR	Quantitative PCR
RAL	Raltegravir
RCF	Relative centrifugal force
Rev / *rev*	Regulator of expression of virion protein
RIG-I	Retinoic-acid-inducible gene-I
RIPA	Radio-immunoprecipitation assay
RLR	RIG-I-like receptor
RLU	Relative light unit
RPMI	Roswell park memorial institute
RRE	Rev-responsive element
RSAD2	Radical S-adenosyl methionine domain containing 2
RT	Reverse transcriptase
RT-PCR	Reverse transcription PCR
RT-qPCR	Reverse transcription-qPCR
SAMHD1	Sterile alpha motif and HD domain-containing protein 1
SDS	Sodium dodecyl sulphate
SDS-PAGE	Sodium dodecyl sulfate polyacrylamide gel electrophoresis
SEAP	Secreted alkaline phosphatase
SIV	Simian immunodeficiency virus
SIV_{Mac}p6 region	SIV macaques p6 region of *gag*
ssRNA	Single-stranded RNA
STAT	Signal transducers and activators of transcription
STING	Stimulator of interferon genes
T-cell	T lymphocyte
TAR	Trans-activation responsive region
Tat / *tat*	Trans-activator of transcription
TBK1	TANK-binding kinase 1
TBS	Tris-buffered saline
TEMED	Tetramethylethylenediamine
TLR	Toll-like receptor
TRAF6	TNF receptor-associated factor 6
TRIF	Toll IL-1 receptor domain-containing adaptor inducing IFN-β
TSS	Transcription start site
Vif	Viral infectivity factor
VLP	Virus-like particle
Vpr	Viral protein R
Vpu	Viral protein U
Vpx	Viral protein X
VSV-G	Vesicular stomatitis virus glycoprotein
WT	Wild-type
WPRE	Woodchuck hepatitis virus posttranscriptional regulatory element
$WPRE_{GFP}$	WPRE minimal lentiviral GFP reporter virus

Abstract

A fundamental defense mechanism against pathogens is the recognition of pathogen-associated molecular patterns (PAMPs) by pattern recognition receptors (PRRs). These PRRs are integral components of the innate immune system. This recognition process initiates the interferon (IFN) response mechanism, triggering expression of interferon-stimulated genes (ISGs). Many of these ISGs possess antiviral properties that inhibit viruses, including HIV-1. The PPRs and their following signal pathways vary based on cell type. Publications have shown that an unknown pathway mediated over MAVS is activated by intron-containing RNA from HIV-1 in monocyte-derived macrophages (MDMs). However, the mechanism behind the sensing of the viral genomic RNA is yet unknown.

This work identified two distinct stages of immune recognition in MDMs triggered by HIV-1 infection. The first stage occurred prior to reverse transcription and was influenced by the stability of the viral capsid. In the second stage, characterized by a more robust immune response, a short peptide sequence encoded by the N-terminus of *gag* was crucial to inducing inflammatory responses. While partially spliced or full-length viral RNA in the cytoplasm was required for Gag protein translation, the myristoylation site of Gag was essential to induce innate sensing in MDMs. Furthermore, we examined whether THP-1 or U937 cells in differentiated state showed a similar phenotype to MDMs during HIV-1 infection to identify the molecular mechanisms involved in sensing the virus. We found that U937 cells exhibited robust innate response at a late-stage of virus replication, whereas pre-integration determinants, observed in MDMs, differ. Surprisingly, THP-1 cells exhibited minimal innate immune responses against HIV-1 and showed significant differences from the responses observed in MDMs and U937 cells. Our findings reveal that HIV-1 sensing in differentiated THP-1 and U937 cells does not parallel the responses seen in primary cells. These results enable new research targets in regard to find the cellular sensor, which induces HIV-1 chronic inflammation in MDMs and highlight the importance of research in primary cell systems.

Zusammenfassung

Ein fundamentaler Verteidigungsmechanismus in der Abwehr von Pathogenen ist die Erkennung von Pathogen-assoziierten molekularen Mustern (PAMPs) durch Mustererkennungsrezeptoren (PRRs). Diese PRRs sind integrale Bestandteile des angeborenen Immunsystems, ein Erkennungsprozess löst die Ausschüttung von Interferonen aus, welche die Expression von Interferon-stimulierten Genen (ISGs) zur Folge hat. Viele dieser ISGs haben antivirale Funktionen die Viren, wie HIV-1, inhibieren. Die PRRs und ihre nachfolgenden Signalwege variieren je nach Zelltyp. In Publikationen wurde gezeigt, dass ein über MAVS vermittelter unbekannter Signalweg durch Intron beinhaltene RNA von HIV-1 in Monozyten-herangereiften Makrophagen (MDMs) aktiviert wird. Der Mechanismus, der hinter der Erkennung der viralen genomischen RNA steht, ist jedoch noch unbekannt.

In dieser Arbeit wurden zwei unterschiedliche Phasen der Immunerkennung in MDMs identifiziert, die durch eine HIV-1-Infektion ausgelöst werden. Die erste Phase findet vor der reversen Transkription statt und wurde durch die Stabilität des viralen Kapsids beeinflusst. In der zweiten Phase, die durch eine robuste Immunreaktion gekennzeichnet ist, spielt eine kurze Peptidsequenz im N-Terminus von Gag eine entscheidende Rolle bei der Auslösung von Entzündungsreaktionen. Während für die Translation des Gag-Proteins die virale einfach gespleißte oder Volllängen RNA im Zytoplasma erforderlich war, erwies sich die Myristoylierung von Gag als wesentlich für die Auslösung der angeborenen Signalerkennung in MDMs. Darüber hinaus wurde untersucht, ob THP-1- oder U937-Zellen im differenzierten Zustand während einer HIV-1 Infektion einen ähnlichen Phänotyp wie MDMs aufweisen, um weiterfolgend die molekularen Mechanismen zu identifizieren, die an der Erkennung des Virus beteiligt sind. Es konnte gezeigt werden, dass U937-Zellen eine robuste angeborene Antwort in einem späten Stadium der Virusreplikation besitzen, während die Determinanten vor der Integration, die in MDMs beobachtet wurden, sich unterscheiden. Überraschenderweise zeigten THP-1-Zellen nur minimale angeborene Immunantworten gegen HIV-1 und wiesen signifikante Unterschiede zu den in MDMs und U937-Zellen beobachteten Reaktionen auf. Unsere Ergebnisse belegen, dass die Erkennung von HIV-1 in differenzierten THP-1- und U937-Zellen nicht mit den in Primärzellen beobachteten Reaktionen übereinstimmt. Diese Ergebnisse ermöglichen neue Forschungsziele im Hinblick auf die Suche nach dem zellulären Sensor, der die chronische Entzündung von HIV-1 in MDMs auslöst, und bestärkt die Bedeutung der Forschung in primären Zellsystemen.

1 Introduction

1.1 The Immune System

The immune system represents the major biological defense system of higher organisms against pathogens such as bacteria, fungi, viruses, parasites, and in a broader sense, degenerated cells. These cells have been stimulated to uncontrolled growth by mutations and can be eliminated by immunological control mechanisms. This system has continued to evolve over millions of years.[1]

In vertebrates a basic distinction of the immune system is made between the innate and adaptive immune systems. The innate immune system functions as an initial barrier of protection, responding rapidly, but unable to recognize certain pathogens and prevent re-infection. In contrast, the adaptive immune system operates slowly and more directed, targeting specific pathogens through the process of clonal selection within a pool of lymphocytes carrying diverse antigen-specific receptors. These receptors equip the immune system with the capability to identify any unknown antigen effectively and establish an immunological memory against pathogens, thereby providing long-term protection against re-infections. The two systems do not act in isolation from each other, but are interconnected via complex signaling pathways and mechanisms (Figure 1).[2,3]

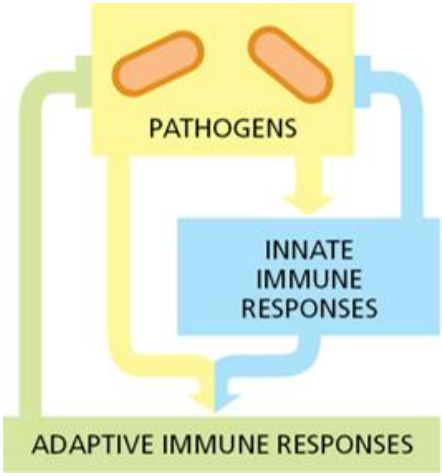

Figure 1: Interplay of the Innate and Adaptive Immune System

Schematic representation of the dynamic interactions between the innate and adaptive immune systems. Illustrated are the synergistic activity to counteract pathogenic threats. Image reproduced with permission from [3] p.1353.

Disruptions within this intricate interplay underlie a diverse array of diseases, manifesting as an inability to differentiate between foreign and host-structures. Furthermore, the immune system must maintain a calibrated tolerance towards foreign elements that pose minimal threat and occasionally even confer beneficial effects on the organism. When the immune system reacts to such harmless structures, it leads to a hypersensitivity reaction, analogous to an allergic response. Conversely, an inverse scenario can also emerge, characterized by an immune deficiency. Such deficiencies originate from defects in one or more components of the immune system. These immunodeficiencies can arise congenitally (primary immune-deficiencies) due to genetic anomalies or they can be acquired through environmental

influences (secondary immunodeficiencies), as in the case of human immunodeficient virus (HIV) infection.[2]

1.1.1 The Myeloid and Lymphoid Cell Lineage

A variety of cell types are involved in the innate as well as the adaptive immune system and all are derived from a single pluripotent cell, the hematopoietic stem cell. They originate from the bone marrow and develop into lymphoid and myeloid progenitor cells, each of which constitutes an individual lineage and matures into a wide range of immune cell types (Figure 2). While the myeloid lineage can directly mature in the environment of the marrow, the lymphoid lineage requires maturation outside of the bone. The mature or immature cells enter the bloodstream, where they are distributed throughout the body.[2]

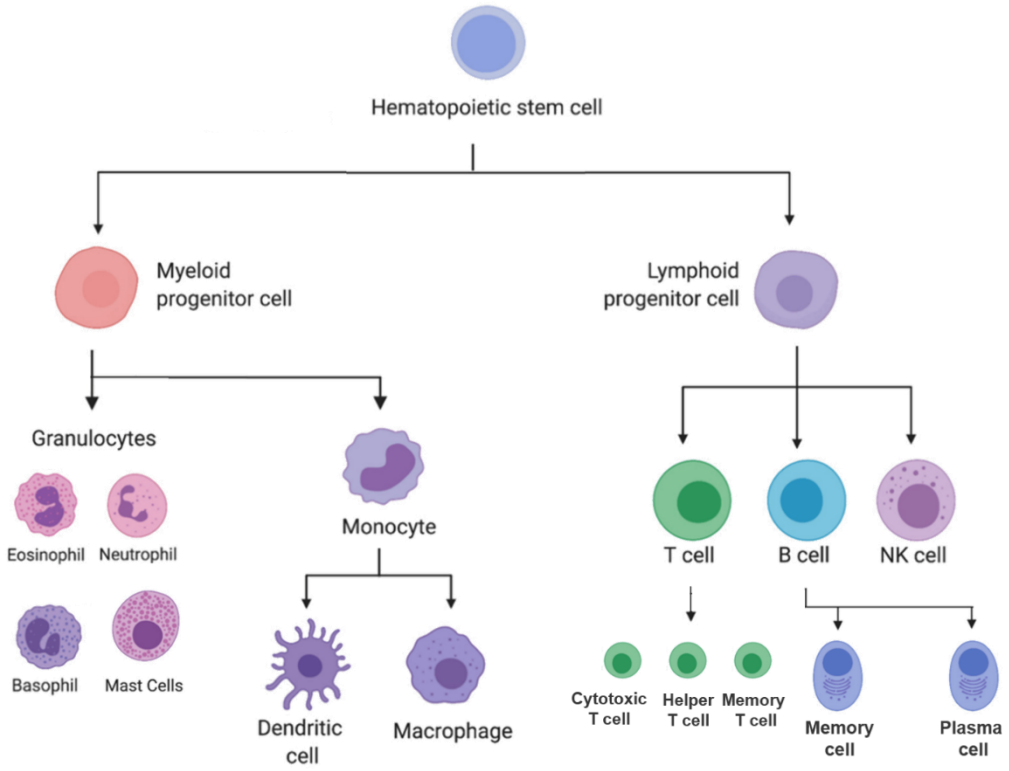

Figure 2: Hematopoietic Differentiation Scheme to Immune Cells

The schematic illustrates the current understanding of hematopoietic lineage in a hierarchical manner. It shows a two-stage progression in which multipotent hematopoietic stem cells transform gradually along a spectrum into myeloid and lymphoid cells of the immune systems. Image adapted from [4].

Myeloid Cell Lineage

The myeloid lineage produces the majority of cells constituting the innate immune system as well as important antigen-presenting cells (APCs) that prime the adaptive immune response (Figure 2). Red blood cells and platelets also arise from myeloid lineages,[2,3] but are omitted in Figure 2 to focus on immune cells.

Within the myeloid lineage, there exists a distinct subgroup referred to as granulocytes, notable for their numerous cytoplasmic granules. This subgroup consists of eosinophils, neutrophils, basophils, and mast cells, each contributing to a range of protective functions.[2,3] Eosinophils are specialized in releasing cytokines to promote immune defense.[5] Neutrophils, on the other hand, function as innate immune cells uniquely equipped to capture and eliminate microorganisms through phagocytosis.[2,6] Basophils are thought to play a role in the immune response against parasites,[2,7] and allergic responses,[2,8] while mast cells take on an active role as effectors in allergic reactions.[2,9]

The myeloid progenitors can also develop into a monocyte, representing the largest population of immune cells. Subsequently, these monocytes undergo further differentiation, branching into dendritic cells (DCs) and macrophages. DCs, which are specialized phagocytic cells, serve as important intermediaries between innate and adaptive immunity. Their crucial role involves the processing and presentation of antigens to T and B lymphocytes (T-cells and B-cells), both of which are essential components of the adaptive immune system.[2,3,10]

Macrophages are part of the innate immune system and are tissue-resident cells that act as primary sentinels for pathogenic invaders. They initiate the elimination of pathogens through phagocytosis, thereby contributing to the non-specific immune defense mechanism. This phagocytic activity leads to the lysis of captured pathogens, generating peptide fragments within the macrophages. These peptide fragments are subsequently displayed as antigens through the major histocompatibility complex (MHC) class II molecules on the cell membrane surface. MHC molecules are referred to as the human leukocyte antigen (HLA) system. This presentation ultimately drives the differentiation of macrophages into activated APCs. Subsequently, the release of pro-inflammatory cytokines triggers a signaling cascade, which recruit T-cells and further amplify the immune response. This process is called inflammation.[2,3,11]

Lymphoid Cell Lineage

The lymphoid progenitor cell undergoes differentiation into three classes of cells: the T-cells, B-cells, and natural killer (NK) cells (Figure 2).

T-cells, belonging to the adaptive immune system, encompass several types. T-cells that have not yet been activated are referred to as naïve T-cells. These cells migrate through the bloodstream to the thymus for maturation, where they recognize antigens presented by APCs via T-cell receptors located on their cell surfaces. This recognition induces their proliferation and differentiation into effector T-cells, which assume specialized functions in immune defense.[2]

Among these effector T-cells, cytotoxic T-cells play a crucial role. They recognize the same antigen, or small pathogen-derived particles, present on infected cells that activates the APCs. Cytotoxic T-cells eliminate these infected cells in a pathogen-specific manner (Figure 3). These cells are commonly identified by the expression of the CD8 receptor on their cell surface, hence referred to as $CD8^+$ T-cells. Similarly, helper T-cells, bearing the CD4 receptor, are known as $CD4^+$ T-cells. Notably, helper T-cells primarily activate B-cells, thereby inducing antibody synthesis. Following T-cell-mediated response, >95% of effector T-cells undergo apoptosis, while a minority develop into long-lived memory T-cells. These memory T-cells serve as a repository of "immunological memory" facilitating a more rapid and potent immune response upon re-infection with the same pathogen.[2,12]

Upon activation through antigen binding, B-cells undergo maturation into either memory B-cells or plasma cells. Plasma cells play a critical role in the adaptive immune response. They are responsible for secreting antibodies that bind to and neutralize the pathogen. These antibodies are specific for the particular activating antigen encountered by the B-cell (Figure 3).[2,3] In parallel, NK cells function as cytotoxic entities within the innate immune system. Their role involves detecting and eliminating virus-infected cells, contributing to the overall defense against infections.[2,13]

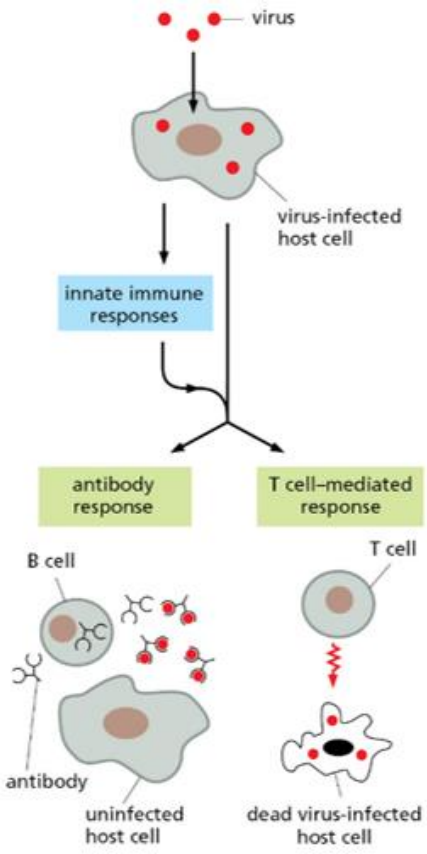

Figure 3: Activation of Adaptive Immune Responses

Schematic illustration depicts the induction of the adaptive immune response involving B-cells and T-cells, demonstrated here in response to a viral infection. B-cells release antibodies that bind to and neutralize the virus, effectively preventing further infection. Conversely, T-cells react directly by neutralizing the virus-infected host cells. Image reproduced with permission from [3] p.1354.

1.1.2 Sensing Pathways of the Innate Immune System

As mentioned above, the innate immune system represents the first barrier of defense against pathogens. The receptors responsible for recognizing conserved microbial molecular motifs are termed pattern recognition receptors (PRRs). These receptors detect non-specific patterns that include foreign molecules like those from microbes and non-foreign molecules like cellular DNA. These patterns are known as pathogen-associated molecular patterns (PAMPs). Additionally, danger-associated molecular patterns (DAMPs), released from dying host cells,

dead cells, or tumor-associated cells, are also detected. These molecular motifs are recognized by multiple PRR families, including Toll-like receptors (TLRs), Nucleotide oligomerization domain (NOD)-like receptors (NLRs), RIG-I-like receptors (RLRs), C-type lectin receptors (CLRs), and other DNA sensors. These PRRs sense various molecules from different pathogens, such as viruses, bacteria, and fungi, initiating downstream signaling cascades that lead to the production of pro-inflammatory cytokines and the three types of interferons (IFNs). These molecular events subsequently activate the adaptive immune response.[2,3,14–17]

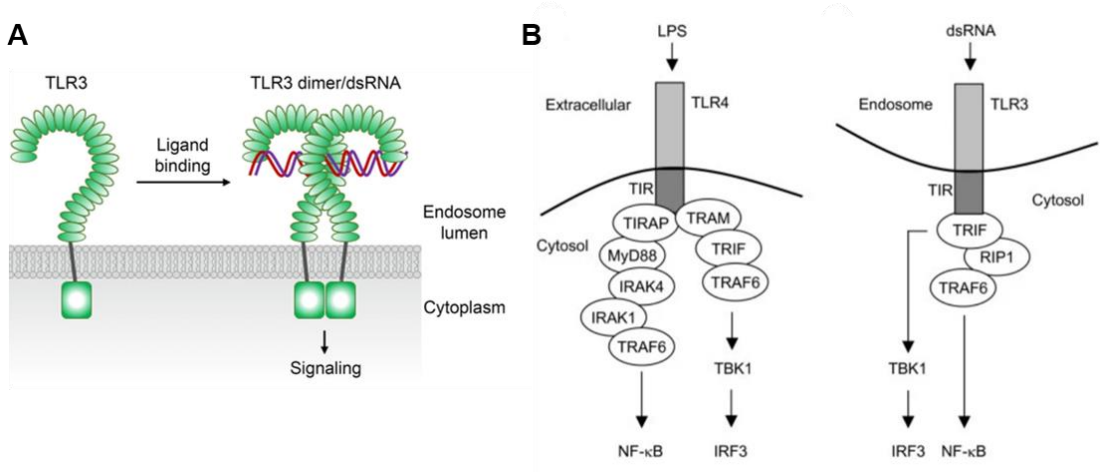

Figure 4: TLR Sensing Pathway

(A) Schematic representation of TLR3 dimerization caused by sensing dsRNA. **(B)** Downstream signaling pathways of extracellular TLR4 and endosomal TLR3. TLR4 mediates NF-κB signaling via myeloid differentiation factor 88 (MyD88) and IRF3 signaling via Toll IL-1 receptor domain-containing adaptor inducing IFN-b (TRIF). TLR3, in contrast, mediates the NF-κB pathway via TNF receptor-associated factor 6 (TRAF6). Images reproduced from (A)[18] and (B)[19].

TLRs are important host-associated PRRs essential for recognizing PAMPs in innate sensing pathways, including molecules of viral origin. Intracellularly anchored TLRs located in endosomes (TLR3, 7-9) play crucial roles in detecting those viral molecules. For instance, TLR3 recognizes double-stranded RNA (dsRNA) viruses, while TLR7 detects single-stranded RNA (ssRNA) viruses.[2] Additionally, TLR4, that is located on the cell membrane and traditionally known for sensing bacterial lipopolysaccharides (LPS), has also been shown to detect viral coat proteins.[20]

Recognition of TLR-specific PAMPs leads to receptor dimerization (Figure 4A). This regulates interactions between their cytoplasmic tails containing adaptor proteins, thus initiating intracellular signaling. It is important to note that other PRRs besides TLRs also have adaptor proteins and these have different downstream signaling cascades depending on the combinations of adaptor proteins. However, e.g., TLR4 activates the MyD88-dependent pathway, leading to the activation of nuclear factor κB (NF-κB), while members of the interferon regulatory factor (IRF) family are activated through the TRIF-dependent pathway, resulting in

their phosphorylation-dependent translocation to the nucleus (Figure 4B). IRFs, including IRF3 and IRF7, play crucial roles in antiviral responses by inducing the production of type I interferons (IFN-I; IFNα and IFNβ), while NF-κB primarily drives the transcription of pro-inflammatory cytokines. IFN-I exerts its effects in both the infected cell (autocrine) and the neighboring, uninfected cells (paracrine) by binding to essential cell-surface interferon-alpha-beta receptors (IFNARs). This binding triggers the Janus kinase/signal transducers and activators of transcription (JAK-STAT) in the intracellular signaling pathway, which leads to the transcription of hundreds of interferon-stimulated genes (ISGs). ISGs inhibit viral replication, direct cellular metabolism to an antiviral state, and regulate the downstream adaptive immune response.[2,3,14–17]

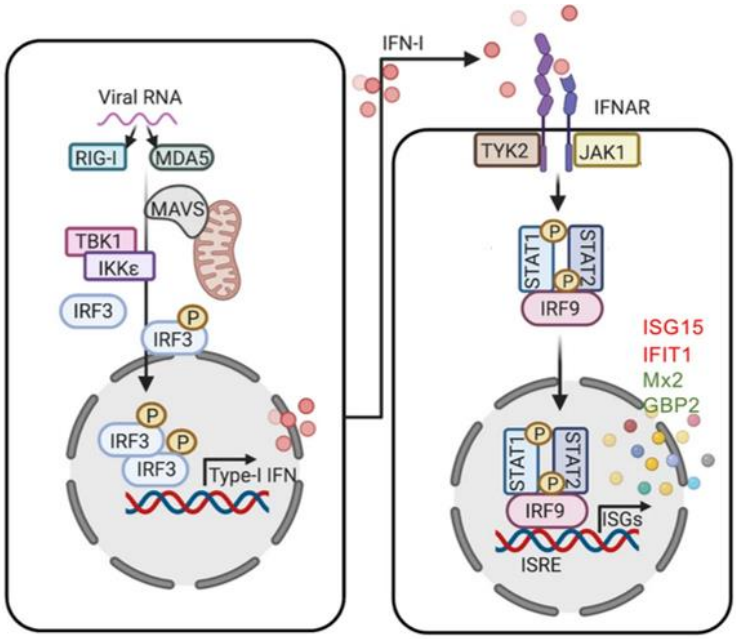

Figure 5: MAVS-Mediated Innate Immune Signaling Pathway

Schematic illustration of viral RNA sensing in macrophages. Sensing of viral RNA through MAVS sensing pathways leads to the transcription of Type-I IFN, which in turn triggers the translation of ISGs via the JAK-STAT pathway, in both autocrine and paracrine cells. Image adapted from [21].

Apart from TLRs, RLRs like retinoic-acid-inducible gene-I (RIG-I) and melanoma differentiation-associated protein 5 (MDA5) play significant roles as cytoplasmic viral RNA sensors. Both sensors activate the adaptor protein mitochondrial antiviral signaling (MAVS), which initiates downstream signaling through TANK-binding kinase 1 (TBK1) and IKB kinase-ε (IKKε) followed by IRF3/7, which is subsequently linked to the IFN-I signaling pathway (Figure 5).[2,16,22] RIG-I detects short uncapped dsRNAs with a 5'-triphosphate, typically synthesized by viral polymerases,[23] while MDA5 senses longer dsRNAs.[24,25] These distinguish viral from cellular RNA, allowing RIG-I and MDA5 to primarily sense foreign RNA.[2,16,22]

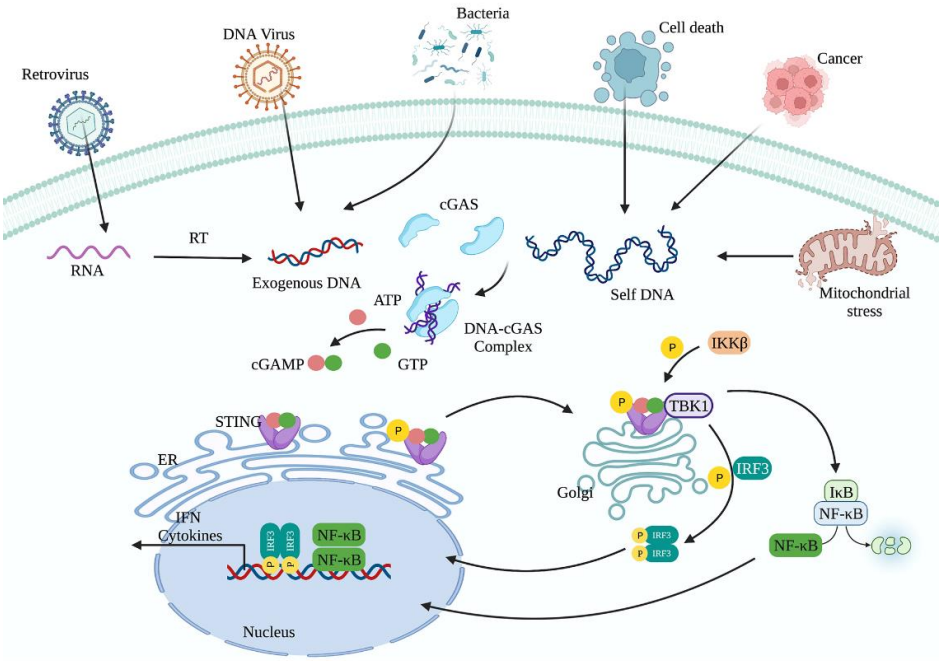

Figure 6: cGAS-STING-Mediated Innate Immune Signaling Pathway

Schematic illustration of viral DNA sensing mediated via the cGAS-STING pathway. Sensing of exogenous DNA or cytoplasmic self-DNA through cGAS mediates downstream actions of the adaptor STING, leading to the transcription of Type-I IFN and cytokines. Image reproduced from [26].

An important DNA recognition pathway for DNA of viral origin is the cGAS-STING pathway. This pathway not only recognizes viral PAMPs but also detects any DNA present within the cytoplasm (Figure 6). Cytoplasmic dsDNA is recognized by cyclic GMP-AMP synthase (cGAS), with the downstream adaptor protein stimulator of interferon genes (STING). Upon DNA detection, cGAS produces cyclic GMP-AMP (cGAMP), which binds to and activates STING. This activation leads to the downstream transcription factor IRF3, similar to TLR3 and RLRs, ultimately resulting in IFN-I production.[2,16,27–30]

1.2 Human Immunodeficiency Virus: A Brief Summary

In 1981, an unknown immunodeficiency was diagnosed in patients suffering from severe opportunistic infections. The following year, the still-unknown condition was described as acquired immunodeficiency syndrome (AIDS).[31] Two years later, a retrovirus was isolated for the first time from a sample of a patient with AIDS,[32] which was identified as the causative agent of the disease in 1984.[33] The retrovirus was named lymphadenopathy associated virus (LAV) but was later changed to human immunodeficiency virus (HIV, now HIV-1).[34] In 1986, another related immunodeficiency syndrome human retrovirus was discovered in West Africa (now called HIV-2).[35] After years of extensive research and discovery, HIV-1 has been classified into four distinct groups (M, N, O, P).[36] It has been established that HIV-1 (chimpanzee, *Pan troglodytes*),[37] as well as HIV-2 (sooty mangabeys, *Cercocebus atys*)[38,39]

originated from the genetically diverse simian immunodeficiency virus (SIV).[36] Among these viruses, the HIV-1 M group emerged as the primary virus driving the ongoing HIV epidemic (>90%).[2,36,40,41]

According to estimates, 38.4 million people worldwide were living with HIV in 2021 and a total number of 40.1 million people have died since the start of the epidemic from AIDS-related illnesses.[42] In the same year, 1.5 million people worldwide were newly infected with HIV.[42,43]

The infection can be controlled through antiretroviral therapy, and infected persons achieve almost the same average life span as uninfected persons.[44] However, only three patients have confirmed complete clearance of the virus in peer-reviewed published cases.[45,46] Three more patients are currently in long-term remission and could soon be declared completely HIV-free.[47–49] This underscores the challenges of research in finding therapeutic approaches to cure HIV infection.

1.2.1 Morphology, Genomic Characteristics, and Proteins of HIV-1/2

The basic structure of an HIV particle consists of an envelope, a core, and two copies of an RNA genome with enzymes, which is analogous to other retroviruses (Figure 7). The outermost layer of the HIV-1 particle consists of a membrane originating from the cytoplasmic membrane. This membrane carries the viral glycoprotein 120 (gp120, SU) positioned on its surface, while glycoprotein 41 (gp41, TM) spans the trans-membrane region, collectively forming the envelope glycoprotein (Env). The isometric structure of the particle is based on the matrix protein (MA) bound to the inner side of the envelope membrane. The core of the particle constitutes the viral capsid (CA), comprising the capsid protein (p24). In the case of the lentivirus HIV-1, it has a conical shape, which is connected to the membrane by a linker protein (p6). The dimer of linear positive-sense ssRNAs (+ssRNAs), which are not linked, constitute the viral genome and are located in the viral capsid along with the reverse transcriptase (RT), protease (PR), integrase (IN), and nucleocapsid protein (NC). The genomic RNA (gRNA) has all the characteristics of a cellular mRNA, a 5'-cap structure at the beginning and a 3'-polyadenylation at the end of the RNA strand.[50–52]

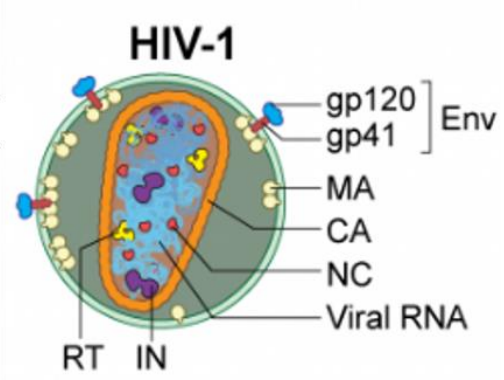

Figure 7: Structure of HIV-1 Virus Particle

Schematic representation illustrates the structure of an HIV-1 virus particle. Image adapted from [77].

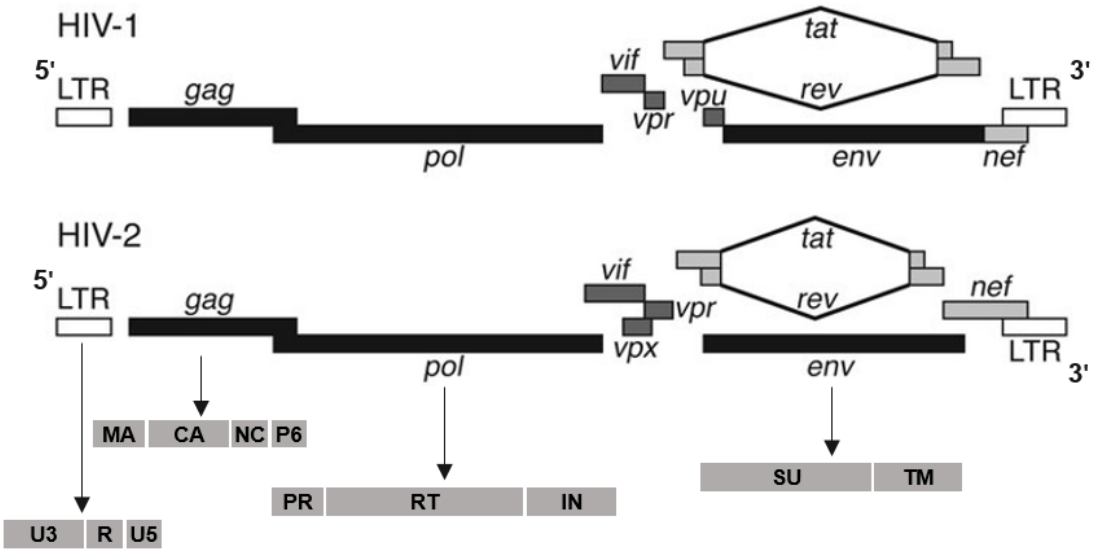

Figure 8: Genomic Maps of HIV-1 and HIV-2

A schematic illustration depicts the genomic structure and organization of both HIV-1 and HIV-2. The maps provide a visual representation of the major genes (*gag*, *pol*, *env*) and their coding proteins (*gag*: MA, CA, NC, p6; *pol*: PR, RT, IN; *env*: SU, TU) as well as, regulatory proteins (*tat*, *rev*), and accessory genes (*vif*, *vpr*, *vpu* HIV-1; *vpx* HIV-2) and the regions of the LTRs (U3, R, U5). Image adapted from [53].

The genomes of HIV-1 and HIV-2 share fundamental similarities with those of other retroviruses, consisting of partially overlapping open reading frames (ORFs) that facilitate the transcription of various genes from the viral RNA genome (Figure 8).[50,51]

The full genome of HIV-1 genome (HXB2; NIH GenBank: K03455.1) around 9.7 kilo base (kb), while the genome of HIV-2 (ROD; NIH GenBank: M15390.1) spans 9.6 kb and encode for nine genes each. The exact length may however vary depending on the specific phylogenetic group or even in a single individual.[54,55] Like all retroviruses, the genome of HIV contains three major genes: group-specific antigen (*gag*), polymerase (*pol*), and envelope (*env*). These segments encode diverse proteins that arise through mechanisms such as alternative splicing, ribosomal frameshifts, and precursor peptide cleavage (Figure 10). The 5'-end of the genomic RNA is flanked by long terminal repeats (LTRs), which play roles in transcriptional regulation and integration into the host genome. The *pol* gene region encodes viral enzymes (RT, PR, IN), while the *gag* gene encompasses the structural proteins CA, MA, p6, and NC. The *env* gene governs the synthesis of gp120 and gp41 proteins. The Gag, Gag/Pol, and Env proteins initially exist as polyproteins, undergoing cleavage by the viral protease during later-stages of viral maturation.[50,51]

In addition to these conserved genes present in all infectious retroviruses, the HIV-1/2 genome also encodes multiple regulatory proteins. The trans-activator of transcription (Tat) binds to a hairpin structure known as the trans-activation responsive region (TAR) element, which is encoded within the R region of the LTR. This binding leads to an increase in the transcriptional

elongation of viral genes, which is amplified 100-fold through the recruitment of host factors. The activation of transcription by Tat is crucial for the replication of the virus.[50,56–59]

Another regulatory protein is the regulator of the expression of virion proteins (Rev). Rev binds to the Rev-responsive element (RRE) located within the HIV-1 *env* gene and, through its interaction with the chromosomal region maintenance 1 (CRM-1, *XPO1*) exporter protein, facilitates the export of unspliced and partially spliced viral RNA from the nucleus. This process allows the expression of gene products from *gag*, *pol*, and *env*.[50,60,61]

The last four genes encoding the HIV-1/2 genome are accessory proteins. These proteins exert a significant influence on viral infectivity by either redirecting regular host factor functions or inhibiting antiviral mechanisms of the host cell to promote viral replication.[50–52]

The viral infectivity factor (Vif) is prominently expressed within the cytoplasm, where it is also encapsulated into virus particles, contributing to increased infectivity. Its role includes the degradation of constituents within the apolipoprotein B mRNA-editing catalytic polypeptide-like 3 (APOBEC3) family, which functions as a cellular restriction factor against HIV.[50,62–65]

The viral protein R (Vpr) is substantially packaged into virus particles, facilitated by its interaction with Gag (p6 domain). It exerts a robust cell cycle arrest, specifically targeting the G2 stage of the cell cycle. This effect is achieved through the ubiquitination and subsequent degradation of cell cycle-related proteins. Vpr achieves this by binding to a ubiquitin ligase complex via DDB1 and CUL4 associated factor 1 (DCAF1)/VprBP. Moreover, Vpr aids in the import of the pre-integration complex (PIC) into the nucleus of non-dividing cells, particularly macrophages.[50,66–70]

HIV-1/2 also possesses a unique, type-specific accessory protein. HIV-1, for instance, encodes the viral protein U (Vpu), a membrane-bound protein that plays a pivotal role in augmenting virus production. It achieves this by inhibiting the activity of Tetherin, a restriction factor of HIV, which prevents the virus from spreading to nearby cells by entrapping them on the cell surface. Additionally, Vpu is involved in facilitating the degradation of CD4 through the ubiquitin-conjugating pathway.[50,71–73]

HIV-2 and a few other SIVs contain the viral protein X (Vpx), which supports the early stages of infection. This support is particularly important in macrophages and DC in a non-proliferative state, which consequently expresses the sterile alpha motif and HD domain-containing protein 1 (SAMHD1). SAMHD1 functions as a nucleosidase, breaking down the pool of available deoxyribonucleoside triphosphates (dNTPs) within the cytoplasm. This degradation impairs RT activity drastically. In a manner similar to other HIV accessory proteins, Vpx contributes to SAMHD1 degradation with the assistance of DCAF1 and the ubiquitin pathway.[50,74,75]

Finally, the genome also encodes the negative factor (*nef*), which induces downregulation of chemokine receptors (e.g. CD4, CD8), restriction factors, and HLA class I antigens on the surface of HIV-1 infected cells.[50,76]

1.2.2 HIV-1 Replication Cycle

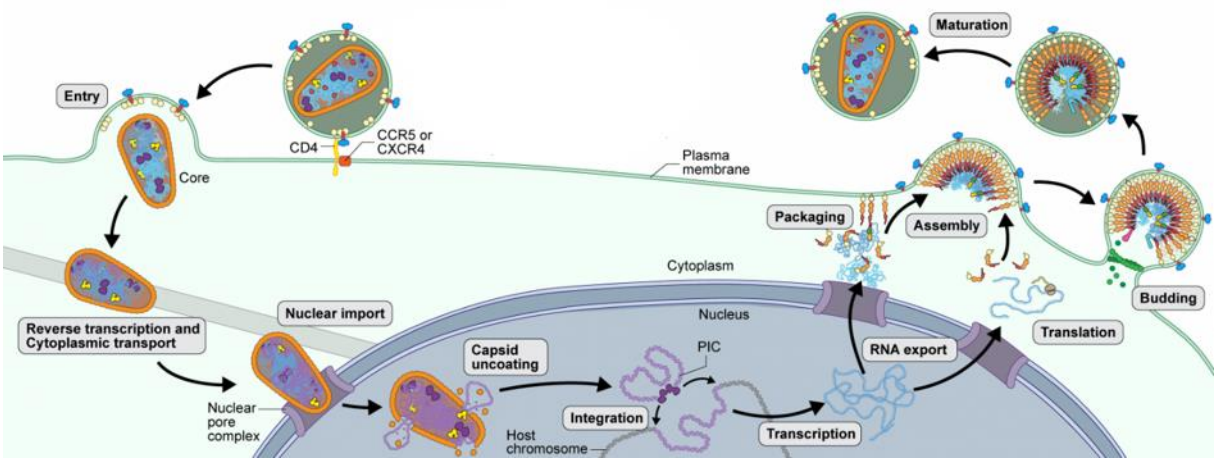

Figure 9: Schematic of HIV-1 Replication Cycle

Illustration depicting the current understanding of the HIV-1 replication cycle. The virus particle first binds to the CD4 and co-receptor (CCR5 or CXCR4) on the host cell membrane, resulting in fusion and the entry of the viral capsid into the cytoplasm. Reverse transcription is initiated in the cytoplasm and is completed after nuclear import. In the nucleus, the capsid falls apart, and the reverse-transcribed cDNA integrates into the host cell genome. The integrated provirus is then transcribed, and the resulting RNA products are exported to the cytoplasm. Unspliced and single-spliced RNA products utilize separate export pathways than multiply spliced RNA. The viral proteins are translated, and Gag and Gag/Pol precursor proteins assemble at the plasma membrane. The Gag/Pol protein binds to the newly transcribed viral genome, and the virus buds from the plasma membrane, subsequently maturing into a new infectious virus. Image adapted from [77].

Entry, Reverse Transcription, and Cytoplasmic Transport

After entering the host bloodstream, HIV-1 binds to macrophages, DC, or T cell CD4 receptors via the gp120 portion of the env protein. To facilitate fusion between the viral envelope and the cell membrane, a chemokine receptor (CCR5 or CXCR4) acts as a co-receptor. After binding, the fusion of viral and plasma membranes is initiated, allowing the capsid to enter the target cell's cytoplasm and initiating the replication cycle of HIV-1.[50,51,78]

In the cytoplasm, reverse transcription of the viral genome begins within the capsid, using host dNTPs and tRNAs to synthesize and initiate the reaction. In this process, the RT synthesizes a complementary double-stranded DNA (cDNA) from the two +ssRNA genome copies present in the capsid. Cellular and viral proteins that are connected with cDNA are called PIC.[79,80] During the process of reverse transcription, the capsid is transported through the cytoplasm to the nucleus by interactions with microtubules and ATP-dependent motor proteins.[81–84]

Nuclear Import, Capsid Uncoating, and Integration

The process of uncoating in HIV has been a topic of debate, particularly regarding its location and timing, whether it occurs in the cytoplasm or the nucleus of the host cell.[85,86] Recent publications tend to support the latter hypothesis. In this scenario, intact capsid reaches the nucleus and gains entry through a nuclear pore, facilitated by the cellular host factor cleavage and polyadenylation specific factor 6 (CPSF6), which binds to the capsid.[83,85–87] This process allows lentiviruses like HIV to also infect non-dividing cells.[88] In the nucleus, reverse transcription is completed and the capsid disassembles. The viral cDNA is then integrated into the host genome with the help of integrase. This integration establishes the virus as a provirus structure within the host's DNA and marks the end of the early stage of the HIV replication cycle.[50,85,89]

Transcription, RNA Export, and Translation

After integration, the late stages of HIV's life cycle start with gene transcription of the provirus. This process may be immediate or the provirus may remain latent for varying periods of time, spanning from days to years, and differing in duration from cell to cell.[90] Post-latency, transcription from the provirus occurs by human RNA polymerase II (Pol II),[50,91] which can bind to three adjacent transcription start sites (TSS) within the promoter U3-R region of the 5' LTR (Figure 8).[92] This region also contains binding sites for the transcription factors like NF-κB, which acts as a positive regulatory factor for transcription.[93] Pol II synthesizes long primary RNA transcripts, that are processed and may be also be spliced into small RNAs.[50,91,94,95] As mentioned previously, during the cellular Pol II-mediated transcription Tat protein binds to the TAR region of nascent viral RNA, forming a protein complex with cellular proteins which significantly enhances Pol II transcription rates, elevating viral RNA levels.[50,56,57] While multiply-spliced viral RNAs can exit the nucleus similar to cellular mRNAs, singly-spliced or unspliced viral RNAs require assistance of the viral Rev protein binding to the RRE in order to exit the nucleus (Figure 10) (1.2.1).[50,60,61]

Once in the cytoplasm, viral RNAs undergo translation into proteins through the cellular translation machinery. The *gag* and *pol* coding sequences are located in separate ORFs (Figure 10). Commonly, unspliced viral RNA translation produces the Gag precursor protein ($Pr55^{Gag}$). However, due to an occasional one-amino acid frameshift occurring approximately 10% of the time near the end of the Gag ORF, ribosomal translation proceeds within the pol reading frame. As a result, the entire *pol* gene is transcribed and the Gag/Pol precursor protein (Gag/Pol) is formed.[50,96]

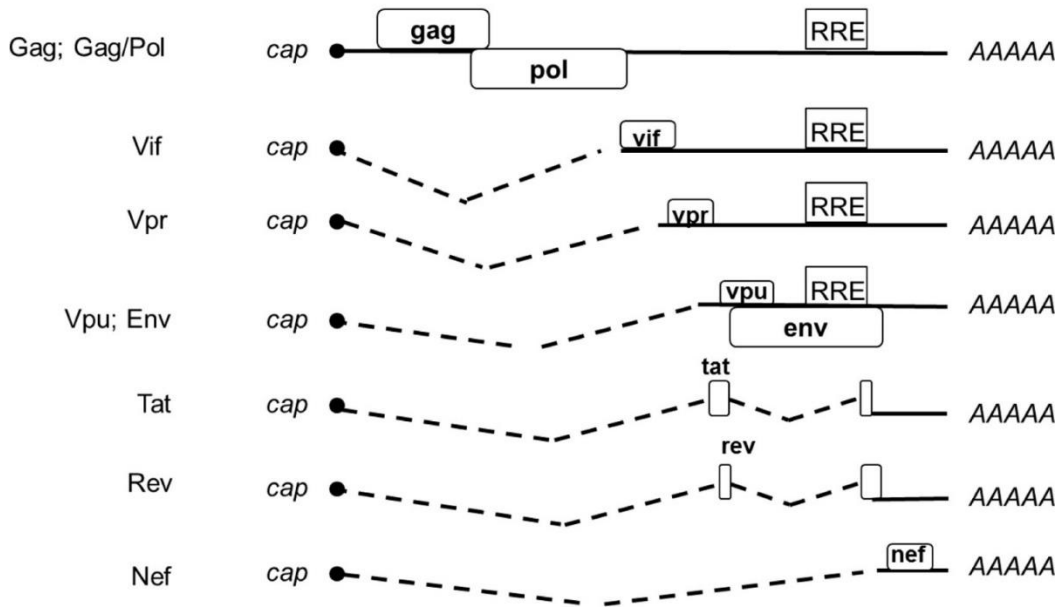

Figure 10: Different splice forms of HIV-1 RNA

This illustration depicts the transcription and processing of RNA from HIV-1 provirus and potential splicing events. Dashed lines showing the connection between major splice donor and acceptor sites. RNAs indicating the RRE site are leaving the nucleus through the CRM-1 pathway with the aid of Rev. The coded proteins of the respective RNA are shown on the left-hand side. Image adapted with permission from [97].

Packaging, Assembly, Budding, and Maturation

The assembly process primarily involves the aggregation of numerous $Pr55^{Gag}$ molecules at the cell membrane through a process known as Gag multimerization.[98–100] During this process, the N-terminal glycine within the MA domain undergoes myristoylation.[50,99,101] This myristoylation remains cloaked within the hydrophobic pocket of monomeric MA. Exposure of the myristate occurs upon the trimerization of MA.[102] This trimerization is induced by the multimerization of $Pr55^{Gag}$, mediated by the CA and NC domains. The binding of the newly transcribed gRNA to the NC promotes the Gag multimerization.[102] This conformational alteration is referred to as the "myristyl switch".[102,103] Additionally, a highly basic region (HBR; amino acids 14-31 of MA) forms a positively charged patch on the surface of the MA domain, promoting the association of $Pr55^{Gag}$ with the plasma membrane.[101,104,105] Remarkably, $Pr55^{Gag}$ itself can generate new particles without requiring additional viral proteins, emphasizing the significance of a few essential sites.[106] The Env glycoprotein is transported from the Golgi apparatus to the plasma membrane, integrating into it.[50,107] Over time, increasing amounts of $Pr55^{Gag}$ and a limited amount of Gag/Pol multimerize, causing the plasma membrane to bulge and form a spherical particle. The gRNA dimer, binding to NC through the “packaging sequence” psi (ψ) within the 5’ LTR, becomes packaged within this particle. [50,96,97,99,108,109]

After completion of the virus assembly, budding occurs in which the immature virus particles detach from the plasma membrane, which is facilitated by proteins of the host cell. Subsequently, immature virus particles are released into the extracellular space.[50,96,99,110]

Afterwards, the PR undergoes autocatalytic cleavage, separating itself from the Gag/Pol and processing other viral proteins that undergo reorganization. This results in the construction of a new conical capsid shell out of the p24, which encapsulates the gRNA-NC-enzyme complex. This completes the maturation process. The virus is now infectious and can infect a new cell.[50,96,99]

1.2.3 HIV Transmission, Pathogenesis, and the Onset of AIDS

This section focuses on medical and some epidemiological aspects of the virus. HIV infection occurs via infectious body fluids. Most cases occur through sexual contact, but transmission can also occur through the exchange of needles and perinatally. Not only free virus particles but also already infected cells represent a source of infection. HIV cannot be transmitted via droplet or smear infection, meaning that HIV is often described as difficult to transmit compared to other pathogens. However, the transmissibility of the virus cannot be understated, since the risk of transmission via the above-mentioned routes is great, especially at high viral loads.[51,111]

The course of HIV pathogenesis can be divided into the following three phases:

Primary Infection

The first phase of the natural HIV pathogenesis lasts approximately one to six months and is often asymptomatic. During this time, HIV establishes itself and builds up reservoirs inside $CD4^+$ memory T cells and macrophages. Flu-like symptoms such as fever, joint pain, lymphadenopathy and skin rashes can occur. During this phase, large amounts of virus particles accumulate in the blood and $CD4^+$ cell counts temporarily decrease but increase again towards the end of this phase. Due to the fact that the viral load is extremely elevated during this phase, the risk of transmission is also higher compared to the later-stages of infection.[51,111]

Latency Phase

The second phase lasts on average 8-10 years, in which the patient is in a symptom-free state. Due to the immune response, HIV-specific antibodies and cytotoxic $CD8^+$ T cells are established against HIV. As a result, the viral load diminishes in the bloodstream, while the $CD4^+$ T cell count decreases only slightly over the years. Overall, there is a balance in the body of the infected person between viral replication, followed by cell death, and the production of new $CD4^+$ cells.[51,111]

Symptomatic Phase

The last phase is defined by the onset of immunodeficiency and the development of the AIDS clinical symptoms. The $CD4^+$ T cell count decreases rapidly while the viral load in the blood spikes once more. The weakening of the immune system leads to HIV-associated infections such as fungal infections, shingles, or bacterial pneumonia. If the $CD4^+$ T cell count drops below approximately 200 cells/µl, opportunistic diseases associated with AIDS occur. These are infections that specifically affect individuals with immune deficiencies. The primary cause of this lies in the diversity of specific antibodies that are no longer present, and a wide variety of pathogen can get a foothold. Eventually, the immune system fails, potentially caused by the drastic loss of $CD4^+$ T cells. The patient dies due to one of the overwhelming burdens of opportunistic infections.[51,111]

1.2.4 A Life With HIV: cART Treatment and Long-Term Consequences

However, HIV infection is no longer a death sentence. This dramatic change is due to the effective highly active antiretroviral therapy (HAART), which is a type of HIV therapy that involves a combination of medications to suppress the replication of HIV and slow down the disease progression. HAART is also known as combination antiretroviral therapy (cART). The previously described phase progression of infection occurred in the pre-HAART era without medical intervention of the infected individual.[50,51,111,112]

cART typically involves the use of three or more antiretroviral medications from different classes, including nucleoside reverse transcriptase inhibitors (NRTIs), non-nucleoside reverse transcriptase inhibitors (NNRTIs), protease inhibitors (PIs), and integrase inhibitors (INIs). By using a combination of drugs with different mechanisms of action, cART is able to attack the virus at multiple points in its life cycle, making it more difficult for the virus to develop resistance against drugs. The goals of cART therapy are to reduce the viral load, increase the $CD4^+$ T cell count, and improve the overall health and quality of life of people living with HIV.[50,51,111,113] cART is highly effective in achieving these goals, with many people living with HIV being able to reach nearly normal life expectancy with proper treatment.[44] However, cART is not a cure for HIV, and it requires lifelong adherence to the medication regimen in order to maintain its effectiveness.[50,51,111,113] Additionally, cART can have side effects, including nausea, vomiting, diarrhea, neurotoxicity, fatigue, and interactions with other medications.[51,111,114]

It is nearly impossible to cure HIV infection (described in section 1.2). The reason for this resiliency is the HIV reservoir, with proviruses being inactive and not affected by the drugs in cART. They do not express viral proteins and the immune system cannot differentiate between healthy cells and provirus containing cells. As a result, the immune system is unable to distinguish between infected and uninfected cells. HIV reservoirs thus enable replication-

competent viruses to persist despite therapy, which means that increased virus production can occur anytime if therapy is interrupted.[51,111,112,115]

The major challenge for research is to find a means to eradicate the HIV reservoir.[111,112,116–118] Attempts are being made to prevent the integration of HIV into the host cell genome, to reactivate it from dormant memory cells by the "shock and kill" strategy,[117] or to epigenetically silence the provirus in the genome by the “block and lock” strategy.[116] Ultimately, the aim is to prevent the expression of viral proteins and the resulting formation of new virions.

HIV-Associated Neurocognitive Disorder and the Role of Macrophages

A complete, safe cure remains the ultimate goal in HIV research. However, despite cART treatment, individuals with HIV infection still experience pathogenic manifestation. Although these symptoms are milder than those associated with AIDS, they continue to have a significant impact on their lives.[119] The life expectancy for those living with HIV is approaching that of people without HIV infection, leading to a growing population of individuals living with HIV.[44] It is therefore essential to understand molecular mechanisms underlying these symptoms and to investigate possible treatments.

One major pathogenic manifestation in current HIV-infected patients is cognitive impairments, which are grouped under the term HIV-associated neurocognitive disorders (HAND).[120–122] This impairment affects up to 50% of individuals with HIV-1 infection, particularly those with advanced states of disease (Figure 11).[121,123] The clinical manifestations of HAND can vary depending on the severity of the disease. Mild neurocognitive disorders (MND) associated with HAND may manifest as subtle deficits in attention, memory, and executive functions, while more severe forms may lead to HIV-associated dementia (HAD), which can include motor deficits and seizures. In developed countries where cART treatment is the standard, asymptomatic neurocognitive impairments (ANI) is the most common group of HANDs, defined by the detectability of HIV in the cerebrospinal fluid, but that does not significantly affect the individual's daily functions.[121,122,124] Despite effective cART treatment, the incidence of HAND remains high, with numbers remaining at levels similar to the pre-cART era, although the severity of HAD cases is less pronounced today (Figure 11). This ongoing prevalence of HAND poses increasing challenges for health systems worldwide.[122–124]

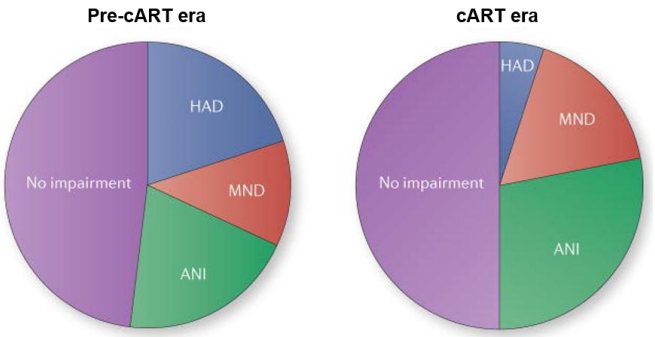

Figure 11: Proportion of HAND in the HIV-Infected Population

Illustration of the distribution of unaffected (purple), as well as HAND affected individuals of the HIV infected population before and with treatment by cART. HAND is split into ANI (green), MND (red) and HAD (blue) cases. Image reproduced with permission from [122].

The pathogenesis of HAND is complex and not yet fully understood. Macrophages, as one of the first cell types encountered by HIV-1 after infection, play a crucial role in the pathogenesis of HAND. During the acute phase, HIV-1 infects monocytes, allowing the virus to migrate through these monocytes across the blood-brain barrier as 'trojan horse' into the central nervous system (CNS).[119,125,126] Within the CNS, monocytes can differentiate into mature tissue-resident macrophages, and HIV-1 establishes persistent infection.[124,127,128] Moreover, newly produced virus particles can infect cells within the CNS, including microglial cells.[129] Viral components in infected cells trigger the release of pro-inflammatory cytokines, leading to neuroinflammation,[128,130,131] and neurotoxicity mediated by viral proteins.[127,132] These processes can damage neurons and contribute to cognitive impairment.

Understanding the interaction between macrophages and HIV-1 is important for the development of new treatments and strategies for controlling chronic inflammation caused by the virus and to improve the health of a growing population of individuals living with HIV-1.

1.3 Aims of This Thesis

This thesis focuses on the innate immune response of monocyte-derived macrophages (MDMs) against HIV-1 infection, investigating the viral and cellular determinants that produce the innate immune response and subsequent inflammation. The aim is to identify and characterize viral or cellular determinants that are crucial for driving innate immune activation in macrophages.

First, we investigate the innate immune response in MDMs. This will involve time-interval experiments using antiviral agents to inhibit reverse transcription or integration of the viral genome to determine the stage of the replication cycle that triggers the innate immune response. A panel of ISGs will be selected to assess nascent inflammation and activated PRRs in MDMs and their expression will be monitored over time using real-time PCR. Activation of transcription factors is measured by western blot analysis.

Subsequently, analytical experiments are carried out using macrophage-like stable cell lines. The utilization of cell lines will minimize genetic variability between experiments and enable the generation of stable knockout (KO) cell lines for identified cellular proteins associated with innate immune recognition of HIV-1. Further experiments involving pharmacological or genetic approaches are conducted to investigate the specific viral determinants required for triggering the innate immune response.

The study will also try to explore the interaction between the identified viral components of HIV-1 and the cellular factors involved in the innate sensing pathway. This analysis aims to provide insights into the cellular mechanisms underlying innate immune recognition. Ultimately, this knowledge will facilitate our understanding of inflammation in HIV-1-infected MDMs at both the viral and cellular levels.

2 Materials and Methods

2.1 Materials

The following tables list the materials used in the preparation of this thesis that could not be assigned to just one of the subsequent method sections (2.2, 2.3, 2.4, 2.5).

Table 1: Antibiotics, Drugs and Stimulants

Antibiotic / Drug / Stimulants	Supplier
Ampicillin	Carl Roth, Germany
cOmplete™ protease inhibitor cocktail	Roche, Switzerland
eBioscience™cell stimulation cocktail (500X)	ThermoFisher Scientific, USA
Gentamicin-solution	Merck, Germany
Gibco pen strep (penicillin-streptomycin)	ThermoFisher Scientific, USA
Human GM-CSF recombinant protein, PeproTech®	ThermoFisher Scientific, USA
Leptomycin-B	InvivoGen, France
Nevirapine	Merck, Germany
Normocin™	InvivoGen, France
Phorbol 12-myristate 13-acetate (PMA)	Merck, Germany
PhosSTOP™ phosphate inhibitor cocktail tablets	Roche, Switzerland
Puromycin	InvivoGen, France
R-33	AdooQ BioScience, USA
Raltegravir	Merck, Germany
Selinexor (KPT-330)	Selleck Chemicals, USA

Table 2: Antibodies and Dyes

Antibody / Dye	Dilution	Organism	Supplier
AG3.0 Anti-p24	1:500	Mouse	Stephen Norley[133] NIH reagent program ARP-4121
Anti-human IgG (γ-chain specific)-peroxidase	1:1,000	Goat	Merck, Germany
c-Myc monoclonal antibody (9E10)	1:1,000	Mouse	ThermoFisher Scientific, USA
eBioscience™ fixable viability dye eFluor™ 660 (FVD-660)	1:1,000		ThermoFisher Scientific, USA
GAPDH monoclonal Ab (FF26A), eBioscience™	1:2,500	Mouse	ThermoFisher Scientific, USA
HIV positive plasma pool	1:10,000	Human	Stephen Norley[133]
IRDye® 680RD goat anti-rabbit IgG	1:15,000	Goat	LI-COR, USA
IRDye® 800CW goat anti-mouse IgG	1:15,000	Goat	LI-COR, USA
IRF3 monoclonal antibody	1:1,000	Mouse	Proteintech Group, USA
IRF3 monoclonal antibody eBioscience™	1:1,000	Mouse	ThermoFisher Scientific, USA
Anti-IRF3 (phospho-S386) [EPR2346] monoclonal antibody	1:1,000	Rabbit	Abcam, UK
MAVS antibody #3993 polyclonal antibody	1:1,000	Rabbit	Cell Signaling Technology, USA
Monoclonal anti-α-Tubulin antibody T6074	1:1,000	Mouse	Merck, Germany

Monoclonal anti-β-Actin antibody	1:1,000	Mouse	Merck, Germany
Phospho-IRF-3 (S396) (D601M) monoclonal antibody	1:1,000	Rabbit	Cell Signaling Technology, USA
Phospho-STAT1 S(S727) (D3B7) monoclonal antibody	1:1,000	Rabbit	Cell Signaling Technology, USA
Phospho-STAT1 S(T701) (58D6) monoclonal antibody	1:1,000	Rabbit	Cell Signaling Technology, USA
Phospho-TBK1/NAK (S172) (D52C2) monoclonal antibody	1:1,000	Rabbit	Cell Signaling Technology, USA
SAMHD1 mouse monoclonal antibody	1:1,000	Mouse	OriGene, USA
STAT1 (9H2) monoclonal antibody	1:1,000	Mouse	Cell Signaling Technology, USA
STING (D2P2F) monoclonal antibody	1:1,000	Rabbit	Cell Signaling Technology, USA
TBK1 monoclonal antibody	1:1,000	Mouse	Proteintech Group, USA
TBK1 monoclonal antibody	1:1,000	Mouse	Proteintech Group, USA

Table 3: Chemicals

Chemical	Supplier
1,2-Bis-(dimethylamino)-ethane,N,N,N',N'-Tetramethylethylenediamine (TEMED)	Carl Roth, Germany
1,4-Dithiohreit (DTT)	Carl Roth, Germany
2-Mercaptoethanol	Carl Roth, Germany
Agarose analyze and prep	Simplebiotech, Germany
Ammonium chloride	Carl Roth, Germany
Ammonium persulfate (APS)	Carl Roth, Germany
Bovine serum albumin (BSA) fraction V	Carl Roth, Germany
D(+)-Saccharose	Carl Roth, Germany
Dimethyl sulfoxide (DMSO)	Merck, Germany
Ethanol	Carl Roth, Germany
Ethidium bromide	Roche, Switzerland
Ethylenediaminetetraacetic acid (EDTA)	Merck, Germany
Formaldehyde	Merck, Germany
Glycerol	Carl Roth, Germany
Glycine	Carl Roth, Germany
Glycogen	ThermoFisher Scientific, USA
Glutaraldehyde 25% aqueous solution	Merck, Germany
Hydrochloric acid (HCl) 37%	Carl Roth, Germany
Isopropanol (2-propanol)	Carl Roth, Germany
Methanol	Carl Roth, Germany
MS2 RNA from bacteriophage MS2	Roche, Switzerland
Nonoxinol 40 (NP-40)	ThermoFisher Scientific, USA
Skimmed milk powder	Carl Roth, Germany
Polyethylenimine hydrochloride (PEI)	Merck, Germany
Polyethylene glycol alkylphenyl ether (Triton X-100)	Carl Roth, Germany
Polyoxyethyelne-20-sorbitan monolaurate (Tween® 20)	Carl Roth, Germany
ROTIPHORESE®Gel 30 (37,5:1)	Carl Roth, Germany
Sodium azide	Merck, Germany
Sodium chloride	Carl Roth, Germany
Sodium deoxycholate	Merck, Germany
Sodium dodecyl sulphate (SDS)	Carl Roth, Germany
Sodium hydroxide (NaOH)	Carl Roth, Germany
Sulfuric acid (H_2SO_4) 95-98%	Carl Roth, Germany
Trichloromethane/chloroform	Carl Roth, Germany

Tris-(hydroxymethyl)-amino methane	Carl Roth, Germany
TRIzol™ reagent	ThermoFisher Scientific, USA

Table 4: Commercial Buffers, Growth Media, and Solutions

Buffer / Solution / Growth medium	Supplier
10X Phosphate-buffered saline (PBS) / 1X PBS, pH 7.2	RKI, Germany
10X Tris-buffered saline (TBS), pH 7.5	RKI, Germany
2-[4-(2-Hydroxyethyl)-1-piperazinyl]-ethane sulfonic acid (HEPES)-Buffer 1 M	Merck, Germany
Accutase® solution	Merck, Germany
Blocking buffer (western blot)	Rockland Inc., USA
Carbonate-bicarbonate buffer, pH 9.6	GENAXXON bioscience, Germany
Dulbecco's modified eagle medium (DMEM), pH 7.2	Nutrient center of RKI, Germany
FastDigest green buffer (10X)	Thermo Fisher Scientific, USA
Gibco™ fetal bovine serum (FBS) origin brazil	Thermo Fisher Scientific, USA
Histopaque®-1077 Hybri-Max™	Merck, Germany
Humanserum heat inactivated, male AB	Merck, Germany
IC fixation buffer	Thermo Fisher Scientific, USA
Incuwater-Clean™	ITW Reagents, Italy
NuPAGE®LDS sample buffer (4X)	ThermoFisher Scientific, USA
QUANTI-Blue™: SEAP detection reagent	InvivoGen, France
QUANTI-Luc™: luciferase detection reagent	InvivoGen, France
Resolving gel buffer 1.5 M Tris-HCl, pH 8.8	Bio-Rad Laboratories, Inc., USA
Roswell Park memorial institute (RPMI)-1640, pH 7.2	Nutrient center of RKI, Germany
ROTIPHORESE®50x TAE buffer	Carl Roth, Germany
S.O.C. medium	Thermo Fisher Scientific, USA
Stacking gel buffer 0.5 M Tris-HCl, pH 6.8	Bio-Rad Laboratories, Inc., USA
Trypsin-EDTA solution 1X	Merck, Germany

Table 5: Compositions of Made Buffers, Growth Media, and Solutions

Buffer / Solution / Growth medium	Composition
10X Tris-glycine	250 mM Tris, 1.92 M glycine in ddH_2O
12% Resolving gel solution	40% (v/v) ROTIPHORESE®Gel 30 (37,5:1), 25% (v/v) resolving gel buffer, 0.1% (v/v) SDS, 0.05% (v/v) APS, 0.05% (v/v) TEMED
5% Stacking gel solution	17% (v/v) ROTIPHORESE®Gel 30 (37,5:1), 25% (v/v) stacking gel buffer, 0.1% (v/v) SDS, 0.05% (v/v) APS, 0.05% (v/v) TEMED
Blocking buffer (ELISA)	2% (w/v) Skimmed milk powder in 1XPBS, pH 7.2
Cell freezing medium	45% (v/v) FBS, 45% (v/v) RPMI-1640, pH 7.2, 10% (v/v) DMSO
Dendritic cell (DC)-medium	5% (v/v) Human serum, 1mM HEPES, 24 µg/mL gentamicin in RPMI-1640, pH 7.2

Disruption buffer	40 mM Tris-HCl, pH 8.1, 50 mM KCl, 20 mM DTT, 0.2% NP-40
DMEM complete	10% (v/v) FBS, 20 Units/mL pen strep-solution in DMEM, pH 7,2
ELISA wash buffer	0,05% Tween 20 in 1XPBS, pH 7,2
LB-medium complete	50µg/mL Ampicillin in LB-medium, pH 7,2
NP40-lysis buffer	100 mM Tris-HCl, pH 8,0, 30 mM NaCl, 0,5% (v/v) NP40 in ddH_2O, 1 tablet each of cOmplete™ Protease inhibitor cocktail for 10 mL buffer
Radio-immunoprecipitation assay (RIPA)-lysis buffer	50 mM Tris HCl, 150 mM NaCl, 1% (v/v) NP-40, 0,5% (w/v) sodium deoxycholate, 1 mM EDTA, 0,1% (w/v) SDS, 0.01% (w/v) sodium azide in ddH_2O, pH of 7.4, 1 tablet each of cOmplete™ protease inhibitor cocktail and PhosSTOP™ for 10 mL buffer
Red blood cell-lysis-buffer	160 mM NH_4Cl, 170mM Tris-HCl, pH 7.2
RPMI-1640 complete	10% (v/v) FBS, 2% (v/v) pen strep-solution, 100 µg/mL normocin in RPMI-1640, pH 7.2
Running buffer	0.1% (v/v) SDS, 10% (v/v) 10X Tris-gylcine in ddH_2O
Sucrose gradient solution	20% (w/v) Sucrose in 1XPBS, pH 7.4,
Transfer buffer	20% (v/v) Methanol, 10% (v/v) 10X Tris-gylcine in ddH_2O
WB sample buffer	5% 2-Mercaptoethanol in 4X NuPAGE®LDS sample buffer
WB wash buffer	0.1% Tween 20 in 1XPBS, pH 7.2 or 1XTBS, pH 7.5

Table 6: Enzymes and Ladders

Enzyme / Ladder	Supplier
FastDigest BamHI	Thermo Fisher Scientific, USA
FastDigest FspAI	Thermo Fisher Scientific, USA
FastDigest NheI	Thermo Fisher Scientific, USA
FastDigest SalI	Thermo Fisher Scientific, USA
FastDigest SpeI	Thermo Fisher Scientific, USA
FastDigest XhoI	Thermo Fisher Scientific, USA
GeneRuler 1 kb DNA-ladder	Thermo Fisher Scientific, USA
GeneRuler 1 kb Plus DNA-ladder	Thermo Fisher Scientific, USA
GeneRuler 100 bp Plus DNA-ladder	Thermo Fisher Scientific, USA
PageRuler™ prestained protein ladder	Thermo Fisher Scientific, USA
Phusion green HS II high-fidelity PCR MM	Thermo Fisher Scientific, USA
T4 DNA ligase, LC (1 U/µL)	Thermo Fisher Scientific, USA

Table 7: Kits

Kit	Supplier
BigDye™ terminator v3.1 cycle sequencing kit	ThermoFisher Scientific, USA
GeneJET gel extraction kit	ThermoFisher Scientific, USA
GeneJET PCR purification kit	ThermoFisher Scientific, USA
Luciferase assay system	Promega, USA
Pierce BCA protein assay kit	Thermo Fisher Scientific, USA
QIAprep® spin miniprep kit	QIAGEN, Germany
QIAamp® DNA mini kit	QIAGEN, Germany
QIAamp® viral RNA mini kit	QIAGEN, Germany
QIAGEN plasmid maxi kit	QIAGEN, Germany
QIAGEN plasmid midi kit	QIAGEN, Germany
QIAquick® gel extraction kit	QIAGEN, Germany
QIAquick® PCR purification kit	QIAGEN, Germany
RevertAid RT reverse transcription kit	Thermo Fisher Scientific, USA
RNeasy® mini kit	QIAGEN, Germany
Lenti RT activity kit	Cavidi, Sweden
SensiFAST™ probe no-ROX kit	Meridian Bioscience, USA
SensiFAST™ SYBR no-ROX kit	Meridian Bioscience, USA
SuperScript™ III first-strand synthesis system	Thermo Fisher Scientific, USA
SV 96 total RNA isolation system	Promega, USA

Table 8: Laboratory Gear

Laboratory gear	Supplier
96PW-Tecan CE micro plate washer	Tecan Group, Switzerland
Avanti™J-20 XP centrifuge	Beckman Coulter, USA
CB 170 CO_2-incubator	Binder, Germany
Cell culture dishes, well-plates, and flasks	TPP, Switzerland
Centrifuge 5415 R	Eppendorf, Germany
Centrifuge 5424 R	Eppendorf, Germany
CFX96™real-time system	Bio-Rad Laboratories, USA
Countess 3 FL	Thermo Fisher Scientific, USA
Ecotron	Infors HT, Switzerland
Eppendorf thermomixer compact 5350 Mixer	Eppendorf, Germany
FACSCalibur flow cytometer: 4-color	BD Biosciences, USA
Heraeus biofuge primo R centrifuge	Thermo Fisher Scientific, USA
Immobilon®-FL transfer membranes 0.45 µm	Merck, Germany
Invitrogen™ nunc MaxiSorp™ flat bottom	Thermo Fisher Scientific, USA
LABSONIC® M	Sartorius, Germany
LUMIstar OMEGA	BMG LABTECH, Germany
Magna-Sep™	Thermo Fisher Scientific, USA
Mastercycler X50s	Eppendorf, Germany
Mini Trans-Blot® cell	Bio-Rad Laboratories, USA
Mini-PROTEAN® tetra handcast system	Bio-Rad Laboratories, USA
Mini-PROTEAN® TGX gels	Bio-Rad Laboratories, USA
Multiskan Go	Thermo Fisher Scientific, USA
NanoDrop™ One/Onec microvolume-UV/Vis Spectrophotometer	Thermo Fisher Scientific, USA
Optima XPN-80 ultracentrifuge	Beckman Coulter, USA
Polymax1040	Heidolph Instruments, Germany
Power supplies	Bio-Rad Laboratories, USA

ROTILANO®Blotting papers, thick 0.75,	Carl Roth, Germany
Sartorius top-loading balance excellence E2000D	Sartorius, Germany
Sigma 3-30KS	Sigma Laborzentrifugen, Germany
Tecan sunrise OEM remote microplate absorbance reader	Tecan Group, Switzerland
Thermo HERAsafe KS 12	Thermo Fisher Scientific, USA
Ultra-Clear™ centrifuge tubes 25 x 89mm	Beckman Coulter, USA
Wide mini-sub cell GT cell	Bio-Rad Laboratories, USA

Table 9: Plasmids

Nr.	Plasmid	Source
1	p89.6	NIH HIV reagent program ARP-3552
2	pcDNA6-SIV_{mac239}-Vpx-Myc-His	Henning Hofmann[134]
3	pCH040.c/2625	NIH HIV reagent program ARP-11740
4	pCMV-VSV-G Myc	Addgene# 80054
5	pLentiCRISPR.v1-Puro-MAVS#1	Oya Cingöz
6	pLentiCRISPR.v1-Puro-MAVS#2	Oya Cingöz
7	pLentiCRISPR.v1-Puro-STING#2	Oya Cingöz
8	pMDLg/pRRE	Addgene #12251
9	pNL.4.3-Luc E- R-	Ned Landau[135] NIH HIV reagent program ARP-4121
10	pNL4.3 GFP CA_{E45A}	Stephen Goff
11	pNL4.3 GFP CA_{K203A}	Stephen Goff
12	pNL4.3 GFP CA_{N74D}	Stephen Goff
13	pNL4.3 GFP CA_{P38A}	Stephen Goff
14	pNL4.3 GFP $CA_{QQ63/67AA}$	Stephen Goff
15	pNL4.3 Luc MA_{G2A} E- R-	Nicolas Arnow
16	pNL4.3 Luc $Rev_{LE76\ 77DL}$ E- R-	Oya Cingöz
17	pNL4.3 Luc Tat_{M1A} E- R-	Oya Cingöz
18	pNL4.3.CMV-GFP SIVp6 (SIV_{mac}gag 17-26) E- R-	Henning Hofmann[136]
19	pNL4.3.CMV-GFP SIVp6 (SIV_{mac}gag 17-26) MA_{G2A} E- R-	Nicolas Arnow
20	pNL4.3.CMV-GFP SIVp6 (SIV_{mac}gag 17-26) $Rev_{LE76/77DL}$ E- R-	Nicolas Arnow
21	pNL4.3.CMV-GFP Δgag/$pol_{(52-3711)}$ E- R-	Nicolas Arnow
22	pNL4.3-Luc CA_{P90A} E- R-	Stephen Goff
23	pNL4.3-Luc IN_{D64A} E- R-	Oya Cingöz
24	pNL4.3-Luc RH_{H539F} E- R-	Oya Cingöz
25	pNL4.3-Luc RT_{D110A} E- R-	Oya Cingöz
26	pRSV.rev	Addgene #12253
27	psPAX2	Addgene #12260
28	pWPXL-GFP	Addgene #12257

Table 10: Plasmids Used for Virus Production

Virus	Plasmids used (**Table 9**)	Ratio of transfection
$WPRE_{GFP}$	4, 19, 28	1: 3: 4
$NL4.3_{GFP}$ CA_{E45A}	4, 10, 19	1: 4: 3
$NL4.3_{GFP}$ CA_{K203A}	4, 11, 19	1: 4: 3
$NL4.3_{GFP}$ CA_{N74D}	4, 12, 19	1: 4: 3
$NL4.3_{GFP}$ CA_{P38A}	4, 13, 19	1: 4: 3
$NL4.3_{GFP}$ $CA_{QQ63/67AA}$	4, 14, 19	1: 4: 3
$NL4.3_{GFP}$ MA_{G2A}	2, 4, 19, 27	1: 1: 3: 4
$NL4.3_{GFP}$ Rev_{M10}	2, 4, 20, 25	1: 1: 7: 1
$NL4.3_{GFP}$	2, 4, 18	1: 1: 7
$NL4.3_{GFP}$ Δgag/pol	4, 19, 21	1: 3: 4
$NL4.3_{Luc}$ CA_{P90A}	4, 19, 22	1: 3: 4
$NL4.3_{Luc}$ IN_{D64A}	4, 19, 23	1: 3: 4
$NL4.3_{Luc}$ MA_{G2A}	4, 15, 19	1: 4: 3
$NL4.3_{Luc}$ Rev_{M10}	4, 16, 19	1: 4: 3
$NL4.3_{Luc}$ RH_{H539F}	4, 19, 24	1: 3: 4
$NL4.3_{Luc}$ RT_{D110A}	4, 19, 25	1: 3: 4
$NL4.3_{Luc}$ Tat_{M1A}	4, 17, 19	1: 4: 3
$NL4.3_{Luc}$	4, 9	1: 7
Virus-like particle (VLP) empty	4, 8, 25	1: 7: 1
VLP Vpx	2, 4, 8, 25	1: 1: 7: 1

Table 11: Software

Software	Version	Supplier
CFX Maestro Software	2.2	Bio-Rad Laboratories, Inc., USA
CMU FireCam	2.03	PHASE, Germany
DeepL	23.9.2	DeepL SE, Germany
FlowJo	10.8.0	FLOWJO, LLC, USA
Geneious Prime	2021.2.2	Biomatters, New Zealand
GraphPad Prism	9.1.0	Graph Pad Software, USA
Image Studio	5.2.5	LI-COR, USA
ImageJ	01.52a.0	National Institutes of Health, USA
MARS	3.32 R5	BMG LABTECH, Germany
Mendeley Desktop	1.19.8	Elsevier Inc., USA
Microsoft Office Professional Plus	2019	Microsoft, USA
ND1000	V 3.8.1	Thermo Fisher Scientific, USA
Omega	5.50 R4	BMG LABTECH, Germany
TECAN Reader	1.0	Steve. Ink.

2.2 Cell Biological Methods

2.2.1 Cell Culture

For cell culture, only cell culture plastics from TPP (Table 8) were purchased. The cells were cultured at 37°C in a 5% CO_2 humidified atmosphere in Binder incubators (Table 8).

Table 12: Cells Used in Cell Culture

Cells	Cell type	Supplier
C8166 $CD4^+$ $CCR5^+$	Suspension	Kindly provided by Oya Cingöz at RKI
HEK-293T	Adherend	ATCC, USA
HEK-Blue™ IFN-α/β Reporter HEK 293 Cells	Adherend	InvivoGen, France
PBMCs (Buffy Coats from anonymous blood donors)	Suspension/ Adherend	DRK Blutspendedienst Nord-Ost, Germany
THP-1	Suspension	Kindly provided by Veit Hornung at Ludwig-Maximilians-Universität Munich
THP-1 Dual™ Cells	Suspension	InvivoGen, France
THP-1 Dual™ KO-STING Cells	Suspension	InvivoGen, France
THP-1 MAVS KO	Suspension	Created by Nicolas Arnow at RKI
THP-1 STING KO	Suspension	Kindly provided by Veit Hornung at Ludwig-Maximilians-Universität Munich
TZM-bl	Adherend	Kindly provided by Uwe Fiebig at RKI
U937	Suspension	Kindly provided by Albrecht F. Kiderlen at RKI
U937 MAVS KO	Suspension	Created by Nicolas Arnow at RKI
U937 STING KO	Suspension	Created by Nicolas Arnow at RKI

Adherent Cells

Adherent cells (Table 12) were cultured in Dulbecco's Modified Eagle Medium (DMEM) complete medium (Table 5). Cells were passaged every two to three days at a ratio of 1:5 to 1:20, depending on cell density. For this purpose, the medium was first removed, and the cells were washed with 1X PBS. Subsequently, the cells were detached from the bottom of the flask using a trypsin/EDTA solution (Table 4). Depending on the ratio, the cells were resuspended in a fresh medium and further cultured.

Suspension Cells

Suspension cells (Table 12) were cultured in Roswell Park Memorial Institute 1640 (RPMI-1640) complete medium (Table 5). Depending on cell density, the cell suspensions were diluted at a ratio of 1: 10 to 1: 20 with fresh medium and then cultured further.

Primary Blood Cells

Isolated primary blood cells from Buffy Coats (Table 12) were cultured in DC-Medium (Table 5).

2.2.2 PBMC Isolation

The following protocol details how peripheral blood mononuclear cells (PBMC) are properly isolated to obtain a pure cell population for downstream applications.

To isolate PBMCs from a fresh buffy coat of samples (Table 12), the buffy coat was first diluted 1: 2 with RPMI-1640 and carefully layered onto 12 mL of ficoll (Histopaque, Table 4) in 50 mL centrifuge tubes. Histopaque, a polysucrose, can penetrate erythrocytes, dead cells, and cell fragments while leaving PBMCs in the interphase. After centrifugation at 1420 x g for 25 minutes with the lowest possible acceleration and braking forces, the buffy coat separated into three phases, and the PBMCs were collected from the interphase.

The collected PBMCs were then washed with RPMI-1640 and centrifuged at 840 x g for 8 minutes. After discarding the supernatant, the pellet was resuspended in 5 mL of RBC Lysis Buffer and incubated at room temperature for 5 minutes to lyse any remaining erythrocytes. Following another wash step with RPMI-1640 and centrifugation at 840 x g for 5 minutes, the supernatant was discarded again. If the pellet was still strongly stained red, indicating the presence of many remaining erythrocytes, the lysis and washing step was repeated.

Finally, the PBMC pellet was resuspended in 10 mL of DC medium, and cell counting was performed. The desired number of cells were either used directly or cultured for further experiments.

The use of Histopaque 1077 as ficoll and RBC Lysis Buffer allows for efficient separation of PBMCs from other blood components, particularly erythrocytes, which can interfere with downstream applications.

Differentiation of MDMs

Macrophages can be differentiated *in vitro* from monocytes isolated out of peripheral blood. First, monocytes of the PBMCs population were selected by adhering to the plate surface for several hours, followed by washing to remove unbound cells. Macrophages were differentiated from monocytes by stimulating the cells with 50 ng/mL Granulocyte-Macrophage Colony-Stimulating Factor (GM-CSF) for one to two weeks with freshly added GM-CSF every other day. The resulting macrophages are referred to as monocytic-derived macrophages (MDM).

2.2.3 Flow Cytometry

Fluorescence-activated cell sorting (FACS) is a method used to analyze and sort cells based on their physical and fluorescent characteristics. FACS involves labeling cells with fluorescently labeled antibodies or dyes, which bind to specific molecules or structures within the cell. The cells are then passed through a flow cytometer, which detects the fluorescence emitted by the cells and measures their physical properties, such as size and granularity.

Adherent cells were harvested by incubating them with Accutase or trypsin/EDTA at 37°C for 20 minutes, or by washing them off with PBS. Suspension cells were harvested by washing them once with PBS. To detect the live and dead cell populations, a fixable-viability dye (FVD) 660 was used. The cells were incubated with PBS containing FVD-660 at a 1: 1,000 dilution for 20 minutes in the dark at room temperature. After the cells were washed, they were fixed in IC fixation buffer for 10 minutes at room temperature or overnight at 4°C. Prior to analysis by flow cytometry, the cells were washed twice and then diluted in PBS.

2.2.4 Production of CRISPR/CAS 9 KOs

The Clustered Regularly Interspaced Short Palindromic Repeats (CRISPR) method, coupled with the lentiviral vector system, enables efficient and precise KO of gene expression in various cell types.

Table 13: Oligonucleotides for CRISPR/Cas9 KO

Name	5'-Sequence-3'
MAVS gRNA-1a	AGT ACT TCA TTG CGG CAC TG
MAVS gRNA-1b	ACT GGA GCA GAT GAT AGG CT
STING gRNA2	CAT TAC AAC AAC CTG CTA CG

In this study, the lentiCRISPR v1 construct, which carries the codon-optimized CRISPR-associated 9 (Cas9) nuclease and a puromycin resistance gene, was used as a lentiviral backbone. A guide RNA (Table 13) targeting the gene of interest (GOI) for KO was cloned into the vector under the control of a U6 promoter. Virus-Like Particles (VLPs) carrying the lentiCRISPR constructs were produced by transfecting (section 2.2.5) HEK-293T cells with the lentiCRISPR construct, psPAX2 packaging plasmid, and VSV-G envelope (Env) plasmid in a 4:3:1 ratio. The VLPs were collected using the same method as virus particles (section 2.2.6). The KO of STING and MAVS genes was then introduced into 5×10^5 target THP-1 and U937 cells via viral transduction with 20 µl of concentrated VLPs. The transduction procedure was similar to spinoculation with virus infection (section 2.2.6). The integrated lentiviral construct then produced Cas9 nuclease, which generated double-stranded breaks at the guide RNA-targeted gene locus, triggering the cell's natural DNA repair mechanisms. These repair mechanisms can result in the KO of the target genes through non-homologous end-joining or homology-directed repair mechanisms. After 72 hours of transfection, the positively transduced cells were selected by puromycin (1 µg/mL) treatment. Non-transduced cells served as a reference for puromycin effectiveness. Typically, after seven days of puromycin selection, all control cells had died. The transduced cells were then diluted for single-cell clones in a 96-well U-bottom plate to establish a genetic homogenous KO cell line. After two weeks of cell growth, wells containing single cells were transferred into small cell culture flasks. Once the cell amount was sufficient, the cells were tested via western blot analysis to confirm the success of the KO.

Positive clones in the western blot were then also verified via sequencing of the KO gene region.

2.2.5 PEI Transfection

Transfection is the process of introducing free, soluble DNA into eukaryotic cells. The current study employed a transfection agent, specifically the synthetic polymer polyethylenimine (PEI) (Table 3). PEI compresses DNA into positively charged particles which interact with the negatively charged cell membranes. This interaction leads to endocytosis of the DNA:PEI complex by the cells, thereby releasing the DNA into the cytoplasm.[137]

The desired plasmid/s and the PEI were taken separately from each other in equal volumes of DMEM and allowed to stand for 5 minutes to homogenize the solutions. The PEI was used in a ratio of 2.5: 1 (w/w) to DNA. Subsequently, the two solutions were combined to form a transfection mixture, which was inverted several times and incubated for 15-20 minutes at room temperature to form particles. The transfection mixture was then added to the cells and removed at the latest 24 hours after transfection.

2.2.6 Virus Production and Infections

Virus stocks were produced by transfecting 293T cells with PEI, followed by a change of medium 24 hours later, and collecting the virus-containing media 48-72 hours post-transfection. The media was then filtered and layered carefully on top of a sucrose cushion (Table 5). The virus was concentrated by ultracentrifugation at 4°C, using a relative centrifugal force (RCF) of 133.900 × g for 3 hours. The concentrated virus was then aliquoted and frozen at -80°C for future use.

Infections were carried out by simply adding the concentrated virus supernatants to the medium, followed by spinoculation[138] at RCF of 1200 × g for 1 hour at 25 °C. Infectious units were determined on TZM-bl cells followed by X-gal staining (section 2.5.4). In the case of GFP viruses, infectious units were also quantified on 293T cells by flow cytometry (section 2.2.3). For luciferase reporter gene-containing viruses, infectious units were relatively quantified via a luciferase assay (section 2.5.1). The p24 levels were quantified using enzyme-linked immunosorbent assay (ELISA) (section 2.3.1), and the reverse transcriptase activity was determined through a PERT assay (section 2.4.4).

2.3 Immunological Methods

2.3.1 p24 Capture ELISA

The capture ELISA is a type of broadly used immunological ELISA method for detecting and quantifying specific proteins or molecules in a sample. The process involves the use of two

antibodies, one that is immobilized on a solid support and another that is linked to a peptide. ELISA utilizes the specific binding of an antibody to its antigen, followed by detection through an enzymatic reaction.

B. Sanders-Beer et al. established the p24-Capture ELISA protocol used in this thesis, and the ELISA was performed using the same materials according to their established protocol [133] (Table 2). The process starts with p24 monoclonal antibody AG.30 is immobilized onto a 96-well polystyrene ELISA plate with high protein binding capacity. The plate is then blocked using the blocking buffer to prevent non-specific binding of other proteins. Viral lysates are added to the AG3.0-coated plate, where the p24 antigen specifically binds. Next, a selected pool of HIV-1 patient plasma is added, and the bound p24 antigen is detected using a horseradish peroxidase (HRP)-labeled secondary antibody.

The concentration of the samples is quantified based on their optical densities in the linear range of the measured standard curve. Dilutions of the samples were prepared to obtain optical densities falling within this linear range.

2.3.2 Western Blot

The western blot is an immunological method that allows the detection of specific proteins in a complex mixture like cellular lysates via immunological reactions on a membrane.

The western blot process was carried out in the following steps. First, we separated protein lysates by SDS-PAGE based on size (section 2.5.3). We used the wet blotting method with the Mini Trans-Blot® cell (Table 8), following the manufacturer's instructions, to transfer the proteins onto a polyvinylidene difluoride (PVDF) membrane that had been activated by immersion in pure methanol. Electrophoresis was performed at 4°C or with a frozen cold cool pack in the blot tank. A constant current of 200 mA was applied for 60-90 minutes, depending on the protein size. After transfer, we blocked the PVDF membrane with a Blocking Buffer (Table 4) for 1 hour at room temperature. We then incubated the membrane with the primary antibody (Table 2), diluted in WB Wash Buffer (Table 5), for 1-2 hours at room temperature or overnight at 4°C. Then, the membrane was washed three times with WB Wash Buffer and incubated with an IRDye® fluorescent dye-labeled secondary antibody (Table 2) for 45-60 minutes at room temperature. The membrane was washed four times and subsequently scanned in the Odyssey.

2.4 Molecular Biological Methods

2.4.1 Creation of NL4.3 Mutated Lentiviral Constructs

Mutations were introduced into the lentiviral vector of the HIV-1 NL.4.3 construct by altering point mutations in an insert of the full-length molecular clone. This was achieved using a

combination of mutagenesis PCR, followed by a two-step PCR (2.4.4). The resulting insert carrying the mutation was then cloned into the same backbone of the full-length molecular clone. First, two overlapping PCR amplicons were generated through mutagenesis PCR with the following cycling parameters: 98°C for 30 seconds, followed by 30 cycles of 98°C for 10 seconds, 58°C for 30 seconds, and 72°C for 2.5 minutes. Next, the PCR products were purified by gel electrophoresis and extraction. Afterwards, PCR was performed using small amounts of the purified PCR amplicons, with the overlapping regions serving as the primer region in the first step. The following cycling parameters were used: 98°C for 30 seconds, followed by 15 cycles of 98°C for 10 seconds, 65°C for 30 seconds, and 72°C for 3 minutes. Since annealing temperatures were determined in advance in touchdown PCR, there was no gradual temperature progression applied. In the second step, the resulting DNA strand was amplified by adding primers with the following cycling parameters: 98°C for 30 seconds, followed by 30 cycles of 98°C for 10 seconds, 58°C for 30 seconds, and 72°C for 3 minutes. After the cycling program, the amplification was completed with a final elongation step of 10 minutes at 72°C.

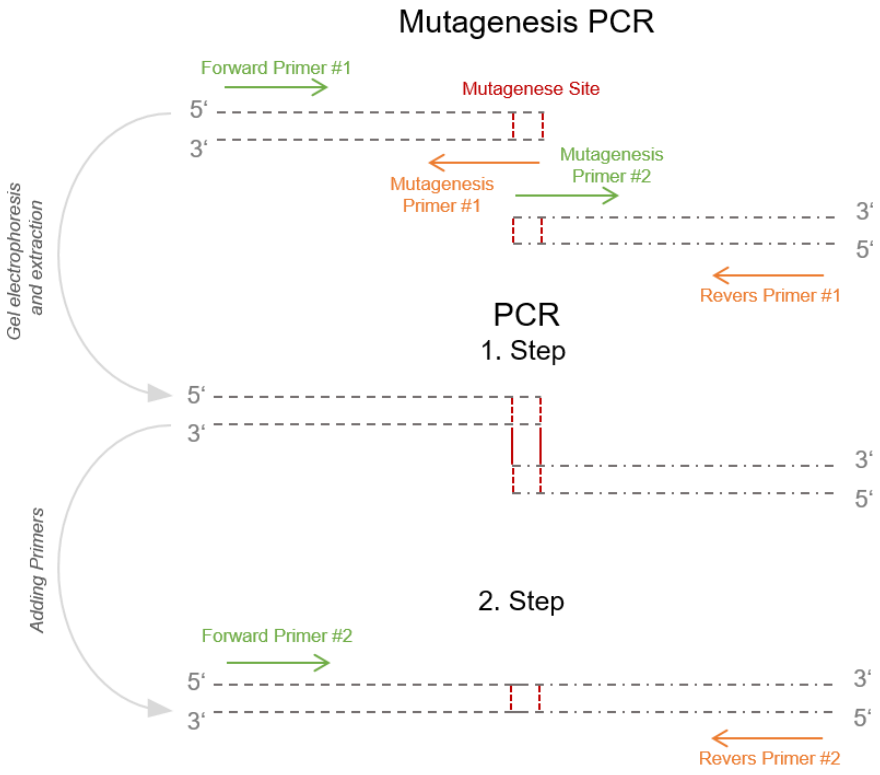

Figure 12: PCR Workflow of NL4.3 Mutant Vector Creation

Schematic showing the PCR workflow of the cloning procedure for NL4.3 mutants. First, mutagenesis PCR was performed to introduce the mutation on two PCR fragments, with the mutagenesis site indicated in red, forward primers binding sites shown in green, and reverse primers in orange. A two-step PCR was used to join the two fragments, with primers added in the second step.

2.4.2 Cloning

Restriction Enzyme Digest

Restriction enzyme digest is a method used to cleave DNA molecules at specific locations using endonucleases, resulting in DNA fragments of predefined sizes.

Two main applications are central to the use of restriction digests. One is the control digest, which is used to verify a plasmid by fragmenting it into expected DNA fragments and analyzing the results via electrophoresis. We typically use 0.5-1 µg of plasmid DNA for control digests at 37°C for 1 hour, followed by heat inactivation of the enzyme as per the manufacturer's recommendations.

The other application is preparative digestion, which represents a crucial step in cloning. In the preparative restriction digest, a selected plasmid serves as the “backbone” of the new vector and is cleaved at a designated section where the new GOI should be inserted. The GOI DNA fragment is amplified via PCR (section 2.4.4) and then cleaved with the same enzymes so that it can be ligated into the resulting gap. We typically perform preparative digestion at 37°C for 3 hours for the backbone and 12 hours for the inserts, followed by heat inactivation of the enzyme according to the manufacturer's recommendations. For the plasmids cloned in this study, we used the FastDigest Green Buffer system and enzymes from ThermoFisher Scientific (Table 4, Table 6).

Ligation

Ligation is a process that allows the joining of two DNA fragments through the formation of a phosphodiester bond.

T4 DNA ligase, LC (1 unit) was utilized to link the free 3'-hydroxy and the 5'-phosphate ends of the insert and vector. To ensure efficient ligation, a 3- or 5-fold molar excess of insert DNA was used relative to the vector DNA, and the DNA concentrations were determined using a NanoDrop™ One spectrophotometer (Table 8).

During the ligation reaction, 50 ng of vector DNA and the excess insert DNA were mixed with T4 DNA ligase in a reaction buffer, and the mixture was incubated at room temperature for two hours to facilitate the ligation reaction. After the ligation reaction, the DNA mixture was transformed into chemically-competent *Escherichia coli* (*E. coli*) cells.

Transformation

Transformation of chemically-competent *E. coli* (Table 14) cells is a process used to transfer and amplify plasmid DNA.

First, the competent cells were thawed on ice and mixed with 5 µL of the ligation product or 10 ng of plasmid DNA. The suspension was then incubated on ice for 10 minutes, followed by heating in a heat block at 42°C for 45 seconds, before being incubated on ice for another two

minutes. Next, 200 µl of pre-warmed S.O.C. medium was added to each batch, and the samples were shaken at 225 rpm and 37°C for one hour. Finally, 50-150 µl of the suspension was plated onto LB ampicillin agar plates and incubated overnight at 37°C in an incubator, placed upside down. This selection allowed the plasmid-bearing clones to be used for plasmid preparation the following day.

Table 14: Bacteria

Bacteria	Supplier
One Shot™ Stbl3™ chemical competent *E. coli*	ThermoFisher Scientific, USA
One Shot™ TOP10™ chemical competent *E. coli*	ThermoFisher Scientific, USA

2.4.3 Nucleic Acid Extraction and Purification

Agarose Gel Electrophoresis

Agarose gel electrophoresis is an analytical separation method used to separate nucleic acid fragments by size through the application of an electrical voltage.

First, 1% (w/v) agarose (Table 3) in 1X TAE buffer (Table 4) was boiled. Ethidium bromide (0,5 µg/mL, Table 3) was added to the gel and then poured into an electrophoresis chamber to harden. The sample was then applied to the gel, and separation was performed at 80-100 V for about 30-60 minutes in 1X TAE buffer. The duration depended on the size of the anticipated bands. During the electrophoresis process, ethidium bromide intercalates with the nucleic acids present in the agarose gel, which changes the excitation spectrum of ethidium bromide and significantly enhances the substance's fluorescence upon excitation with ultraviolet (UV) light. Nucleic acids that have intercalated with ethidium bromide were excited and visualized by the UV light. The intensity of the light emitted is directly proportional to both the concentration of DNA/RNA present and the length of the nucleic acid.

Gel Extraction and PCR Purification

Purification of PCR products after amplification is a crucial step in cloning to remove residual buffers or enzymes that may interfere with downstream applications. Subsequently, the size-separation of amplicons through agarose gel electrophoresis.

PCR purification and gel extraction were performed using QIAGEN or Thermo Fisher kits (Table 7) according to the manufacturers' protocols. Before extraction, the desired nucleic acid band was cut out on a UV table. The purified DNA was eluted in 30 µl of ddH_2O.

Genomic DNA Isolation

QIAGEN QIAamp® DNA Mini Kit (Table 7) was used for the preparation of genomic DNA, following the manufacturer's instructions. The purified DNA was eluted in 200 µl ddH_2O. Samples were stored at -20°C until further use.

Measuring of Nucleic Acid Concentrations

The concentrations of RNA and DNA were determined using a NanoDrop™ (Table 8) spectrophotometer by measuring absorbance at 260 nm. The solvent (e.g. water, buffer) used to dissolve the sample was used as a reference for the measurement.

Plasmid DNA Purification

QIAGEN Plasmid preparation kits (Table 7) were used for the preparation of plasmid DNA, following the manufacturer's instructions. The purified DNA pellet was eluted in ddH_2O. Samples were stored at -20°C until further use.

RNA-Isolation

The QIAGEN RNeasy® Mini Kit (Table 7) was utilized for the preparation of total RNA of cell lysates for RT-qPCR downstream application, following the manufacturer's instructions. The purified RNA was eluted in 30 µl ddH_2O. Samples were stored at -20°C until further use.

TRIzol Extraction

The TRIzol™ Reagent enables the sequential precipitation of RNA, DNA, and proteins from a sample.[139] The manufacturer's instructions for TRIzol™ extraction were followed in order to isolate RNA. After homogenization of the sample with TRIzol™ reagent, chloroform was added to allow separation into three layers. The first layer is a clear upper aqueous phase containing the RNA, followed by an intermediate phase and a red lower organic phase at the bottom containing the DNA and proteins. To the aqueous phase, 10-20 µg/sample of glycogen was added as a carrier. The glycogen co-precipitated with the RNA but did not interfere with subsequent applications. Isopropanol was used to precipitate RNA from the aqueous layer. The precipitated RNA was washed to remove impurities and was then resuspended in 30 µl of ddH_2O for downstream applications.

Viral RNA Isolation

The QIAGEN QIAamp® Viral RNA Mini Kit (Table 7) was used to prepare concentrated virus RNA for downstream RT-qPCR measurement of viral genomic RNA copies, following the manufacturer's instructions. The purified viral RNA was eluted in 60 µl of the AVL buffer provided in the kit. Samples were stored at -20°C until further use

2.4.4 PCR-Methods

Polymerase chain reaction (PCR) is used for the in vitro amplification of a specific DNA segment. In the subsequent sections, the specific PCR methods and primers used during this study are described in detail.

All primers and probes used in this work were manufactured and supplied by Integrated DNA Technologies (Germany).

Mutagenesis PCR

The oligonucleotide-directed mutagenesis (ODM) technique was used in this study as a form of mutagenesis PCR to introduce specific mutations into a vector DNA sequence. This technique uses a synthetic oligonucleotide primer that is designed to hybridize with the DNA template at a specific site. The mutations are introduced by replacing one or more nucleotides in the template with corresponding nucleotides in the primer.

Table 15: Oligonucleotides Used for Mutagenesis PCR

Name	5'-Sequence-3'
NL43 BamHI Rev	GGT GGT AGC TGA AGA GGC AC
NL43 FspAI outFwd	CCC ACT CGG CTT TGC TTT CC
NL43 NheI Fwd	GTA GAG CAA AAT GGA ATG CC
NL43 SalI Fwd	CCA TTT CAG AAT TGG GTG TCG ACA TAG CAG AAT AGG CG
NL43 SalI Fwd2	GGC AGG AGT GGA AGC CAT AAT
NL43 SalI Rev2	TCC TCT GTC GAG TAA CGC CTA
NL43 SpeI2 Rev	TCT CCT ACT GGG ATA GGT GGA
NL43 XhoI outRev	CAC AAG CAG CAT TGT TAG CTG C
pri64_NheI_outRev	CCC CTC CAC AAT TAA AAC TGT GC
delta Gag-Pol Mut55	GGA GAA TTA GAT AAA TGG GAAΔGGC CAG TAA AAA CAG TAC
delta Gag-Pol Mut56	GTA CTG TTT TTA CTG GCCΔTTC CCA TTT ATC TAA TTC TCC
Gag (start codon) Mut7	GAC TAG CGG AGG CTA GAA GGA GAG AG**G** **C**GG GTG CGA GAG CGT CGG TAT TAA GCG
Gag (start codon) Mut8	CGC TTA ATA CCG ACG CTC TCG CAC CC**G** **C**CT CTC TCC TTC TAG CCT CCG CTA GTC
MA-G2A Mut11	GCG GAG GCT AGA AGG AGA GAG ATG **GCT** GCG AGA GCG TCG GTA TTA AGC G
MA-G2A Mut12	CGC TTA ATA CCG ACG CTC TCG C**AG** **C**CA TCT CTC TCC TTC TAG CCT CCG C
RevM10 mutation Mut10	CCT CGT TAC AAT CAA GAG TAA GTC T**CA** **GAT** **C**CG GTG GTA GCT GAA GAG GCA CAG GC
RevM10 mutation Mut9	GCC TGT GCC TCT TCA GCT ACC ACC G**GA** **TCT** **G**AG ACT TAC TCT TGA TTG TAA CGA GG
Tat-M1A Mut13	GTT ACT CGA CAG AGG AGA GCA AGA A**GC** **G**GA GCC AGT AGA TCC TAG ACT AGA G
Tat-M1A Mut14	CTC TAG TCT AGG ATC TAC TGG CTC **CGC** TTC TTG CTC TCC TCT GTC GAG TAA C

Touchdown PCR

Touchdown PCR is a technique that can improve the specificity of PCR reactions. It achieves this by gradually reducing the annealing temperature during a cycling program, typically by 1-2°C every second cycle. The starting annealing temperature is set several degrees higher than the estimated melting temperature (Tm) of the primers to prevent non-specific binding. The annealing temperature is then gradually decreased until it reaches the calculated annealing temperature of the primers, or a few degrees below, which facilitates specific primer binding. The amplification is then continued at this annealing temperature to amplify the target DNA sequence.

Table 16: Oligonucleotides for Touchdown PCR

Name	5'-Sequence-3'
NL43 BamHI Fwd	GGT GGA GAG AGA GAC AGA GAC A
NL43 FspAI Fwd	GCG TTC AGC CAA GGT CTG AAA CTA G
NL43 NheI Rev	CTC CTG AGG ATT GCT TAA AGA
NL43 SalI Rev	CGC CTA TTC TGC TAT GTC GAC ACC CAA TTC TGA AAT GG
NL43 SpeI Rev	TGT TCC TGA AGG GTA CTA GTA GTT CCT GCT ATG TC
NL43 XhoI Rev	GCT ACT TGT GAT TGC TCC ATG T

F-PERT-Assay

The Fluorescent Product-Enhanced Reverse Transcriptase (F-PERT) assay is used to detect and quantify the presence of RT activity. The F-PERT assay is a fluorescence-based method that allows for the real-time monitoring of RT activity during the reverse transcription process.[140] The F-PERT assay was employed to quantify the RT activity per mL of virus production. The primer and probe set, as well as the materials and protocol, were based on the previously published description by *Horie et al*.[141]

Briefly, virus or cell supernatants were added to a pre-cooled 96-well plate containing a 1: 1 mixture of disruption buffer (Table 5), RNase (0.8 U/µl), and lysed for 10 minutes at room temperature. The lysis was stopped by adding 9: 1 ratio of ddH_2O. The RT standard consisted of 12 dilutions of the HIV-1 rRT Standard Lenti from the Cavidi kit (Table 7), which were prepared according to the manufacturer's protocol. Next, 9 µl of the lysate was added to the 11 µl RT-master mix (2x SensiFast MM, Horie primer (500 nM) and probe (250 nM), and 1.5 ng MS2 RNA; Table 4, Table 17, Table 3). Real-time PCR was performed in a CFX96™ Real-Time System (Table 8) using the following parameters: 95 °C for 10 minutes, followed by 45 cycles of 94 °C for 30 seconds and 64 °C for 1 minute.

Table 17: Oligonucleotides for F-PERT-Assay

Name	5'- Dye/Sequence-3'
Horie2010_PERT-F	TCC TGC TCA ACT TCC TGT CGA G
Horie2010_PERT-R	CAC AGG TCA AAC CTC CTA GGA ATG
Horie_Probe	**FAM**-TCT TTA GCG AGA CGC TAC CAT GGC TA

HIV-1 qPCR

Malnati et al. described and established a qPCR assay targeting a conserved region of the HIV-1 genome that is present in all group-M HIV-1 subtypes, including subtypes A, B, C, D, F, G, H, J and K, marking it a universal assay capable of detecting and qualifying all major subtypes of group-M HIV-1.[142] We utilized this qPCR, referred to as the "HIV-1 qPCR," to quantify the genomic copies of our produced viruses or to determine the amount of integrated provirus in infected cells. The wild-type (WT) $NL4.3_{GFP}$ and $NL4.3_{Luc}$-plasmid DNA (Table 9) used as a standard in our experiments. The corresponding copy numbers were calculated by

determining the number of molecules/weight (10 ng $NL4.3_{Luc}$ ≈ 565.928.271,4 molecules/10 ng; $NL4.3_{GFP}$ ≈ 633.332.874,2 molecules).

Table 18: Oligonucleotides for HIV-1 qPCR

Name	5'- Dye/Sequence-3'
CCR5-F (h)	ATG ATT CCT GGG AGA GAC GC
CCR5-P (h)	**VIC**-AAC ACA GCC ACC ACC CAA GTG ATC A
CCR5-R (h)	AGC CAG GAC GGT CAC CTT
HIV1-Malnati-For	TAC TGA CGC TCT CGC ACC
HIV1-Malnati-Probe	**FAM**-CTC TCT CCT TCT AGC CTC
HIV1-Malnati-Rev	TCT CGA CGC AGG ACT CG

Real-Time PCR (qPCR)

In real-time PCR or quantitative PCR (qPCR), the amplification process is continuously monitored during each amplification cycle, allowing for the measurement of the amount of amplified DNA or RNA in real-time. This is achieved using a fluorescent probe (Taqman®) or a DNA-binding dye (SYBR) that emits fluorescence when it binds to the amplified DNA or RNA. The emitted fluorescence is measured after each cycle, providing a quantification of the target DNA or RNA molecules in the sample without the need for post-amplification analysis.

The qPCRs were performed using the SensiFAST™ SYBR or Probe Kits (Table 7) with a duplex probe approach (FAM/HEX) carried out in the CFX96™ Real-Time System (Table 8), following the manufacturer's recommendations. Primers were used at a final concentration of 500 pmol, and probes at 125 pmol. The underlined primers were excluded for qPCRs with SYBR Green (Table 19). 3 µl of genomic DNA and for reverse transcription-qPCR (RT-qPCR), 2.5-3 µl of cDNA were used as templates. The cycle threshold (Ct) value for each sample was automatically calculated using the CFX Maestro Software (Table 11). Subsequently, the evaluation data and determination of the ΔΔCt value and fold change value were performed using Excel. The calculation followed the method published by the ΔΔCt method[143] as described below:

$$\Delta \boldsymbol{C_T}(\boldsymbol{target\ or\ control\ sample}) = C_T(gene\ of\ interest) - C_T(housekeeping\ gene)$$

$$\Delta\Delta \boldsymbol{C_T} = \Delta C_T(target\ sample - \Delta C_T(control\ sample)$$

$$\boldsymbol{Fold\ change} = 2^{-\Delta\Delta C_T}$$

Table 19: Oligonucleotides for SYBR Green or Taqman® Probe qPCR

Name	5'- Dye/Sequence-3'
CXCL10 Prob Hu	**FAM**-TGC CAT TCT GAT TTG CTG CC
CXCL10-F	TGG CAT TCA AGG AGT ACC TC
CXCL10-F Taq Hu	GAA CCT CCA GTC TCA GCA CC
CXCL10-R	TTG TAG CAA TGA TCT CAA CAC G
CXCL10-R Taq Hu	GCT GAT GCA GGT ACA GCG TA
HPRT-probe (h)	**HEX**-AGT GAT AGA TCC ATT CCT ATG ACT GT
HPRT-R (h)	TTA TGT CCC CTG TTG ACT GGT
HRPT-F (h)	TCT TTG CTG ACC TGC TGG ATT
IFI27-F	GGC AGC CTT GTG GCT ACT CT
IFI27-R	ATG GAG CCC AGG ATG AAC TTG
IFI44L-F	GTA TAG CAT ATG TGG CCT TGC TTA CT
IFI44L-R	ATG ACC CGG CTT TGA GAA GTC
IFIT1-F	AAC AGG TTT TCG CAA TCA GGC
IFIT1-probe	**FAM**-AGA TTG CCT CCT CCC TGG AA
IFIT1-R	GCT CCA GAC TAT CCT TGA CCT G
IFIT2-F	AAC AGC TGA GAA TTG CAC TGC
IFIT2-probe	**FAM**-TTC CTT GGA GAG CAG CCT AC
IFIT2-R	GCC AGT AGG TTG CAC ATT GTG
IFNB1-F	TTG ACA TCC CTG AGG AGA TTA AGC
IFNB1-P	**HEX**-CCA GAA GGA GGA CGC CGC ATT GAC C
IFNB1-R	TTA GCC AGG AGG TTC TCA ACA ATA G
ISG15-F	ACT CAT CTT TGC CAG TAC AGG AG
ISG15-R	CAG CAT CTT CAC CGT CAG GTC
MX1-F	ATC CTG GGA TTT TGG GGC TT
MX1-R	CCG CTT GTC GCT GGT GTC G
Viperin Prob Hu	**HEX**-TCG CTA TCT CCT GTG ACA GC
Viperin-F	TGG GTG CTT ACA CCT GCT G
Viperin-F Taq Hu	CGT GAG CAT CGT GAG CAA TG
Viperin-R	GAA GTG ATA GTT GAC GCT GGT T
Viperin-R Taq Hu	TCT TCT TTC CTT GGC CAC GG

RT-PCR

Reverse Transcription PCR (RT-PCR) involves the conversion of RNA into cDNA using a reverse transcriptase enzyme, followed by amplification through PCR. In this study, we utilized the SuperScript™ III First-Strand Synthesis System for RT of RNA isolates which was used for following ISG transcription analysis by qPCR. For all other RT reactions, the RevertAid RT Reverse Transcription Kit was utilized. The reaction conditions and PCR protocols were carried out following the manufacturer's instructions.

Sequencing

The BigDye™ Terminator v3.1 Cycle Sequencing Kit was utilized for Sanger sequencing with the following primers (10 pmol/µl, Table 20). 100-300 ng of vector DNA was used as the initial template for sequencing. After the sequencing reaction was completed, the sequencing department at the Robert Koch Institute performed an analysis of the sequencing reaction and

provided the sequence results in AB1-data format. Subsequently, the sequencing results underwent further analysis using the Geneious Prime software (Table 11).

Table 20: Oligonucleotides for Sequencing

Name	5'-Sequence-3'
1SeqFor_#1MAVS KO	GGG CCA TAT TAA TCC AAG GCT
2SeqRev_#1MAVS KO	CCC TCC CTC TCT CCT CCT TC
3SeqFor_#2MAVS KO	GAG AGG AAA AAG CGG AGA GAA
4SeqRev_#2MAVS KO	CCC ACA CCA TGT TCT CCA GG
MAVS gRNA-1a	AGT ACT TCA TTG CGG CAC TG
MAVS gRNA-1b	ACT GGA GCA GAT GAT AGG CT
neoCMVF	CGC AAA TGG GCG GTA GGC GTG
seq16-4658F	TAG CAG GAA GAT GGC CAG TA
seq18-5675F	GAC AGA TGG AAC AAG CCC CAG
seq22-10234R	GAT GGG AGG GGC ATA CAT TGC
seq23-8232F	GCA GGA AGC ACT ATG GGC GC
seq25-8830F	CGA GGG GAC CCG ACA GGC C
seq7-3347F	TAG CAG TGG CGC CCG AAC AG

2.5 Protein Biochemistry Methods

2.5.1 Luciferase Reporter and SEAP Assay

The luciferase reporter assay represents a method in molecular biology for studying gene expression, promoter activity, and protein-protein interactions. It involves fusing the luciferase gene to the GOI, followed by measuring the amount of luciferase activity produced by the cells. Luciferase is an enzyme that catalyzes the oxidation of luciferin to produce light, allowing the measurement of gene expression or promoter activity in real-time.

The secreted alkaline phosphatase (SEAP) assay is in many ways comparable to the luciferase assay, as it represents a biochemical method to detect and quantify the activity of a reporter gene. Compared to intracellular reporters like firefly luciferase, SEAP as well as the Lucia luciferase has the advantage of being secreted from cells into the culture medium.

Firefly Luciferase

The assay was performed using the luciferase assay kit (Table 7). 72 hours after infection with a luciferase reporter virus, the cells were washed with PBS and lysed with 25 µl of the 1x passive lysis buffer included in the kit for 10 minutes at room temperature. 2-20 µl of the lysate was then transferred into a white, opaque 96-well luminometer plate. The measurement of relative light units (RLU) was performed using the LUMIstar OMEGA plate reader (Table 8). The automated measurement program proceeded as follows: injection of 50 µl of the luciferase substrate (Table 7), a delay of 1 second, and a measurement time of 6 s/well.

Lucia Luciferase

Lucia luciferase assays were performed exclusively with THP-1-Dual™ cells, which feature the Lucia gene. These cells secrete a luciferase reporter gene that is under the control of an ISG54 minimal promoter in combination with five IFN-stimulated response elements. The assays were performed in accordance with the specifications provided by the manufacturer.

At the designated time points throughout the experiment, 20 µl of the THP-1-Dual™ cell supernatants were collected and transferred into a 96-well luminometer plate. Then, 50 µl of QUANTI-Luc™ substrate (Table 4) was injected into the plate and the resulting mixture was measured using the LUMIstar OMEGA, as described previously.

SEAP

SEAP assays were carried out using THP-1-Dual™ and HEK-Blue™ IFN-α/β Reporter cells, which contain a SEAP reporter gene. The THP-1-Dual™ cells secrete the reporter gene that is governed by an IFN-β minimal promoter fused to five copies of the NF-κB consensus transcriptional response element, while the HEK-Blue™ IFN-α/β Reporter cells regulate the SEAP reporter gene using the IFN-α/β inducible ISG54 promoter.

The levels of SEAP in the supernatant were evaluated using QUANTI-Blue™ solution (Table 4). In the presence of SEAP, the color of QUANTI-Blue™ changes from pink to purple/blue, and the intensity of the purple/blue color reflects the activity of SEAP. The levels of SEAP can be determined quantitatively by using a spectrophotometer at 620-655 nm.

At the designated time points during the experiment, 20 µl of the THP1-Dual™ or HEK-Blue™ IFN-α/β Reporter cell supernatants were collected and mixed with 100 µl of QUANTI-Blue™ in a clear, flat-bottom 96-well plate. The mixture was then incubated for 15-120 minutes at 37°C before measuring the optical density (OD) using the microplate reader Multiskan Go (Table 8).

2.5.2 Protein Sample Preparation

Determination of Protein Concentration

The protein concentration of the lysates was determined using the BCA assay following the manufacturer's protocol. The Pierce BCA Protein Assay Kit (Table 7) was used, and the protocol provided by the manufacturer was followed.

Western Blot Lysate Preparation

To extract proteins from cells, either the NP-40 or the RIPA lysis buffers (Table 5) were used, depending on the protein being investigated. For phosphorylated proteins, the RIPA buffer was used to ensure complete lysis of cells, including the nucleus. Prior to lysis, 1-2 million cells were washed with PBS. Adherent cells were kept in wells, and suspension cells were pelleted before lysis. Lysis was then performed using 15-100 µl of lysis buffer for 15-60 minutes at 4°C. Adherent cells were then scraped off using a cell scraper. The lysate was sonicated for 30

seconds on ice using the Sartorius Labsonic M (50-watt, 0.7 seconds continuous action, Table 8) to prevent DNA clumping. The lysate was then centrifuged in a centrifuge at 16,100 × g for 15 minutes at 4°C, and the supernatant was stored at -20°C until further use.

2.5.3 SDS-PAGE

Sodium dodecyl sulfate polyacrylamide gel electrophoresis (SDS-PAGE) is a widely used laboratory technique for separating proteins based on their size. This method involves denaturing the proteins with SDS and separating them in a polyacrylamide gel matrix through an electric field.

In this study, we performed SDS-PAGE using gradient gels (4-20%, Table 8) or hand-cast polyacrylamide gels. The hand-cast gels were prepared by mixing acrylamide/bis-acrylamide solution (30%) and a polymerization initiator (APS+TEMED) with a buffer solution (Table 5). The gels were cast between two glass plates with a 10 or 15 well-comb inserted to create wells for loading the protein sample (Table 8).

The protein lysates were prepared for running by mixing them with the WB Sample Buffer (Table 5) at a ratio of 1: 4 and then boiling at 95°C for 5-10 minutes to denature the proteins. Loading and electrophoresis involved adding the protein sample to the wells along with 5 µl of the PageRuler™ ladder in a well (Table 6). An electric field with a voltage of 120-150V was then applied for 60-120 minutes to the gel to separate the proteins based on their size. Subsequently, the proteins were blotted on a membrane (western blot; 2.3.2).

2.5.4 β-Gal Staining in TZM-bl Cells

The TZM-bl cells utilized in this study are a type of adherent, HeLa-based cell line. TZM-bl cells have been genetically modified to overexpress the CD4 receptor, as well as the co-receptor CCR5. The CXCR4 receptor is constitutively expressed. Both receptors are used by HIV-1 to enter cells. These cells were originally derived from HeLa cells and are frequently used as an indicator cell platform for HIV-1 research.[144] The TZM-bl cells also contain an HIV Tat-responsive LTR promoter, which activates the expression of beta-galactosidase and firefly luciferase.[145] This allows us to determine the multiplicity of infection (MOI) of produced viruses that have a functional Tat accessory protein, using β-gal staining, which detects the activity of beta-galactosidase and is easily visualized as a blue color resulting from the hydrolysis of X-gal.

In this study, 25.000 TZM-bl cells were plated out in each well of a 96-well plate one day before infection. On the following day, infection was carried out with 1-10 µl of the virus of interest, as previously described. The infection was titrated out on the plate, typically with a 1:3 dilution with eleven dilution steps. 48 hours after infection, β-gal staining was performed.

To prepare for staining, cells were washed with PBS and fixed with 50 µl fixative solution (included in the staining kit) or 0.5% glutaraldehyde in PBS for 10 minutes at room temperature. Cells were then washed twice and incubated with 75 µl of the kit staining solution at 37°C for 30-120 minutes. Infected cells appeared stained, allowing us to determine the MOI of produced viruses that have a functional Tat accessory protein. After staining, the solution was removed, and the cells were overlaid with 75% glycerol for preservation. The cells were then counted and stored at 4°C for further analysis.

3 Results

3.1 Characterization of the Innate Immune Response of MDMs Against HIV-1

Our primary aim was to analyze the innate immune response of MDMs upon HIV-1 infection (Figure 13). The MDMs used in this study were derived from isolated monocytes obtained from different blood donors (*n*=3-6). These monocytes were differentiated into macrophages through treatment with GM-CSF. To accurately determine the timing of the innate immune response in macrophages following HIV-1 infection, we decided to conduct a time-course experiment between 16-72 hours-post infection (hpi) spanning five different conditions. The first two conditions served as control groups, for which no virus was added and no DMSO treatment was administered. The remaining conditions involved infections with HIV-1. Among these, two conditions included drug treatments, while one condition had no drug treatment. The drug treatments consisted of Nevirapine (NVP), an NNRTI, one hour prior to infection to inhibit reverse transcription or Raltegravir (RAL), an INI, to inhibit the integration process of the virus. These treatments aimed to identify the stage of the replication cycle triggering the innate immune response. The MDMs were infected with a vesicular stomatitis virus glycoprotein (VSV-G) pseudotyped HIV-1 green fluorescent protein (GFP) reporter virus (hereafter $NL4.3_{GFP}$) at a MOI of 6. Additionally, the $NL4.3_{GFP}$ virus carries the HIV-2 accessory protein Vpx, which prevents the block of SAMHD1-mediated depletion of extracellular dNTPs by promoting the degradation of the protein.[146] Packaging is mediated through a change of ten amino acids of SIVp6 within the p6 region of *gag* (SIV_{Mac}p6 region).[134]

In the absence of drug treatment, we observed robust infection levels in MDMs, reaching over 50% in three representative donors, depicted in Figure 13A. The measurements were performed through FACS analysis by counting GFP^+ living cells at 72 hpi. In the case of NVP treatment, no GFP signal was observed, as expected. With RAL treatment, a minimal GFP signal remained, which is due to the transcriptional activity of the non-integrated viral DNA in the cell nucleus. We selected the *IFNB1* gene and an ISGs transcription panel, consisting of *IFIT1*, *IFIT2*, *CXCL10*, and *RSAD2* (for full-lengths gene names, see abbreviations list), to serve as a readout for innate immune signaling activation. These genes have been widely studied and documented in the literature as established ISGs that indicate innate immune signaling in MDMs and other immune-responsive cells.[147–156]

Our RT-qPCR measurement of *IFNB1* transcriptional changes (Figure 13B) shows a 10-fold change between 16-24 hpi in the presence of virus infection, regardless of drug treatment. Over time, significant differences of over 100-fold were observed at 72 hpi between conditions

with and without drug treatment compared to the virus-free condition. Neither NVP nor RAL showed any significant differences in *IFNB1* transcriptional levels compared to each other. The same observations were made for the genes in the ISGs transcription panel (Figure 13C). The same result was observed in an infection with RT and IN defective mutants (Supplementary Figure 25A-B).

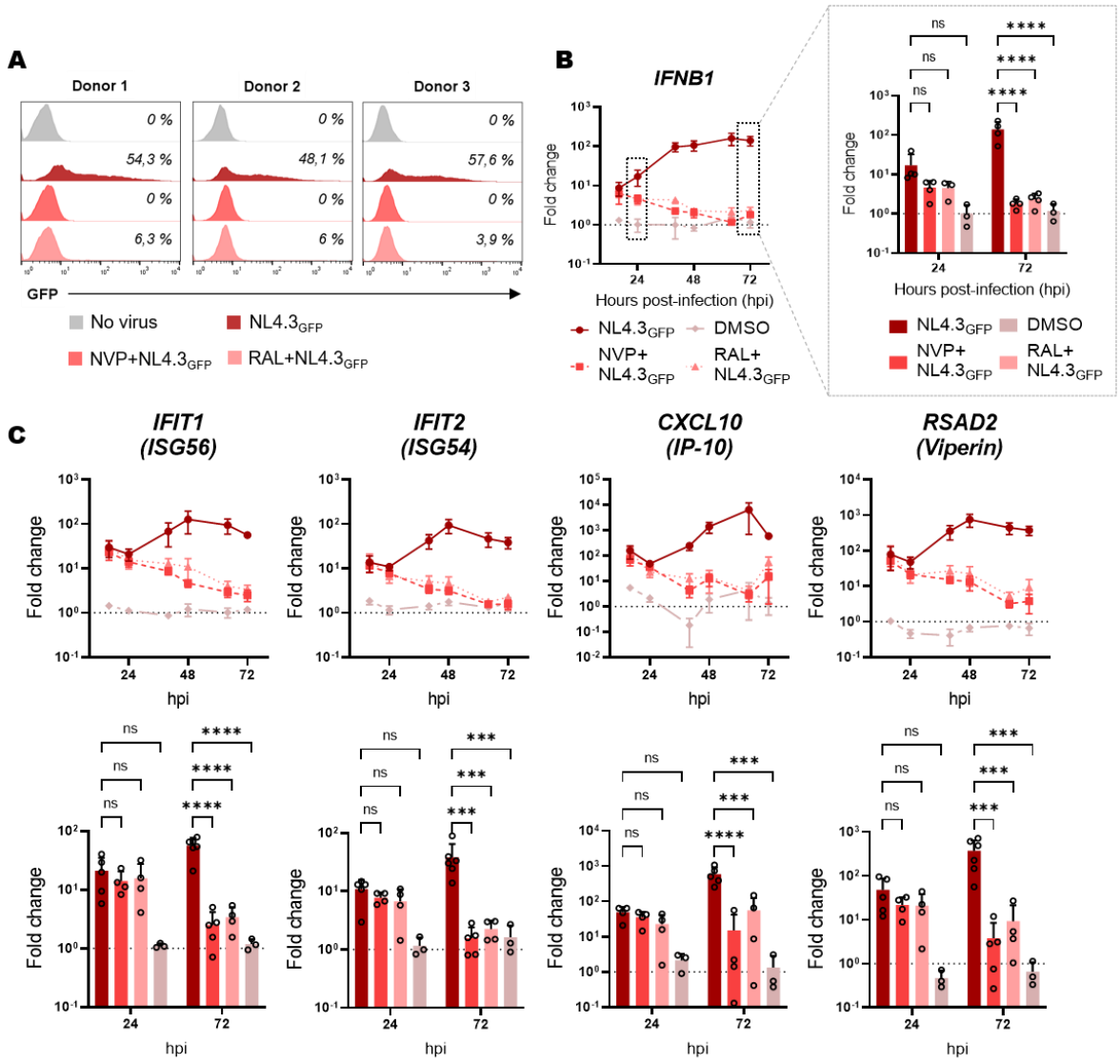

Figure 13: Macrophages Detect HIV-1 in Two Stages of the Virus Infection Cycle

(A) Infection levels of three representative donors infected with HIV-1 single-round GFP reporter virus (NL4.3$_{GFP}$, MOI=6) were harvest 72 hpi and GFP levels analyzed by FACS. **(B)** Temporal fold change gene expression of *IFNB1* of detailed time-course (16-72 hpi) as well as **(C)** *IFIT1*, *IFIT2*, *CXCL10*, and *RSAD2* of infected MDMs from different patient blood-isolated PBMCs (n=3-6) with NL4.3$_{GFP}$ infections (MOI=6) to uninfected cells. Cells were untreated or treated with NVP (10 µM) or RAL (10 µM) one hour before infection and harvested at timepoints as indicated. Gene expression was measured by RT-qPCR. **(B, C)** Dot plots display the means ± SEM, while bar graphs show the means ± SD, with each symbol representing an independent donor. **(B, C)** Two-tailed p-values: two-way mixed ANOVA followed by Tukey post-test, ***p < 0.001, ****p < 0.0001, ns: not significant.

Furthermore, we investigated the activated innate sensing pathways in MDMs in the presence of HIV-1 infection via western blot analysis. We were able to detect latent activation of the JAK-STAT pathway through phosphorylation of STAT1 (Figure 14A). Consistent with our previous observations, increased phosphorylation of STAT1 was detected with increasing duration of infection in NL4.3$_{GFP}$-infected MDMs without drug treatment (Figure 14A). However, the observed intensity of the bands, relative to the $^{+}$Ctrl, did not exhibit as pronounced differences as observed at the transcriptional level of *IFNB1* in infected cells (Figure 14B). Interestingly, no phosphorylation of IRF3, which acts upstream of STAT1, was detected.

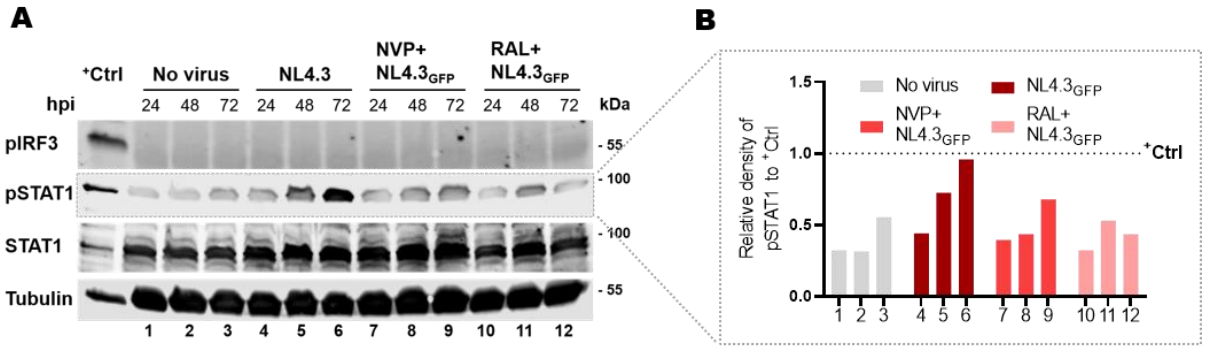

Figure 14: HIV-1 Infection in MDMs Induces STAT1 but Not Upstream IRF3 Phosphorylation

(A) Representative western blot of NL4.3$_{GFP}$ infection (MOI=6) in MDMs showing IRF3-pS386 and STAT1-pS727 phosphorylation as well as STAT1 and α-Tubulin as loading control at time points as indicated **(B)** Relative density of STAT1-pS727 signal to positive control (Lysate of differentiated THP-1 cells 4 hours after transfection with ct-DNA) analyzed with ImageJ. Bands there normalized to STAT1 signal.

In summary, two distinct stages of innate immune signaling in MDMs during HIV-1 infection were observed. The initial stage of detection occurs before reverse transcription takes place, resulting in a comparatively weak innate immune response (observed in NVP-treated cells at 16-24 hpi). In contrast, the second stage triggers a significantly stronger response following the integration of the virus into the host cell genome (compare NL4.3$_{GFP}$ infected cells in the presence vs. absence of RAL at 72 hpi). This phenomenon is further supported by the enhanced activation of the JAK-STAT pathway (Figure 14A), leading to the transcription of ISGs (Figure 13C). Notably, IRF3, which acts in multiple innate sensing pathways upstream of the JAK-STAT pathway, is not activated.

3.2 Macrophage-like Cell Lines as a Model for Studying the Interaction between MDMs and HIV-1 Components

Now that we have provided evidence for two distinct stages of the innate immune response in MDMs in response to HIV-1, we wanted to employ established macrophage-like cell line model systems to investigate interaction between viral and cellular components. We decided to use the human myeloid THP-1 cell line, originally derived from a 1-year-old human male with acute

monocytic leukemia.[157] THP-1 cells differentiate by stimulation with phorbol 12-myristate 13-acetate (PMA) into adherent, macrophage-like cells. These cells are often used in the literature as a possible alternative for macrophages derived from blood monocytes as a cell culture system and are therefore widely used in research of innate immunity.[158–160]

3.2.1 The Phenotype of HIV-1-Infected PMA-Differentiated THP-1 Cells Differs from MDMs

After conducting preliminary experiments to optimize the experimental settings, we initiated time-course experiments in THP-1 cells. Based on our observations in MDMs, we selected 24, 48, and 72 hpi as time points of interest for investigating the innate immune response. Additionally, we changed the MOI to 1.5 and achieved comparable infection levels in MDMs (compare Figure 13A with Figure 15A). One notable finding was that the amount of GFP signal in RAL-treated samples was five times higher than in MDMs, indicating an increased transcription rate of the unintegrated viral genomes. GFP signal with NVP treatment was comparable to the virus-free samples as assumed.

Differentiated THP-1 cells infected with NL4.3$_{GFP}$ exhibited significantly lower gene expression of *IFNB1* and our ISG panel compared to MDMs (compare Figure 13B-C and Figure 15B). For example, after 72 hpi, the expression of *IFNB1* is around 50-fold less in THP-1 cells compared to macrophages. Interestingly, both NVP and RAL treatments in NL4.3$_{GFP}$-infected THP-1 cells had a marginal impact on the detected *IFNB1* and ISG expression compared to infection the absence of drugs (Figure 15B). Notably, we did observe a significant change in the expression level of *RSAD2* only at 72 hpi (Figure 15B). We repeated the time-course experiments in THP-1 cells four times to account for potential variations, but the results remained consistent. Also, in STING or MAVS KO variants of THP-1 cells, no noteworthy changes in ISG expression compared with WT cells were observed (Supplementary Figure 26B)

The results suggest the use of a different sensing pathway or a lack of effective sensing of HIV-1 in differentiated THP-1 cells in comparison to MDMs. Furthermore, we observed that IRF3 phosphorylation was absent in NL4.3$_{GFP}$ infected differentiated THP-1 cells at 16 and 24 hpi (Figure 15C). This finding is in agreement with the results of MDMs experiments (compare Figure 14A and Figure 15C).

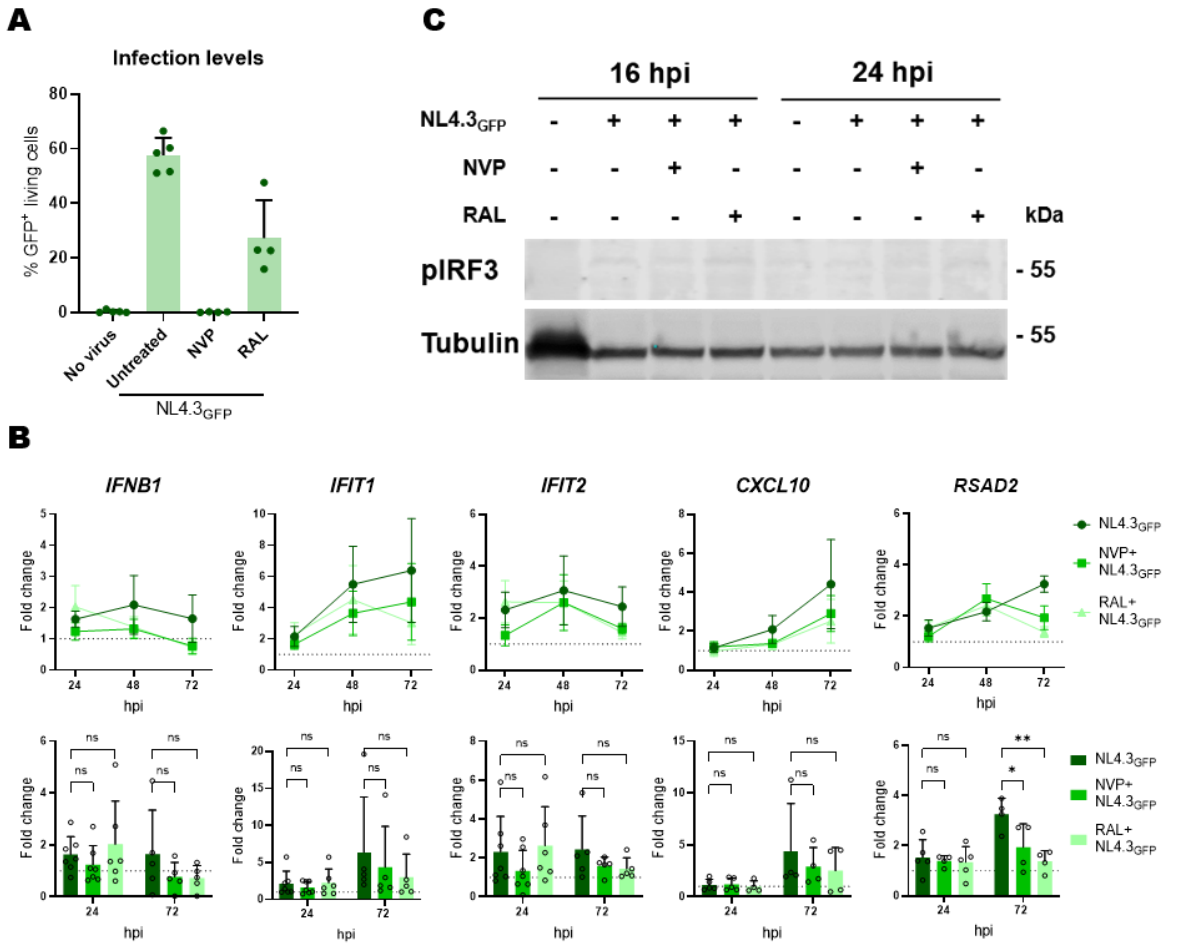

Figure 15: THP-1 Cells Phenotype Against HIV-1 Differs to MDMs

(A) Infection levels of four independent time-courses (24-72 hpi) with PMA (25 ng/mL, 24 h) differentiated THP-1 cells that were infected with NL4.3$_{GFP}$ (MOI=1.5) were harvested 72 hpi and GFP levels analyzed by FACS. The percentage of live/dead cells was determined by FVD-660 staining. **(B)** Temporal fold change gene expression of *IFNB1*, *IFIT1*. *IFIT2*, *CXCL10*, and *RSAD2* in time-course experiments above. Cells were untreated or treated with NVP (10 µM) or RAL (10 µM) one hour before infection and harvested at timepoints as indicated. Gene expression was measured by RT-qPCR. **(C)** Representative western blot of time-course (16 and 24 hpi) showing IRF3-pS386 and α-Tubulin as loading control at time points as indicated. **(A, B)** Dot plots display the means ± SEM, while bar graphs show the means ± SD, with each symbol representing an independent well. **(B)** Two-tailed *p*-values: two-way mixed ANOVA followed by Tukey post-test, **p* < 0.05, ***p* < 0.01, ns: not significant.

3.2.2 U937 Cells Are Highly Immune Competent Against HIV-1

After determining that THP-1 cells were unsuitable for studying the innate immune response due to significant phenotypic differences invoked by the HIV-1 infection, an alternative myeloid cell line, U937, was selected for further study. The U937 cell line is commonly used in the field of innate immune response studies and was initially derived from a histiocytic lymphoma isolate taken from a 37-year-old male patient in 1974.[161] Like THP-1 cells, U937 cells have the ability to differentiate into macrophage-like cells, which can be induced by treatment with PMA.[162,163] Compared to THP-1 cells, U937 cells originate from a more mature tissue state.[159] This

characteristic implies their potential as an alternative cell line model for studying the viral and cellular interactions of HIV-1 infection.

Similar to previous experiments, validation experiments in U937 were conducted before proceeding with the actual time interval experiments. Similar to THP-1 cells, an MOI of 1.5 with $NL4.3_{GFP}$ was found to be sufficient for infecting 50-60% of the U937 cells like in MDMs. Furthermore, approximately 10% of RAL treated cells exhibited GFP signal from non-integrated viral genomes (Figure 16A).

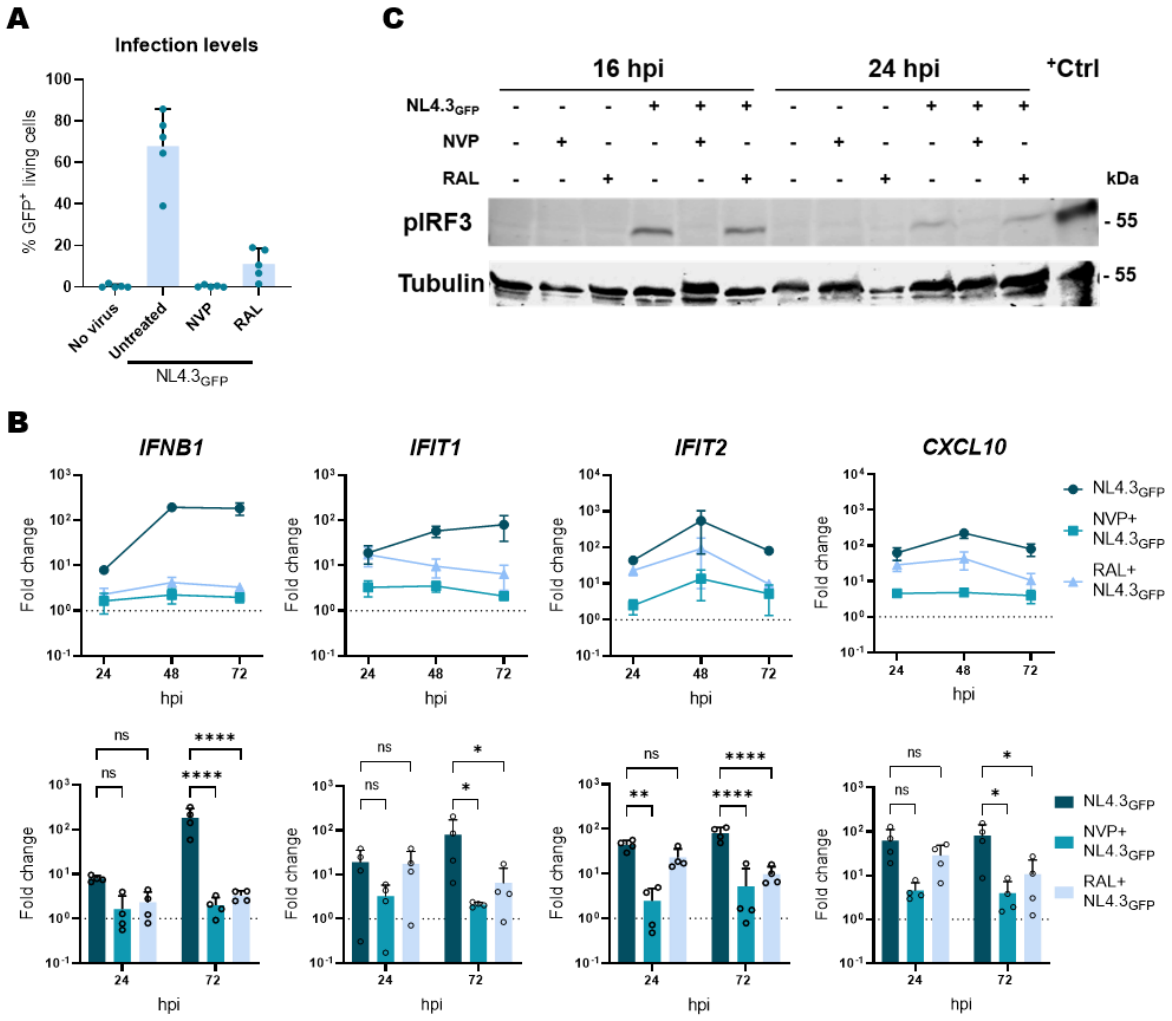

Figure 16: U937 Cells Detected RT-Produces Additionally to Late-Stage Sensing

(A) Infection levels of four independent time-courses (24-72 hpi) with PMA (100 ng/mL, 24 h) differentiated U937 cells that were infected with $NL4.3_{GFP}$ (MOI=1.5) were harvested 72 hpi and GFP levels analyzed by FACS. The percentage of live/dead cells was determined by FVD-660 staining. **(B)** Temporal fold change gene expression of *IFNB1*, *IFIT1*, *IFIT2*, and *CXCL10* in time-course experiments above. Cells were untreated or treated with NVP (10 µM) or RAL (10 µM) one hour before infection and harvested at timepoints as indicated. Gene expression was measured by RT-qPCR. **(C)** Representative western blot of time-course (16 and 24 hpi) showing IRF3-pS386, positive control (Lysate of differentiated THP-1 cells 4 hours after transfection with ct-DNA), and α-Tubulin as loading control at time points as indicated. **(A, B)** Dot plots display the means ± SEM, while bar graphs show the means ± SD, with each symbol representing an independent well. **(B)** Two-tailed *p*-values: two-way mixed ANOVA followed by Tukey post-test, **p* < 0.05, ***p* < 0.01, *****p* < 0.0001, ns: not significant.

Four independent time interval experiments were performed following the design of the previous experiments. Interestingly, a significantly higher immunoreactivity against HIV-1 in *IFNB1* and the chosen ISGs expression panel was observed in differentiated U937 cells compared to THP-1 cells (compare Figure 15B and Figure 16B). One notable finding was the nearly identical expression of measured ISGs in RAL-treated cells after 24 hpi, while this was not the case with NVP-treated cells. This difference was not consistent with the observations made in MDMs (compare Figure 13B and Figure 16B). Moreover, the immune response in RAL-treated cells remained elevated even after 48 hpi and plateaued thereafter. This observation also differs from the results observed in HIV-1-infected MDMs. Additionally, western blot analysis revealed the phosphorylation-mediated activation of IRF3, indicating its involvement in the expression of the ISGs in the innate immune signaling pathway (Figure 16C). This activation was observed in both $NL4.3_{GFP}$ infected cells without drugs and with RAL treatment. However, from 16 hpi to 24 hpi, the intensity of the detected band decreased.

The results suggest that U937 cells identify viral components that are not detected in MDMs. The fact that this occurs at the early-stages of infection and that RAL treatment does not result in a loss or reduction of gene expression, unlike NVP treatment, suggests the involvement of DNA-RNA intermediates or viral cDNA in the detection mechanism within U937 cells. It is worth noting that while U937 and THP-1 cells exhibit phenotypic differences compared to MDMs in response to HIV-1, they also share certain similarities, which underscores the importance of further investigating the cellular determinants of the innate immune response to fully characterize these differences.

3.2.3 Detection of RT-Products is STING-Dependent, but MAVS Plays a Role in Late-Stage Sensing

To further investigate innate immune pathways and cellular determinants in differentiated U937 cells, stable CRISPR/Cas9 KO cell lines were generated for STING and MAVS, which are crucial adaptor proteins for viral DNA and RNA sensing in innate immunity (section 1.1.2). Resulting clones were analyzed by western blot, and KO clones selected for further experiments are illustrated in Figure 17A. Similar levels of infection were achieved in the KO cell lines compared to U937 WT under the same conditions (Figure 17B). The expression of *IFNB1* and ISG genes showed a significant reduction after 72 hpi in both STING and MAVS KO cell lines (compare Figure 17C and Figure 16B). However, the expression of *IFIT2* and *CXCL10* appeared to be more dependent on STING than MAVS. These findings suggest that both adapter proteins play a role in the innate immune recognition of HIV-1 in U937 cells. The western blot analysis demonstrated that the phosphorylation of IRF3 is dependent on STING in U937 cells (Figure 17D). MAVS, on the other hand, seems to not affect IRF3 activation in

U937 cells under HIV-1 infection, as the activation of IRF3 can be detected even in the presence of RAL and without drug treatment (Figure 17D).

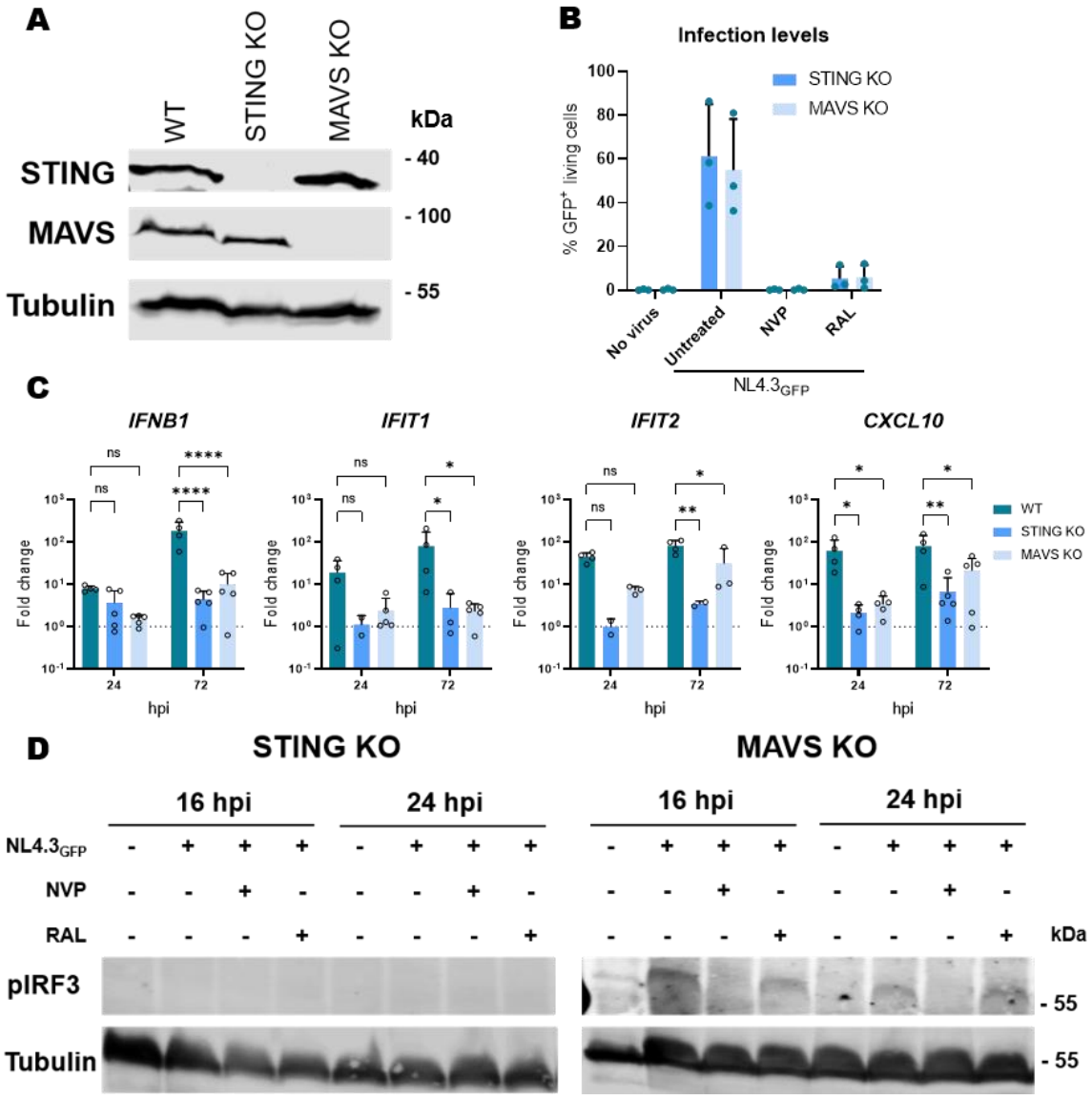

Figure 17: STING and MAVS Are Critical for Sensing HIV-1 Infection in U937 Cells

(A) Western blot of U937 WT, STING, and MAVS KO cells showing STING, MAVS and α-Tubulin as loading control. **(B)** Infection levels of five-time-courses (24-72 hpi) with PMA (100 ng/mL, 24 h) differentiated U937 STING KO and MAVS cells that were infected with NL4.3$_{GFP}$ (MOI=1.5) were harvest 72 hpi and GFP levels analyzed by FACS. The percentage of live/dead cells was determined by FVD-660 staining. **(C)** Temporal fold change gene expression of *IFNB1*, *IFIT1*, *IFIT2*, and *CXCL10* in time-course experiments above. Gene expression was measured by RT-qPCR. **(D)** Representative western blot of time-course (16 and 24 hpi) showing IRF3-pS386 and α-Tubulin as loading control at time points as indicated. **(B, C)** Dot plots display the means ± SEM, while bar graphs show the means ± SD, with each symbol representing an independent well. **(C)** Two-tailed *p*-values: two-way mixed ANOVA followed by Tukey post-test, **p* < 0.05, ***p* < 0.01, *****p* < 0.0001, ns: not significant.

Taken together, these results suggest that U937 cells differentiated by PMA are immunocompetent against HIV-1. They are capable of recognizing RT-products and non-integrated viral DNA. The STING adapter protein is necessary for the signaling pathway and

plays a role in the downstream activation and phosphorylation of IRF3. Additionally, a secondary recognition pathway involving MAVS appears to exist in U937 cells.

Therefore, it can be concluded that U937 cells, due to their ability to detect pre-integrated viral DNA genomes, exhibit a distinct phenotype compared to MDMs in response to HIV-1. However, U937 cells seem to serve as a more suitable model for studying macrophages in the context of HIV-1 infection and detection compared to THP-1 cells. Further investigation is needed to elucidate the specific viral determinants responsible for early detection in MDMs, which will contribute to a clearer understanding of whether U937 cells can be utilized as an appropriate model cell line.

3.3 Finding the Viral Determinants that Induce Innate Response in Macrophages

3.3.1 Early Sensing in MDMs is Dependent on the Viral Capsid

Our previous experiments have shown that the initial response of MDMs to HIV-1 occurs before the reverse transcription process. We speculated that there must be a viral component that triggers this response between the entry of the virus into the cell and its reverse transcription. Previous studies have shown that fusion of virus particle is essential for this early-stage of sensing in MDM.[164]

To investigate this finding further, we focused on the viral capsid and its potential effects on early sensing in MDMs. We tested various known CA mutants, and their different effects on *IFNB1* and ISG expression levels (Figure 18A). One of the mutants, E45A, resulted in a hyperstable CA, while the K203A, P38A, and Q63/67A mutations made the CA hypostable compared to the WT CA core. We also tested a known host cofactor binding mutant, N74D, which disrupts the capsid-CPSF6 interaction.[155] The CA-mutants were engineered to carry a GFP reporter gene. Due to their less efficient virus production, we reduced the MOI to 3, and the virus amount used was normalized to the WT reporter virus using p24 ELISA. During infection, we introduced VLPs containing Vpx in trans, as the CA-mutants were produced without Vpx due to the absence of the SIV_{mac}p6 region, which would result in very low levels of Vpx packaging.[134]

Upon analyzing the MDMs 24 hpi, we made an intriguing discovery. Every single CA-mutant virus-induced higher expression of ISGs compared to the WT virus infection (Figure 18A). This led us to focus on the stability of viral capsid and whether RT-products in CA-mutants might be involved in sensing targets in MDMs, resulting in enhanced gene expressions compared to WT virus. In contrast, U937 cells infected with capsid stability mutants showed a decrease in

IFNB1 and ISG expressions when the cells were treated with NVP. The CPSF6 non-binding mutant also showed a decrease when treated with RAL (Supplementary Figure 26D).

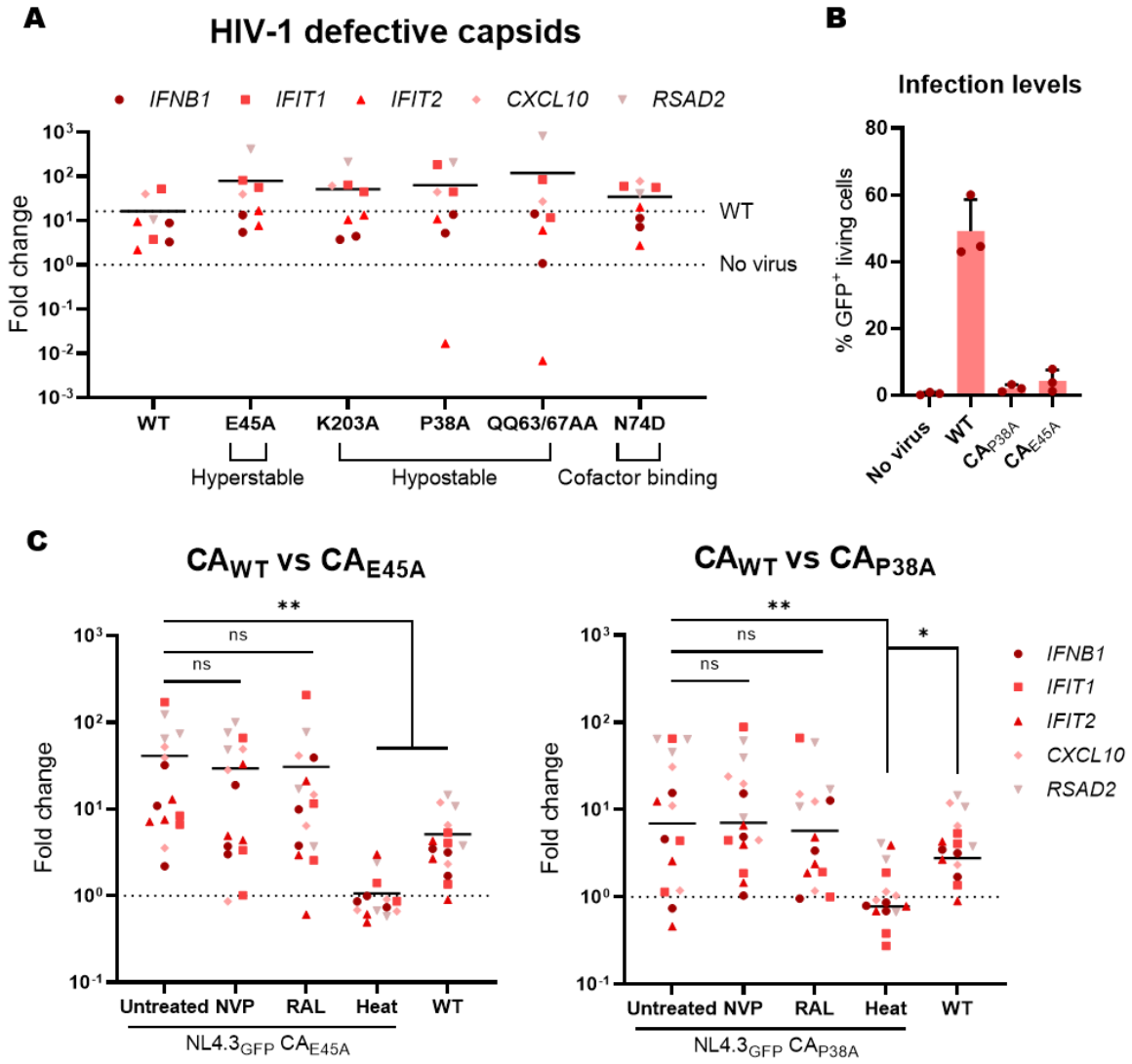

Figure 18: A Change in HIV-1 Capsid Stability Enhances Early-Innate Immune Response in MDMs

(A) Fold change gene expressions of *IFNB1*, *IFIT1*, *IFIT2*, *CXCL10* and *RSAD2* from infected MDMs (n=2) with NL4.3$_{GFP}$ WT-CA or defective-CA (MOI=3) to uninfected cells **(B)** Infectious levels of MDMs (n=3) infected with NL4.3$_{GFP}$ WT-CA or mutant-CA (E45A, P38A; MOI=3). Cells were harvested 72 hpi and analyzed by FACS. The percentage of live/dead cells was determined by FVD-660 staining. **(C)** Comparison of fold change gene expression levels (uninfected) of those infections (B). **(A, B, C)** VLP$_{Vpx}$ were added in trans and viruses were normalized by p24 levels measured via ELISA. **(B)** The means ± SD or **(A, C)** grand means are shown and each symbol represented by the measured expression of a gene 24 hpi or **(B)** donor 72 hpi. **(C)** Two-tailed p-values: two-way ANOVA followed by Tukey post-test, *p < 0.05, **p < 0.01, ns: not significant.

Therefore, we infected MDMs from three individual donors with NL4.3$_{GFP}$, CA$_{E45A}$, and CA$_{P38A}$ GFP reporter viruses. In addition, we treated the cells as before with NVP and RAL. We also tested heat-inactivated CA-mutants. Interestingly, we observed low GFP signals in CA-mutant infected cells by FACS analysis, although the p24 amounts of used viruses were normalized

(Figure 18B). We previously made the same observation during the infection presented in Figure 18A but it was only observed via fluorescence microscopy (Supplementary Figure 25E). Notably, the ISG expression induced by the CA-mutants remained higher than in WT infection, regardless of drug treatments. Heat-inactivated virus did not induce any response at all (Figure 18C).

From these findings, we conclude that RT-products still do not trigger a response in MDMs as suspected previously (section 3.1). Instead, the conformation of the capsid itself appears to play a crucial role in sensing, even when the capsid is more stable. This strongly suggests that the HIV-1 capsid acts as a viral determinant in MDMs, responsible for the observed innate immune sensing at 24 hours post-infection. It is worth noting that the amount of integrated provirus in the CA mutants seems significantly lower than in the case of the WT virus.

Summarizing the results from U937 and MDMs, it becomes evident that early sensing in U937 and MDMs differs in phenotype across both viral and cellular determinants. We have not yet identified a simple and suitable myeloid model cell line to study infected MDMs with HIV-1. Although there are other cell lines like MonoMac6, ML-2, or HL60 cells that could potentially serve as models, our testing of the two most frequently used cell lines, THP-1 and U937, has indicated that neither is suitable for studying cellular and viral determinants in innate immune signaling during HIV-1 infection in MDMs. For this reason, further experiments had to be carried out in MDMs.

3.3.2 Minimal Lentiviral Genome Does Not Induce an Innate Immune Response

Next, our focus was to identify the viral determinants responsible for the robust innate immune response observed between 48 and 72 hpi (Figure 13B-C). Previous experiments indicated that this sensing mechanism occurs after viral integration into the host genome (section 3.1).

To investigate this further, we questioned whether a minimal provirus with only essential genetic elements for integration could still induce a similar expression of our ISG panel. For this purpose, we utilized a GFP reporter lentiviral construct, WPXL (Table 9), which contains minimal genetic elements for viral infection. The construct included the sequence of the woodchuck hepatitis virus posttranscriptional regulatory element (WPRE) to enhance expression. Additionally, it carried the RRE from HIV-1 for gRNA transportation outside of the nucleus, the HIV-1 ψ site for viral gRNA packaging, and the central polypurine tract (cPPT) to enhance transduction efficiency. The vector is driven by the human elongation factor-1α (EF-1α) promoter.

Despite the comparable infection efficiency of MDMs with $WPRE_{GFP}$, there was hardly any stronger mRNA expression of *IFNB1* or ISGs compared to the NVP-treated $NL4.3_{GFP}$ infection

after 72 hpi (Figure 19C). This difference in the innate immune response was evident in both NL4.3$_{GFP}$ infections, whether using a MOI of 3 or 6 (Figure 19C).

Based on these observations, it can be inferred that a viral component within the HIV-1 genome plays a crucial role in triggering the strong immune response following provirus integration. Furthermore, it is evident that a simple lentiviral infection in MDMs does not induce such a pronounced immune response. Additionally, it can be ruled out that the reporter protein GFP is the reason for this induction, as well as the HIV-2 protein Vpx, which was added in trans as VLP during the infection. Nevertheless, Vpx is an essential component to effectively infect MDMs, which is crucial to induce strong expression of *IFNB1* and ISGs during infection of MDMs (Supplementary Figure 25C-D).

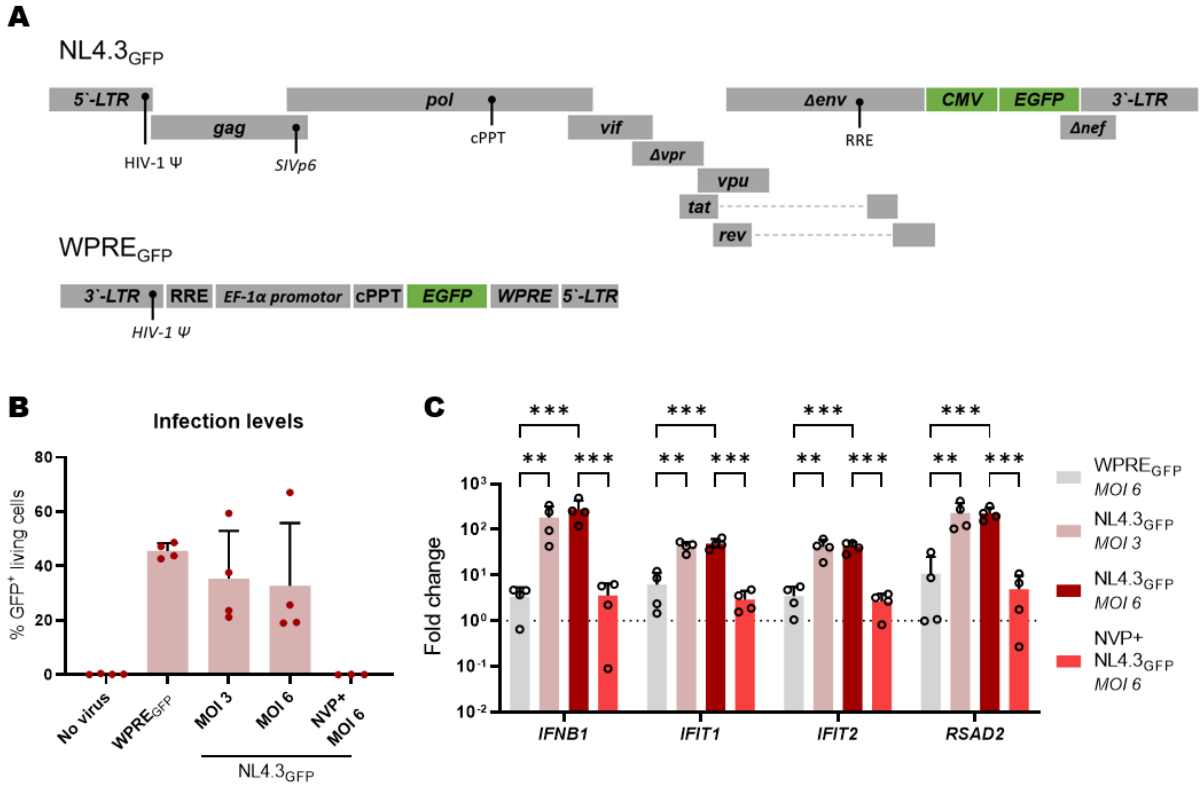

Figure 19: Minimal Lentiviral Genome Differs from HIV-1 Genome Sensing

(A) Schematic genome map of NL4.3$_{GFP}$ and WPRE$_{GFP}$ used in infection experiment in MDMs. **(B)** Infection levels of MDMs (n=4) infected with NL4.3$_{GFP}$ (MOI=3 or 6) or the minimal lentivirus WPRE$_{GFP}$ (MOI=6). Cells their harvested 72 hpi and GFP levels were analyzed by FACS. The percentage of live/dead cells was determined by FVD-660 staining. **(C)** Comparison of fold change gene expression levels (uninfected) of those infections (B). VLP$_{Vpx}$ were added in trans and viruses were normalized by p24 levels measured via ELISA. **(B, C)** The means ± SD are shown, and each symbol representing an independent donor. **(C)** Two-tailed p-values: two-way ANOVA followed by Tukey post-test, $^{**}p < 0.01$, $^{***}p < 0.001$, ns: not significant.

3.3.3 The Nuclear Export of gRNA is Essential for Late-Stage Sensing in MDMs

To explore the pronounced late-stage immune response in MDMs, we adopted a step-by-step approach to examine the virus replication cycle.

Initially, the provirus would produce the first proteins, namely Tat, Rev, and Nef. Subsequently, the accessory proteins and the Gag; Gag/Pol polyprotein would follow, leading to the budding process. Since most of the accessory proteins and Nef are not expressed by our NL4.3$_{GFP}$, following they are not essential for the observed phenotype, our focus shifted to the crucial viral proteins of the replication. Attempts using a pharmacological approach to inhibit later-stages of viral replication would have impacted cellular processes significantly. Therefore, we opted for a less cell-invasive approach.

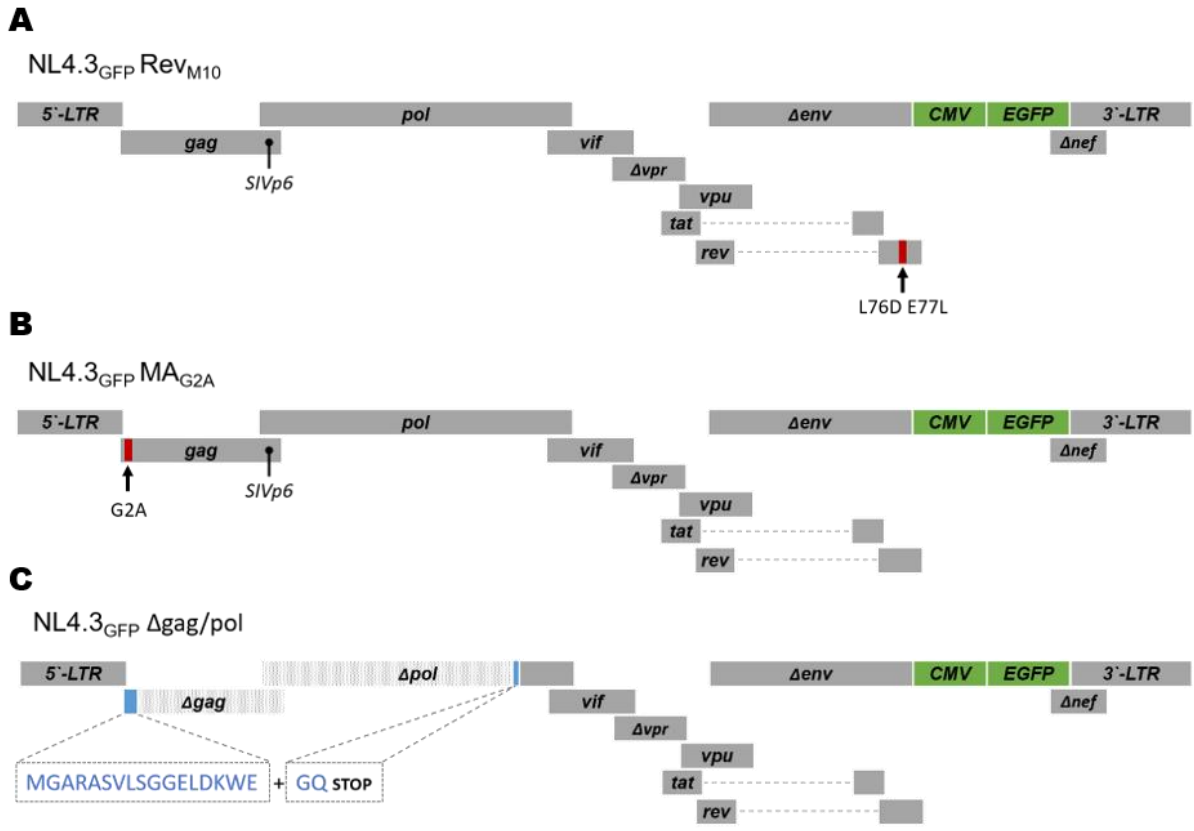

Figure 20: Late-Stage of HIV-1 Defective Mutants

Schematic figure illustrating the generated viral genome mutants using the NL4.3$_{GFP}$ vector. Three distinct mutants were generated: **(A)** Rev$_{M10}$**;** Designed to produce a Rev binding-deficient protein. **(B)** MA$_{G2A}$**;** Engineered to result in a myristoylation-deficient gag/pol-polyprotein. **(C)** Δgag/pol**;** Characterized by a wide deletion in the gag/pol region of the virus. Only the RNA-binding Ψ-side remains, and the shown amino acid sequence (blue) can be expressed.

To determine the specific impact of viral determinants on the immune response, we created mutants that inhibited key replication proteins, thus generating infections that progressed only to particular stages of the HIV-1 replication cycle. This allowed us to individually assess the

role of each viral determinant. Notably, we generated mutants by overlap PCR based on literature findings for Rev[151,165] (Figure 20A), and the myristoylation site of the MA[151,166,167] (Figure 20B). Additionally, we designed a sequence with almost the entire gag/pol region deleted, which still retained the ability to package gRNA (Figure 20C), as well as a Tat mutant where the start codon (M1A) is shifted, resulting in the translation of a non-functioning protein. We introduced the mutations into two different vector systems, one with GFP ($NL4.3_{GFP}$) and the other with a luciferase reporter gene ($NL4.3_{Luc}$; Supplementary Figure 24). The primary difference between these two vector systems is the absence of the *SIVp6* site in $NL4.3_{Luc}$.

The viruses were produced using Tat, Rev, or gag/pol expressing packaging plasmids transfected in trans during virus production to generate infectious viral particles, including the $NL4.3_{GFP}$ Δgag/pol variant (Table 10). However, due to the absence of the SIV_{mac}p6 region in this variant and $NL4.3_{Luc}$, Vpx could not be co-packaged into the virus particles during production.[134] In contrast, Vpx could be co-packaged into the virus particles of other mutants like WT virus particles. Therefore, we initiated our study first by examining the innate immune responses of $NL4.3_{GFP}$, Rev_{M10}, and MA_{G2A} in MDMs.

In infection experiments, varying amounts of GFP^+ cells were observed with fluorescence microscopy when infecting cells with the same p24 amount of virus (Figure 21B). These observations were further validated using FACS analysis (Figure 21A). On average, Rev_{M10} showed more GFP^+ cells, while MA_{G2A} showed fewer GFP^+ cells compared to the WT infection.

To investigate the temporal dynamics of *IFNB1* and ISGs mRNA expression, we monitored their levels over a 24 - 72-hour time interval like in previous experiments (section 3.1, 3.2). Initially, the infections did not exhibit significant differences in their responses (Figure 21C, 24 hpi). However, at 72 hpi, WT infection showed the previously observed increase in *IFNB1* and ISG expression (Figure 13B-C), which did not occur in either mutant (Figure 21C). Notably, both virus mutants demonstrated immune activity beyond that of the heat-inactivated WT control. Moreover, a slightly stronger expression of ISGs was observed in MA_{G2A} compared to the Rev_{M10} mutant, although this difference was not statistically significant. In addition to the $NL4.3_{GFP}$ mutant infection experiments (Figure 21), we also conducted infections with the $NL4.3_{Luc}$ Tat_{M1A} virus. However, we could not detect any significant *IFNB1* or ISG expression compared to uninfected MDMs (Supplementary Figure 27C). Furthermore, as expected, the mutation resulted in a drastic reduction of the Firefly luciferase reporter gene expression (Supplementary Figure 27B).

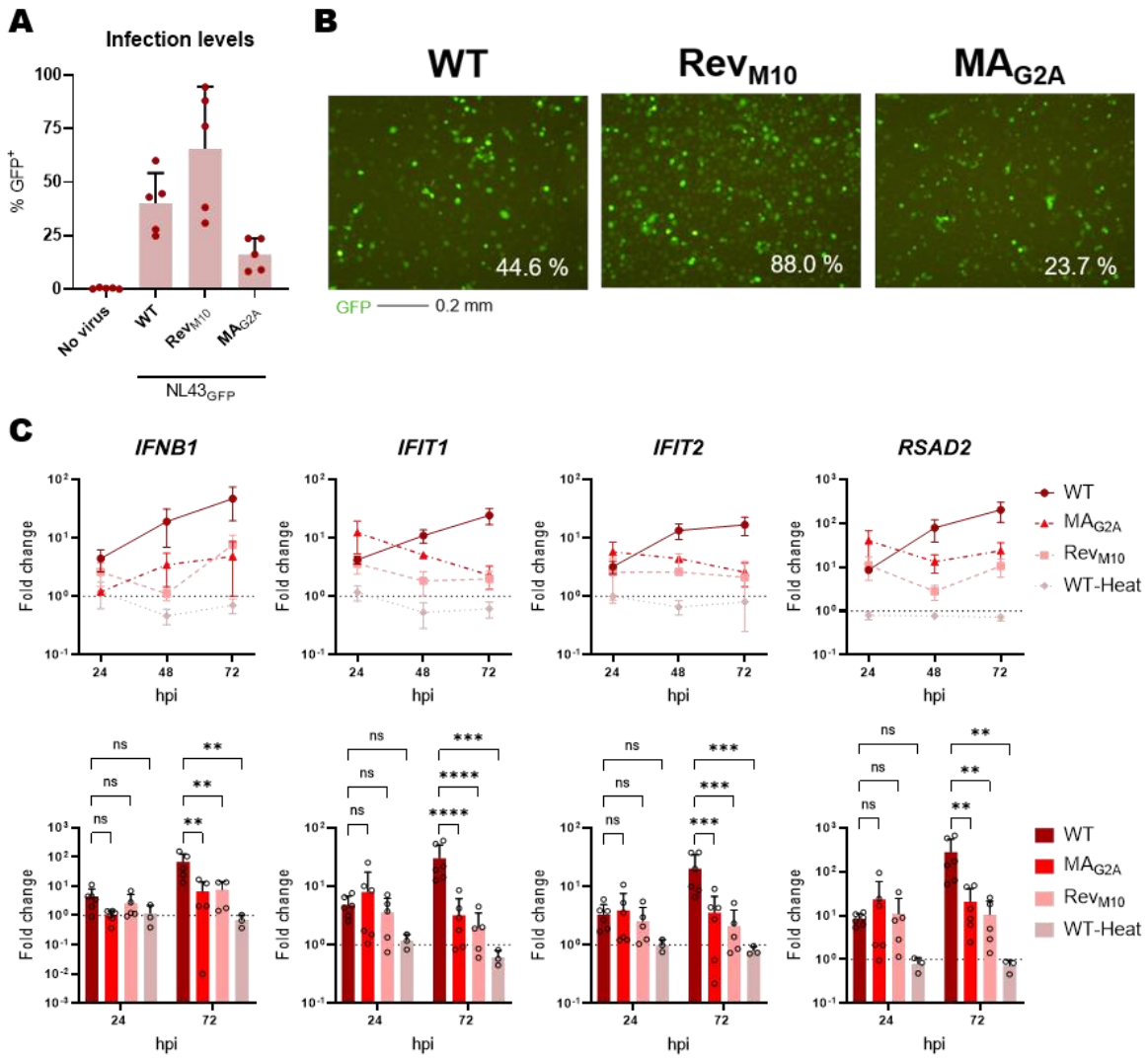

Figure 21: The Nuclear Export of gRNA is Essential for Strong Late-Stage Innate Sensing in HIV-1 Infected MDMs

(A) Infection levels from time-course (24-72 hpi) of MDMs from different donors (*n*=5) infected with NL4.3$_{GFP}$ WT, MA$_{G2A}$, Rev$_{M10}$ virus, or left uninfected as control (MOI=3). After 72 hpi, cells were harvest and GFP$^+$ levels were analyzed by FACS **(B)** Representative fluorescence microscopy images of GFP signals (green) of infected MDMs with different viruses (left to right WT, MA$_{G2A}$, and Rev$_{M10}$) are shown. A scale bar of 0.2 mm is provided under the images and the percentage of GFP$^+$ cells measured by FACS analysis is indicated. **(C)** MDMs (*n*=5) were infected with the viruses mentioned in (A), and cells were also treated with heat-inactivated WT virus (WT-Heat) as a control. Cells were harvest at time points as indicated. The gene expression of *IFNB1*, *IFIT1*, *IFIT2*, and *RSAD2* was measured using RT-qPCR. **(A, C)** Dot plots display the means ± SEM, while bar graphs show the means ± SD, with each symbol representing an independent well. **(C)** Two-tailed *p*-values: two-way mixed ANOVA followed by Tukey post-test, ***p* < 0.01, ****p* < 0.001, *****p* < 0.0001, ns: not significant.

3.3.4 Newly-Produced Gag-Particles Are Not Sensed by MDMs

Next, it was necessary to ensure that the newly produced viral particles resulting from the integrated proviruses did not impact the observed immune response in MDMs. Even in the case of a single-round infection, we expected the production of Gag-particles carrying gRNA, but lacking an envelope, rendering them non-infectious. This approach also enabled us to investigate the likely phenotype of our viral mutants.

To accomplish this, we initiated the experiment by infecting MDMs from two different donors with our HIV-1 WTs and mutants (GFP and Luc; Table 10). Four hours after spinoculation, we washed the cells and replenished them with fresh medium. At 48 and 72 hpi, we collected the supernatants, centrifuged the VLPs present in them, and lysed the cells at each time point. A fraction of the supernatants was used to determine the associated p24 levels using ELISA, while the lysates were subjected to analysis using western blot.

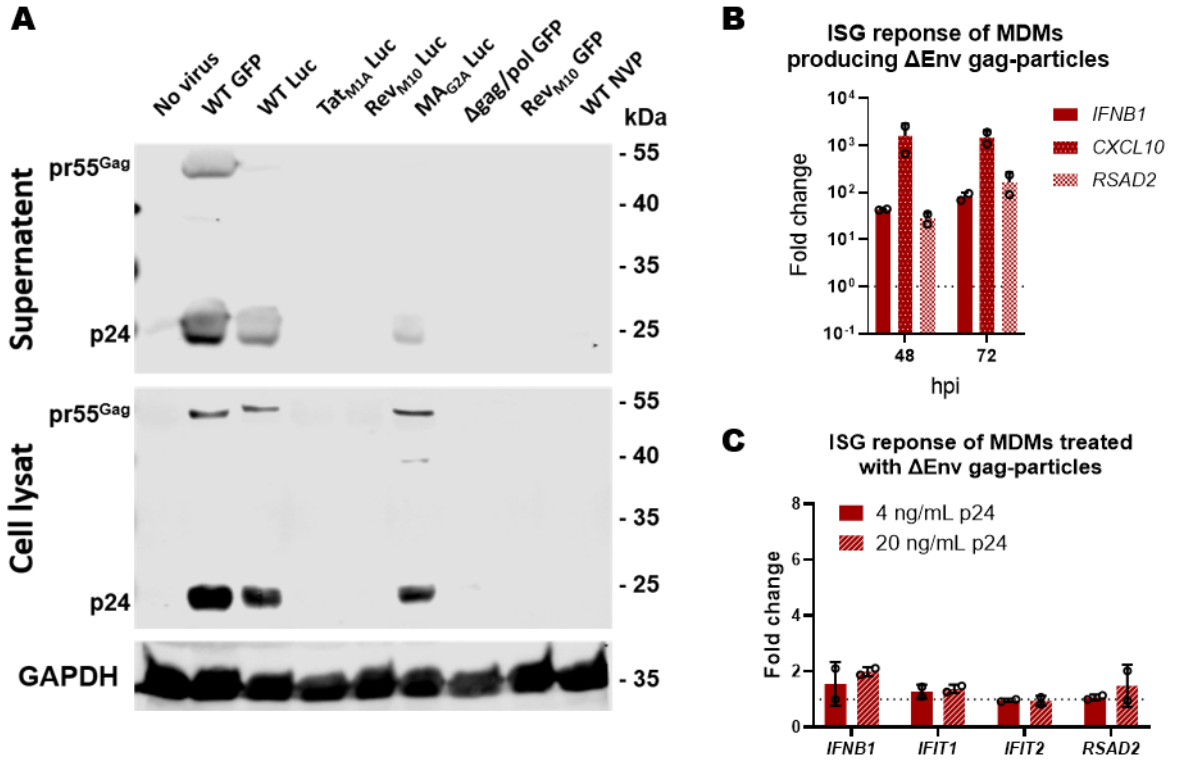

Figure 22: Extracellular ΔEnv Viruses Do Not Induce Innate Immune Activation of MDMs

(A) Western blot of infected MDMs with different NL4.3 GFP or Luc single-round reporter viruses (MOI=3, 72 hpi). Viruses are indicated. The blot showing provirus newly produced ΔEnv viruses from cell lysate or supernatant. Blot is incubated with AG3.0 and α-GAPDH antibodies. **(B)** Temporary fold change gene expression of *IFNB1*, *CXCL10*, and *RSAD2* at indicated time points in infected and ΔEnv viruses producing MDMs (*n*=2). The p24 amount at 48 and 72 hpi was measured via ELISA and **(C)** MDMs (*n*=2) were treated with ΔEnv viruses based on the p24 amount. At 48 hours post-treatment, cells were harvested, and gene expression of *IFNB1*, *IFIT1*, *IFIT2*, and *RSAD2* was measured by RT-qPCR. **(B, C)** The means ± SD are shown and each symbol represents an independent infection in MDMs.

In the western blot analysis, we detected p24 and $Pr55^{Gag}$ of the WT viruses and to our surprise also the MA_{G2A} mutant in both the cell lysate and the supernatant (Figure 22A). The infection of WT viruses showed a comparable expression of *IFNB1* and ISGs (*CXCL10* and *RSAD2*) as observed previously, even after 48 and 72 hpi (compare Figure 21C and Figure 22B). Based on the ELISA results, we determined p24 levels of 4 - 20 ng/mL in the 48 and 72 hpi supernatants (Supplementary Figure 27D). Subsequently, we produced HIV-1 without an envelope (ΔEnv viruses) through transfection, concentrated them, and added p24 amounts of 4 and 20 ng/mL to the MDMs from the same donor used earlier. We then examined *IFNB1* and ISGs expressions 48 hours after the addition and found it to be similar to the untreated control (Figure 22C).

The results of this experiment indicate that only the WT and MA_{G2A} proviruses were capable of producing VLPs in MDMs. Furthermore, these particles did not have any significant effect on the induced innate immune response that we could detect.

3.3.5 Myristoylation is the Major Driver for Enhanced Late-Stage Innate Immune Response in Human MDMs

Having excluded any potential side effects from nascent VLPs, our attention turned towards studying our Δgag/pol viruses. One intriguing aspect of this mutant is its capacity to package gRNA and accurately translate the first 17 amino acids of the gag protein, which includes the myristoylation site. Most residues of the following HBR (14-31 amino acid of MA) site are deleted (18-31 amino acid). To investigate the specific impact of myristoylation, we included the MA_{G2A} mutant in the infection experiment, effectively eliminating the myristoylation site. To distinguish this parameter from the previous infection experiment with the $NL4.3_{GFP}$, and MA_{G2A} we increased the MOI compared to earlier experiments, aiming to potentially observe stronger effects on the immune response. We infected MDMs from three different donors at the same time points.

Under fluorescence microscopy, the infection levels of WT and the MA_{G2A} virus infections showed similarities to previous experiments (compare Figure 21B and Figure 23B), which were further confirmed by FACS analysis (Figure 23A). Additionally, the Δgag/pol mutant exhibited a visually stronger GFP signal saturation within the cells compared to the WT, indicating a potentially higher level of GFP and viral protein expression. However, the number of GFP^+ cells remained similar based on FACS results (Figure 23A).

A surprising finding emerged from the evaluation of RT-qPCR results. We were not able to observe difference in *IFNB1* and ISG expression levels between the WT and the Δgag/pol mutant virus infection (Figure 23C), suggesting that the presence of a complete gag/pol polyprotein is not critical for inducing late-stage innate immune response in MDMs. In contrast,

the MA_{G2A} mutant displayed a similar reduction in *IFNB1* and ISG expression as previously observed (compare Figure 21C with Figure 23C and Figure 27C with Figure 27F). These different transcription levels were also notable compared with the Δgag/pol mutant virus infection (Figure 23C).

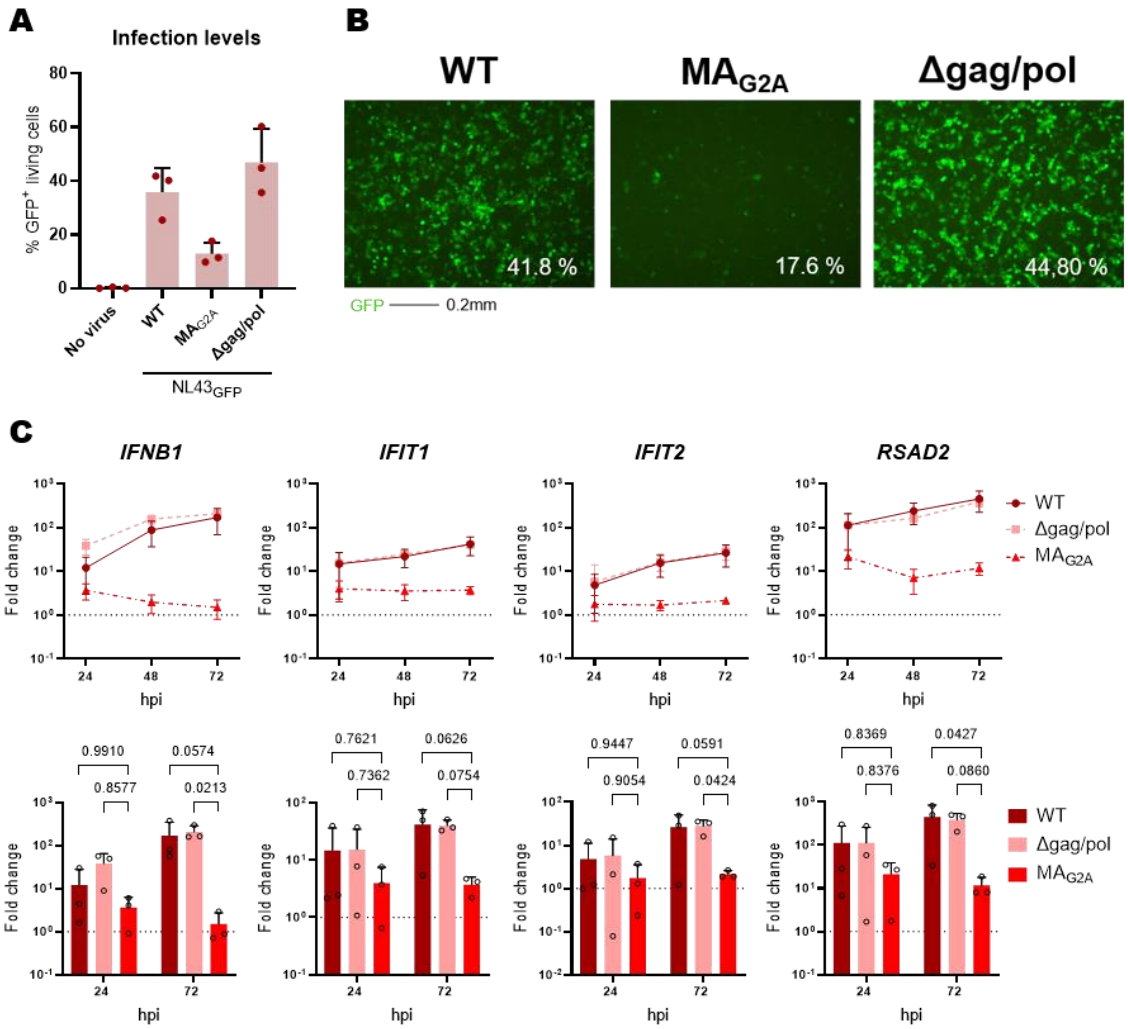

Figure 23: Binding of HIV-1 gRNA to Gag is Not Critical to Induced Late-Stage Sensing in MDMs

(A) Infection levels from time-course (24-72 hpi) of MDMs from different donors (*n*=3) infected with $NL4.3_{GFP}$ WT, MA_{G2A}, Δgag/pol virus, or left uninfected as control (MOI=6). After 72 hpi, cells were harvest and GFP^+ levels were analyzed by FACS. The percentage of live/dead cells was determined by FVD-660 staining. **(B)** Representative fluorescence microscopy images of GFP signals (green) of infected MDMs with different viruses (left to right WT, MA_{G2A}, and Δgag/pol) are shown. A scale bar of 0.2 mm is provided under the images and the percentage of GFP^+ cells measured by FACS analysis is indicated. **(C)** MDMs were infected with the viruses mentioned in (A) and treatment with NVP (10 µM; not shown) as control. Cells were harvested at time points as indicated. The gene expression of *IFNB1*, *IFIT1*, *IFIT2*, and *RSAD2* was measured using RT-qPCR and the fold change is shown (uninfected). **(A, C)** Dot plots display the means ± SEM, while bar graphs show the means ± SD, with each symbol representing an independent well. **(C)** Two-tailed *p*-values: two-way mixed ANOVA followed by Tukey post-test; *p*-values are shown.

Furthermore, the absence of the NC region in the Δgag/pol mutant indicates that the binding of gRNA to the gag/pol polyprotein is not necessary for sensing, highlighting the significance of myristoylation at the $Pr55^{Gag}$ or Gag/Pol as the viral determinant for triggering the late immune response in the virus life cycle in MDMs. The cellular sensing determinants remain to be discussed.

These results indicate that myristoylation at the $Pr55^{Gag}$ protein plays a crucial role as a viral determinant for detecting and triggering late immune responses in the virus life cycle in MDMs. Furthermore, the findings suggest that $Pr55^{Gag}$, Gag/Pol, and packaging of the gRNA into assembling virus particle is not necessary for this response, and the initial MA peptide sequence is sufficient. Conversely, a non-myristoylatable $Pr55^{Gag}$ or Gag/Pol leads to a significantly reduced immune response.

4 Discussion

The primary objective of this thesis was to explore the intricate interplay between cellular and viral components, which induce the innate immune response of macrophages against HIV-1. The research objective is based on understanding the mechanisms behind the inflammation caused by HIV-1 in immune cells, as it likely contributes to the various symptoms observed in long-term HIV infected patients.[119,124,128,131,168,169]

Considerable effort in research has been dedicated to investigate the viral components of HIV-1 and their interactions with cellular factors.[169,170] Much of these efforts focus primarily on $CD4^+$ T cells, given their central role in the HIV infection process, viral latency, and AIDS development.[171–174] However, further studies extend beyond T cells to include myeloid cells, such as DCs and macrophages, which also play an essential role in the immune response to HIV-1.[126,128,175] Monocytes in particular are postulated to facilitate the crossing of the blood-brain barrier during HIV infection, where they eventually persists and mature into resident macrophages.[130,176] This is relevant considering the frequency of neurodegenerative symptoms observed in chronically infected HIV-1 patients, even throughout long-term antiviral therapy and undetectable virus levels. In such instances, inflammation within the CNS has emerged as the likely cause for these symptoms.[121,124,128,177] Intriguingly, despite minimal detectable virus presence within the CNS, inflammation seems to originate from the integrated HIV-1 provirus in CNS-resident cells like macrophages.[128,151,152]

Considering these findings, a study of the innate immune response that is induced by HIV-1-infected macrophages becomes a key for further investigation. This research potentially reveals the determinants that fuel the inflammation observed within the central nervous system of chronically infected HIV-1 patients.[127,128] The exact mechanisms of inflammation have not yet been clarified and are therefore of great interest. Identifying critical determinants of inflammation, whether they are of cellular or viral origin, therefore remains essential. Such findings are needed to formulate precise therapeutic strategies aimed at containing and alleviating the inflammation triggered by the virus. This thesis and the presented research within therefore aim to contribute towards gaining these additional vital insights into HIV and immunological research.

4.1 Two Stages of HIV-1 Innate Immune Sensing in Macrophages

Our objective was to establish a baseline understanding of the innate immune response in MDMs against HIV-1. Since HIV-1 is known to be a poor inducer of the innate immune system,[178] we infected the MDMs with a high viral load (MOI 6) in order to maximize the chances of triggering a response. Samples treated with NVP, an RT inhibitor, and RAL, which

suppresses the integration process, were used to determine at which stage of the HIV-1 life cycle the innate immune response in MDMs was induced.

As shown in Figure 13B-C, we observed an initially moderate innate immune response in MDMs, which increased significantly across time. This increase was not observed in cells where the RT or IN enzymatic activity was inhibited. This suggests that there exists two distinct stages of recognition and induction of an immune response in MDMs. First sensing before the process of reverse transcription takes place and the second after the provirus is established in the host cellular genome. It is further noteworthy that in a comparable experimental setting of another study, two distinct stages were also identified, even when lower amounts of virus were utillized.[156]

Notably, the results from the NVP (RT inhibitor), and RAL (IN inhibitor)-treated cells illustrated similar levels of *IFNB1* and ISG expression after 24 hpi compared to the untreated infection. This indicates comparable levels of innate immune induction and inflammation in MDMs, regardless of the treatment and virus inhibition. However, these levels plateaued as time progressed. In contrast, *IFNB1* and ISG expression in the untreated infected cells continued to increase significantly over time. This implies that the early *IFNB1* and ISG expression observed at 16-24 hpi in the NVP-treated cells cannot be due to RT products or pre-integration events. Otherwise, a strong *IFNB1* and/or ISG expression in the untreated infection compared to the NVP-treated infection would have been detected. Additionally, it has been demonstrated that macrophages detect HIV-1 upon entry into the cell,[164] which underline the recognition process observed within this work. However, this finding contradicts previous observations that macrophages recognize RT products via STING mediation in MDMs.[179] It is therefore worth noting that the measured type-I IFN amounts in human macrophages in the above-mentioned study were low. Furthermore, the absence of ISG induction 72 hpi of HIV-1 when the integration process was inhibited through RAL-treatment suggests that the recognition of a cellular sensor in MDMs must be related to the viral components of the integrated provirus. Previous research has shown that macrophages can sense various stages of the HIV life cycle after integration, including intron-containing RNA,[151,152] PR activity,[160] or virus assembly[180], supporting the findings of this thesis.

To further explore the sensing pathways involved in induction of the innate response of MDMs towards HIV-1 infection, we examined STAT1 and IRF3 phosphorylation through western blot analysis (Figure 14). Interestingly, we observed that the MDMs used in the experiments contained a basal level of JAK-STAT pathway activation. However, the intensity of phosphorylated STAT1 increased significantly throughout the course of the experiment in infected cells, in line with prior observations.[181] The expression of *IFNB1* and STAT1 phosphorylation indicates an increased activation of the JAK-STAT pathway, making them the primary cause of the strong increase in ISG expression and likely contributors to the

inflammatory response. However, we did not detect IRF3 phosphorylation, which would be expected since many signaling pathways proceed via downstream activation of this transcription factor. In the context of cGAS dependency, IRF3 phosphorylation by HIV-1 infection has been demonstrated several times in monocyte-derived dendritic cells.[182–185] This opens the question of which signaling pathway induces the observed ISG expression in MDMs. Previous studies obtained similar findings[186,187] and concluded that HIV-1 activates macrophages independently of TLRs.[187] If this is the case, we cannot draw firm conclusions from the results to this point. Additionally, HIV-1 has been shown to employ the NF-κB pathway to significantly increase transcription levels of its viral genes.[188] Our results suggest that activation of the NF-κB pathway occurred without downstream signaling through IRF3. Consequently, additional questions arise regarding the mechanisms by which NF-κB is activated and if TLRs are involved in these mechanisms. Furthermore, it is still unclear which viral and cellular determinants play a key role in the initial increase in *IFNB1* and ISG expression levels at 16-24 hpi.

4.1.1 Early Sensing: The Issue Lies in the Viral Capsid

Previous studies have shown that deficient viral CA, which are unable to bind the host protein CPSF6 (CA_{N74D}), induce increased levels of innate activation in macrophages compared to WT HIV-1 infection.[155] In addition, the viral CA itself may also represent a PAMP that is recognized by multiple host factors and triggers a downstream signaling cascade via NF-κB.[182,189] Therefore, the CA is likely the viral determinant that is recognized and responsible for triggering the observed innate immune response after 16-24 hpi in MDMs.

To investigate this hypothesis further, we generated NL4.3 variants carrying various known mutations in the CA. These included CA-mutants producing more stable (CA_{E45A})[190] or less stable CA (CA_{K203A}, $CA_{QQ63/67AA}$, CA_{P38A}),[190,191] as well as a CA-mutant which disrupts the interaction between the cellular host factor CPSF6 (CA_{N74D})[192] and CA. It is important to note that these mutants do not impair the conical formation of the CA.[190–192] After 24 hpi, we observed that all illustrated mutants increased expression of *IFNB1* and ISGs compared to the WT infection (Figure 18A). The CA-mutants generally exhibited dramatically reduced expression of the GFP reporter protein compared to the WT-CA, even though we infected cells with the same p24 levels of viruses (Figure 18B). This reduction suggests a lower integration rate of the viral genomes due to fewer CAs entering the nucleus. Previous studies have demonstrated that $CA_{QQ63/67AA}$, CA_{E45A}, and CA_{P38A} mutants can undergo the reverse transcription process but are unable to enter the nucleus, further supporting the observation of reduced GFP expression.[190,191] Achieving equal amounts of GFP^+ cells with CA-mutants compared to WT-CA infection seems unlikely. It is worth noting that there are inconsistencies in the literature regarding the CA_{P38A}-mutation. A study observed that virus particles with CA_{P38A}

may not be able to complete reverse transcription without an additional mutation[193], which could significantly impact the viral components that can be sensed by the cell. However, other studies have observed that RT activity is present with the CA_{P38A}.[190] It should further be considered that these studies were performed on different cell types, including T cells[190] and HeLa cells.[193] We therefore place more confidence in the results obtained from the T cells, as we believe this model is more physiologically-relevant.[190]

We continued to investigate mutations affecting CA-stability. We hereby hypothesized that the reason for the observed phenotype might be related to stability changes affecting the timing of the CA uncoating. This, in turn, could influence gRNA or RT-product recognition and consequently *IFNB1* and ISG expression compared to WT CA. Surprisingly, inhibiting the establishment of the provirus by RAL treatment had no effect on the observed *IFNB1* and ISG expressions in $NL4.3_{GFP}$ CA_{E45A} or CA_{P38A} infected MDMs compared to untreated infections (Figure 18C). This suggests the presence of RT products and recognition by cGAS in the cell, which should lead to increased ISG expression.[154,182] However, even with NVP treatment, innate immune recognition remained at equal levels compared to the untreated cells (Figure 18C). This indicates that the recognition by RT products was not the reason for elevated ISG expression levels over WT-CA infection in MDMs. Therefore, the viral determinant must be present before reverse transcription takes place.

To sum up, the CA itself or the packaged viral gRNA within the CA triggers recognition in MDMs. Consequently, defective CAs are likely also present throughout WT infection, as not all viral particles successfully infect the host cells. The reduced expression of ISGs compared to the CA-mutants are therefore likely due to the presence and number of defective CAs, leading to increased recognition of the virus. However, it cannot be excluded that the entry process may contribute to some of the observed *IFNB1* and ISG expression.[20,164] Nevertheless, it can be concluded that variations in HIV-1 CA-stability have a significant effect on the innate detection of HIV in MDMs and therefore play a major role in the early-stage of HIV infection.

4.1.2 Post-Integration Sensing: What is it About the Gag?

Based on our finding that CAs are essential PAMPs for MDMs in early detection, the question arose whether CAs could also impact the late-stage of infection. We ruled out the possibility of re-detection observed in the early-stage, possibly caused by the entry process[20,164], gRNA, or CA of newly produced viruses by the provirus, as we had previously used single-round viruses. The integrated provirus does not contain the *env* gene region, which should lead to production of ΔEnv viruses. Therefore, the newly produced particles were not able to fuse with the plasma membrane due to the lack of an envelope. However, there was a possibility that these ΔEnv viruses, containing all essential virus components, could trigger recognition in the extracellular space of MDMs or find their way into the cells, for instance by phagocytosis. It

was previously shown that Gag-VLPs can activate human monocyte-derived dendritic cells and subsequently activate NK cells.[194] This is important to note, as that these Gag-VLPs contained an envelope but no vital viral components. We found that even with the highest amount ΔEnv viruses in the supernatants of infected MDMs at 72 hpi, there was no significant difference in *IFNB1* or ISG expression when treated with equivalent p24 levels of ΔEnv viruses compared to the untreated MDMs (Figure 22C). The levels of *IFNB1* and ISG expression observed is negligible compared to the high expression observed in late-stage of infection in MDMs. Therefore, the ΔEnv viruses type of stimulation of MDMs can be excluded as a cause for innate immune induction in the later-stages of infection. Additionally, we investigated whether VLP_{Vpx} treatment, which included an envelope and was used in several experiments (Figure 18, Figure 19, Figure 23), would have impacted the immune response in MDMs. We observed a minor increase in *IFNB1* and ISG expression in MDMs transduced with VLP_{Vpx} (Supplementary Figure 25B). Therefore, it cannot be excluded that the expression of *IFNB1* and ISG in experiments presented in this study is completely independent of the influence of Vpx. We have recently shown in another study that Vpx enhances the innate immune response independently of SAMHD1 during HIV-1 infection.[195]

Next, we questioned whether a minimal lentiviral genome packaged in HIV-CA would also induce similar *IFNB1* and ISG expressions. We achieved comparable infection levels between the $NL4.3_{GFP}$ and $WPRE_{GFP}$ viruses, with $WPRE_{GFP}$ containing a minimal lentivirus genome and $NL4.3_{GFP}$ containing a full-length HIV-1 genome, indicating successful integration of both viruses and expression of the encoded proteins (Figure 19B). It is worth noting that we observed increased variability in the infection levels of those MDMs infected with $NL4.3_{GFP}$. We attribute this variability to the induced immune response in $NL4.3_{GFP}$ infected cells, which can affect the establishment of the provirus and GFP levels. Another contributing factor may be the cell preparation process required for the FACS measurements, as we noticed variations in counts under the microscope of the GFP^+ cells when comparing to those obtained through FACS measurements (Figure 27A). These differences may be attributed to challenges in the detaching process of MDMs from the well surface. In some experiments, increased cell death occurred throughout FACS measurements, resulting in differences between the amount of GFP^+ living cells and those observed under the microscope. Handling MDMs can be challenging, and this issue is well-documented in research involving these cells.[196] Nevertheless, the *IFNB1* and ISG expression in MDMs at 72 hpi induced by $NL4.3_{GFP}$ infection was significantly elevated, although it was barely present in the $WPRE_{GFP}$ infected cells (Figure 19C). Similar observations have been made by other studies investigating minimal lentiviruses in myeloid cells.[151,152] Thus, it became evident that the strong immune induction in MDMs at 72 hpi depends on the viral components encoded by the HIV-1 genome.

We further investigated the potential viral determinants using single defective mutants of the proteins Tat, Rev, Gag/Pol, as well as a Gag myristoylation mutant in order to gain a deeper insight into the late-stage sensing process in MDMs causing innate immune activation. Tat and Rev were hereby found to be essential, indicating that transcription and export of unspliced and partially spliced viral RNA from the nucleus is required for the innate immune response after 72 hpi, as shown by the loss of *IFNB1* and ISG expression (Figure 21C, Figure 27C). However, the initial stage of the innate immune activation remained. This indicates that multiply-spliced viral RNAs, capable of nuclear export without the assistance of Rev, are not involved in the late-stage sensing processes. Instead, it appears that partially spliced or full-length RNA transcripts containing introns of the viral genome, are required to trigger the observed immune activation. In addition, *Akiyama et al.* had highlighted the indispensable role of HIV-1 partially spliced or full-length RNA transcripts exported by the CRM-1 pathway to activate innate immune response in MDMs.[151] It is likely that the export of the partially spliced and full-length RNA transcripts via CRM-1 is crucial for late-stage sensing, as it affects trafficking within the cytoplasm. Indeed, export via a different nuclear export system would lead to a different process of intracellular trafficking.[197] Our results therefore support the findings of early studies in presenting the partially spliced or full-length RNA transcripts of HIV-1 as an essential viral determinant for late-stage signaling in MDMs and within general myeloid cells.[128,152,176]

In subsequent experiments with the Δgag/pol mutant, which lacks nearly the entire Gag/Pol region, we investigated the role of $Pr55^{Gag}$ or Gag/Pol in triggering the late-stage immune response in MDMs. A surprising discovery was that this mutant exhibited a similar level of *IFNB1* and ISG expression compared to the WT infection. Previous studies demonstrated the immune induction in MDMs without expression of Gag, although this was significantly weakened in contrast to the WT infection.[151] Another study has also demonstrated that DCs and macrophages were activated similarly and even matured when transduced with HIV-1 WT or a Δgag/pol mutant, which contains a deletion ranging from the start of *gag* until the cPPT region.[152] However, in our Δgag/pol mutant a short *gag* region that encoded a peptide sequence and induced solid *IFNB1* and ISG expression in MDMs similar to our WT infections. The question therefore remains as to which structures are recognized by the MDMs in this short peptide of Gag that triggers an innate immune response. It can be assumed that the connection through the NC domain and the gRNA was no longer present in the short peptide sequence due to the absence of the domain. Therefore, binding of the gRNA to Gag does not appear to be necessary for the observed late-stage *IFNB1* and ISG expression.

Intriguingly, infection with the myristoylation-incapable mutant, which was otherwise identical in genomic sequence to the WT, did not induce an immune response. This strengthened our assumption that the binding of gRNA to the NC domain of Gag does not ensure recognition.

Furthermore, we observed that the NL4.3$_{GFP}$ MA$_{G2A}$ was capable of producing VLPs and processing Pr55^{Gag} into p24 (Figure 22A) and p24 were also detected in the supernatant of MDMs. However, the absence of myristylation at the first glycine can affect the membrane association potential of Gag, by which Gag should not be detectable in the supernatant. Previous studies have already demonstrated that the MA$_{G2A}$ mutant is able to process Pr55^{Gag} to p24, but these failed to identify Gag in the supernatant.[166] While others have demonstrated that VLP production by HIV can be detected in the supernatant when myristoylation of Gag was substituted[198] or even in the complete absence of MA.[199] Our observations support the findings that production of new HIV viral particles is still possible in the absence of Gag myristoylation.

Furthermore, myristoylation of the first glycine in the MA domain of Pr55^{Gag} or Gag/Pol appears to be essential for late-stage *IFNB1* and ISG expression, therefore recognition by cellular PRRs. *Akiyama et al.* concluded that myristoylation and membrane targeting of Pr55^{Gag} and Gag/Pol are essential for HIV recognition in myeloid cells due to their role in membrane targeting of the full-length gRNA.[151] They further associated the inflammatory response to the adaptor protein MAVS and excluded the classic upstream PRRs RIG-I and MDA5.[151] What would challenge these findings from our site is that we cannot detect IRF3 phosphorylation in HIV-1 infected MDMs, which is strongly associated with the activation of MAVS.[200]

Nevertheless, our results with the Δgag/pol mutant (Figure 23C), our observation of p24 in the supernatant of MA$_{G2A}$ mutant (Figure 22A), and the report of virus assembly being possible without myristoylation of MA,[198] led us to the conclusion that full-length gRNA membrane association is highly unlikely as the trigger for late-stage sensing in MDMs. However, we also consider the export of the partially spliced or full-length RNA transcripts of HIV-1's provirus via the CRM-1 pathway to be a significant contributor to this late-stage innate immune response in MDMs.

Furthermore, it would be crucial to investigate whether the short Gag peptide is also capable of myristoylation. Involvement of N-myristoylation in Gag itself as a PAMP for cellular PRRs seems logical, as evidenced by the loss of *IFNB1* and ISG expression observed in infection with the N-myristoylation-deficient virus (NL4.3$_{GFP}$ MA$_{G2A}$; Figure 21C and Figure 23C). However, this is challenged by the recent discovery of heme oxygenase 2 binding to N-myristoylation of Gag. Heme oxygenase 2 hereby interrupts the virus assembly process and negatively regulates the inflammatory responses of TLR4 via its associated adaptor protein.[201] This implies that myristoylation can have a negative impact on virus replication and possibly inflammatory responses. The exact role of N-myristoylation of MA however requires further study. What is clear is that partially spliced or full-length RNA transcripts of HIV, and its presence in the cytoplasm, are crucial for driving MDMs activation and inflammatory response

in cell culture, as shown in this and other studies.[128,151,176] Whether these results can be directly linked to HAND symptoms needs to be investigated in further studies.

4.2 Differentiated Monocyte Cell Lines as a Model to Study the Immunological Role of Macrophages Against HIV-1

The importance of cell line models in simplifying biomedical studies represents an essential aspect of modern biology-related research. The use of cell lines is also very common in immunological research due to their advantageous properties such as ease of use, genetic uniformity, ability to modify, and experimental reproducibility. Among the most commonly used cells for research of innate immunity are THP-1 and U937 cells.[125] However, it's worth noting that the phenotype of these cell line models may differ from those of primary cell systems.[125,202]

4.2.1 THP-1 Cells

We aimed to use differentiated THP-1 cells as a macrophage model system to further investigate the cellular and viral determinants responsible for the observed *IFNB1* and ISG expression in HIV-1-infected MDMs (Figure 13). THP-1 cells have been widely used in numerous studies as a macrophage cell line to investigate signaling pathways and various mechanisms within the context of innate immune system research.[159] However, in our experiments, we observed significant differences in phenotype between differentiated THP-1 cells and MDMs. We faced challenges when trying to detect significant increases in *IFNB1* and ISG expression upon HIV-1 infection of THP-1 cells (Figure 15). In contrast, we observed robust expression of *IFNB1* and the same ISGs in MDMs, with a similar level of measured infectivity (compare Figure 13 and Figure 15). Although a robust immune response could be detected in several reports of PMA-treated THP-1 cells previously.[154,160,203] Interestingly, in the reports referenced here, only one utilized SAMHD1 downregulation via the addition of Vpx.[154] The other used shRNA knockdown to overcome the SAMHD1 block.[160] It is important to note, that SAMHD1 influences on the differentiation of THP-1 cells,[204] and variations in the results may be attributed to differences of how the SAMHD1 block were bypassed.

Further, we did not detect phosphorylation of IRF3 in HIV-1-infected differentiated THP-1 cells, which is in line with what we observed in MDMs. The reason for this lack of phosphorylation in the THP-1 cell line remains uncertain, raising questions about whether it reflects a similar phenotypic expression as observed in MDMs or if HIV-1 fails to activate IRF3 at detectable levels in these cells in their differentiated stage. We did not find any study demonstrating pIRF3 expression in differentiated THP-1 cells upon HIV-1 infection. Our control experiments, involving differentiated THP-1 cells stimulated with ct-DNA, demonstrated their capability to exhibit IRF3 phosphorylation. Additionally, a separate study revealed that IRF3 dimerization, a process contingent on phosphorylation, is induced by HIV-1 infection in undifferentiated

THP-1 cells.[183] In summary, we conclude that IRF3 is not activated in differentiated THP-1 cells by HIV-1 infection, consistent with our findings in MDMs.

Furthermore, STING or MAVS KO variants of differentiated THP-1 cells illustrated minor differences in *IFNB1* and ISG expression compared to WT cells, but these differences remained far from the immune activity observed in MDMs (Supplementary Figure 26B). It is worth noting that in undifferentiated THP-1 cells, HIV-1 infection did result in robust ISG expression, but also led to an increased amount of cell death, depending on the virus dose.[205] Previous studies have frequently demonstrated higher innate immunoreactivity in undifferentiated THP-1 cells compared to PMA-treated THP-1 cells.[206–209]

We conclude that undifferentiated THP-1 cells in their monocyte stage exhibit increased immunoreactivity towards HIV-1 compared to their differentiated counterparts, as evidenced by enhanced inflammation and cell death. Due to these significant differences in phenotype between THP-1 cells and MDMs during HIV-1 infection, we do not consider THP-1 cells to represent a suitable model for studying cellular interactions with HIV-1 in MDMs.

4.2.2 U937 Cells

We decided to discontinue experiments with THP-1 cells and instead focused on U937 cells as a potential cell line for investigating the cellular and viral determinants in HIV-1-infected MDMs. This decision was influenced by previous reports showing significant induction of proinflammatory cytokines in differentiated U937 cells infected with various viruses.[149,210,211]

In subsequent infection experiments using differentiated U937 cells, we observed a comparable induction of *IFNB1* and ISG expression, similar to what we had observed in MDMs (compare Figure 13B-C and Figure 16B). However, we noticed slight differences in *IFIT1*, *IFIT2* and *CXCL10* gene expression among drug-treated cells. In RAL-treated cells, ISG expression was similar to those in untreated infected cells at 24 hpi, but it reached NVP expressions levels after 72 hpi. The distinction is also apparent in the phosphorylation of IRF3. RAL-treated and untreated infected cells demonstrated the activation of IRF3 after 16 and 24 hpi, whereas NVP did not exhibit activation. These results suggest that viral components are detected prior to virus integration and after or during reverse transcription. It is likely that the PIC or RNA:DNA hybrid formed during reverse transcription is sensed by DNA sensors, triggering the observed response at 24 hpi. The cGAS-STING pathway is likely involved in this sensing process. This is strongly supported by the fact that we observed a loss of *IFNB1* and ISG expression and IRF3 phosphorylation in STING KO cells, while IRF3 phosphorylation is still detectable in MAVS KO cells (Figure 17D). Importantly, *IFNB1* and ISG expression in MAVS KO cells revealed significantly lower levels compared to WT U937 cells and do not differ significantly from STING KO cells. This indicates that both adaptor proteins, STING and MAVS, are involved in the innate immune activation in HIV-1-infected differentiated U937 cells.

Our experiments demonstrate a dependence on both the STING and MAVS pathways for innate immune activation in early- and late-stage HIV-1 infection in differentiated U937 cells (Figure 16). IRF3 activation depends on STING-mediated signaling, possibly indicating cGAS-mediated signaling, which requires further investigation. Therefore, recognition and immune response via the recently discovered DNA-PK STING-independent signaling pathway seems unlikely.[149] However, we also observed a significant influence of MAVS on *IFNB1* and ISG expression in MAVS KO cells. The absence of IRF3 phosphorylation in STING KO cells suggests that IRF3 is not required for MAVS-dependent immune activation in U937 cells (Figure 17). This implies immune activation independent of IRF3 phosphorylation, similar to what we observed in MDMs, and suggests that the same signaling pathway may also be activated in U937 cells. Further experiments with HIV-1 mutants used in MDM experiments could help to clarify whether the late-stage viral and cellular determinants in U937 are comparable to those in MDMs. It can be assumed that *IFNB1* and ISG expression would differ due to the influenced by STING-mediated signaling in U937 cells.

In summary, although differentiated U937 cells provide a valuable tool for studying innate recognition of HIV-1, their phenotype differs from that observed in MDMs. However, U937 cells exhibit closer similarities to MDMs compared to THP-1 cells in the context of HIV-1 infection.

As a result, we have determined that both differentiated THP-1 cells and U937 cells do not represent ideal choices for studying the cellular virus-host interactions that occur in MDMs. We strongly recommend the use of MDMs or other primary cells in conducting comprehensive and in-depth studies within cell culture systems to identify the viral and cellular determinants of HIV-1-induced innate immune activation. Our findings align with those of other studies which have highlighted the limitations of using cell line models to draw conclusions about the behavior of MDMs.[125,202]

4.3 Conclusion and Outlook

We have identified two distinct stages of innate immune response activation in MDMs, which are independent of IRF3 activation. The first stage occurs independently of reverse transcription or integration of HIV-1. The intensity of this immune response is influenced by the stability of the CA, with hyper- or hypostable CA variants inducing significantly elevated *IFNB1* and ISG expression compared to infection with the WT CA. This strongly suggests that the CA is a viral determinant for the first stage of innate immune response in MDMs. Further investigation is needed to determine whether capsid stability is related to recognition of the attached gRNA or not. Subsequent experiments with minimal lentiviral genomes enclosed in different stable capsids will provide insights into whether the gRNA is recognized in the early-phase or not.

The second stage of innate immune activation depends on the export of viral partially-spliced or full-length RNA into the cytoplasm. Activation likely occurs through the presence of N-myristoylated Gag, but it is not dependent on Gag NC-Domain binding to gRNA. An infection with $NL4.3_{GFP}$ Δgag/pol encoding only a short peptide sequence of Gag, primarily consisting of the N-terminus associated with myristoylation, was sufficient to trigger late-stage innate immune response similar to WT infection. Therefore, it is assumed that Gag/Pol polyproteins or binding of gRNA to Gag are not required for the recognition of this late response. The cellular determinants that interact with these viral PAMPs in late-stage infection are still unclear. To gain deeper insights, future experiments, such as pull-down assays involving the short Gag peptide sequence or myristoylation-deficient and WT gRNA, could shed light on which cellular PRRs sense these viral determinants.

Furthermore, we have demonstrated distinct phenotype differences between differentiated THP-1 and U937 cells compared to MDMs. Differentiated THP-1 cells exhibited limited immune reactivity when exposed to HIV-1. Conversely, U937 cells displayed a unique phenotype compared to MDMs in response to HIV-1 infection, with immune response involving both STING and MAVS. We suspect that RT products are sensed by cGAS, which would be an interesting area to explore in future experiments. In addition, an investigation of the possible role of myristoylation of Gag in the MAVS-associated response is needed. In conclusion, our findings suggest that THP-1 and U937 cells are not ideal cell model systems for studying the interaction between macrophages and HIV-1 due to their inadequacies. For future studies focusing on innate sensing mechanisms in macrophages against HIV-1, we recommend prioritizing the use of MDMs over cell line models.

Ultimately, our research has provided valuable insights into cell system-based research of the innate immune system. We have confirmed the significance of the CA and Gag myristoylation in HIV-1 infection. We believe that further research in these areas could pave the way for the

development of drug interventions aimed at reducing inflammation in chronic HIV patients, particularly those experiencing HAND.

References

1. Angelika Vollmar, Ilse Zündorf, T. D. *Immunologie: Grundlagen und Wirkstoffe*. (Wissenschaftliche Verlagsgesellschaft Stuttgart, 2012).
2. Kenneth Murphy, Casey Weaver, L. J. B. *Janeway's Immunobiology*. (Norton & Company, 2022).
3. Bruce Alberts, Rebecca Heald, Alexander Johnson, David Morgan, Martin Raff, Keith Roberts, P. W. *Molecular Biology of the Cell*. (Norton & Company, 2022).
4. Raza, Y., Salman, H. & Luberto, C. Sphingolipids in Hematopoiesis: Exploring Their Role in Lineage Commitment. *Cells* **10**, 2507 (2021).
5. Simon, H. U. *et al.* The Cellular Functions of Eosinophils – Collegium International Allergologicum (CIA) Update 2020. *Int Arch Allergy Immunol* **181**, 11 (2020).
6. Liew, P. X. & Kubes, P. The Neutrophil's Role During Health and Disease. *Physiol Rev* **99**, 1223–1248 (2019).
7. Webb, L. M. & Wojno, E. D. T. The role of rare innate immune cells in Type 2 immune activation against parasitic helminths. *Parasitology* **144**, 1288–1301 (2017).
8. Chirumbolo, S., Bjørklund, G., Sboarina, A. & Vella, A. The role of basophils as innate immune regulatory cells in allergy and immunotherapy. *Hum Vaccin Immunother* **14**, 815 (2018).
9. Williams, C. M. M. & Galli, S. J. The diverse potential effector and immunoregulatory roles of mast cells in allergic disease. *J Allergy Clin Immunol* **105**, 847–859 (2000).
10. Collin, M. & Bigley, V. Human dendritic cell subsets: an update. *Immunology* **154**, 3 (2018).
11. Mosser, D. M., Hamidzadeh, K. & Goncalves, R. Macrophages and the maintenance of homeostasis. *Cell Mol Immunol* **18**, 579–587 (2021).
12. Mahnke, Y. D., Brodie, T. M., Sallusto, F., Roederer, M. & Lugli, E. The who's who of T-cell differentiation: Human memory T-cell subsets. *Eur J Immunol* **43**, 2797–2809 (2013).
13. Vivier, E. *et al.* Innate or adaptive immunity? The example of natural killer cells. *Science (1979)* **331**, 44–49 (2011).
14. Freed, E. O. & Gale, M. Antiviral Innate Immunity: Editorial Overview. *J Mol Biol* **426**, 1129 (2014).
15. Thompson, M. R., Kaminski, J. J., Kurt-Jones, E. A. & Fitzgerald, K. A. Pattern recognition receptors and the innate immune response to viral infection. *Viruses* **3**, 920–940 (2011).
16. Cui, J., Chen, Y., Wang, H. Y. & Wang, R. F. Mechanisms and pathways of innate immune activation and regulation in health and cancer. *Hum Vaccin Immunother* **10**, 3270 (2014).
17. Akira, S., Uematsu, S. & Takeuchi, O. Pathogen Recognition and Innate Immunity. *Cell* **124**, 783–801 (2006).

18. Chen, C.-Y., Shih, Y.-C., Hung, Y.-F. & Hsueh, Y.-P. Beyond defense: regulation of neuronal morphogenesis and brain functions via Toll-like receptors. *J Biomed Sci* **26**, 90 (2019).

19. Hippenstiel, S., Opitz, B., Schmeck, B. & Suttorp, N. Lung epithelium as a sentinel and effector system in pneumonia – molecular mechanisms of pathogen recognition and signal transduction. *Respir Res* **7**, 97 (2006).

20. Halajian, E. A., LeBlanc, E. V., Gee, K. & Colpitts, C. C. Activation of TLR4 by viral glycoproteins: A double-edged sword? *Front Microbiol* **13**, (2022).

21. Chen, X. *et al.* Type-I interferon signatures in SARS-CoV-2 infected Huh7 cells. *Cell Death Discov* **7**, 114 (2021).

22. Kasuga, Y., Zhu, B., Jang, K.-J. & Yoo, J.-S. Innate immune sensing of coronavirus and viral evasion strategies. *Exp Mol Med* **53**, 723–736 (2021).

23. Hornung, V. *et al.* 5'-Triphosphate RNA is the ligand for RIG-I. *Science* **314**, 994–997 (2006).

24. Kang, D. C. *et al.* mda-5: An interferon-inducible putative RNA helicase with double-stranded RNA-dependent ATPase activity and melanoma growth-suppressive properties. *Proc Natl Acad Sci U S A* **99**, 637–642 (2002).

25. Kato, H. *et al.* Differential roles of MDA5 and RIG-I helicases in the recognition of RNA viruses. *Nature* **441**, 101–105 (2006).

26. Wang, D., Zhao, H., Shen, Y. & Chen, Q. A Variety of Nucleic Acid Species Are Sensed by cGAS, Implications for Its Diverse Functions. *Front Immunol* **13**, e826880 (2022).

27. Ishikawa, H. & Barber, G. N. STING is an endoplasmic reticulum adaptor that facilitates innate immune signalling. *Nature* **455**, 674–678 (2008).

28. Wu, J. *et al.* Cyclic GMP-AMP is an endogenous second messenger in innate immune signaling by cytosolic DNA. *Science* **339**, 826–830 (2013).

29. Sun, L., Wu, J., Du, F., Chen, X. & Chen, Z. J. Cyclic GMP-AMP synthase is a cytosolic DNA sensor that activates the type I interferon pathway. *Science* **339**, 786–791 (2013).

30. Ishikawa, H., Ma, Z. & Barber, G. N. STING regulates intracellular DNA-mediated, type I interferon-dependent innate immunity. *Nature* **461**, 788–792 (2009).

31. Greene, W. C. A history of AIDS: Looking back to see ahead. *Eur J Immunol* **37**, 94–102 (2007).

32. Barré-Sinoussi, F. *et al.* Isolation of a T-Lymphotropic Retrovirus from a Patient at Risk for Acquired Immune Deficiency Syndrome (AIDS). *Science (1979)* **220**, 868–871 (1983).

33. Gallo, R. C. *et al.* Frequent detection and isolation of cytopathic retroviruses (HTLV-III) from patients with AIDS and at risk for AIDS. *Science* **224**, 500–503 (1984).

34. What to call the AIDS virus? *Nature* **321**, 10 (1986).

35. Clavel, F. *et al.* Isolation of a new human retrovirus from West African patients with AIDS. *Science* **233**, 343–346 (1986).

36. Hahn, B. H., Shaw, G. M., De Cock, K. M. & Sharp, P. M. AIDS as a zoonosis: scientific and public health implications. *Science* **287**, 607–614 (2000).

37. Gao, F. *et al.* Origin of HIV-1 in the chimpanzee Pan troglodytes troglodytes. *Nature* **397**, 436–441 (1999).

38. Chen, Z. *et al.* Genetic characterization of new West African simian immunodeficiency virus SIVsm: geographic clustering of household-derived SIV strains with human immunodeficiency virus type 2 subtypes and genetically diverse viruses from a single feral sooty mangabey troop. *J Virol* **70**, 3617–3627 (1996).

39. Hirsch, V. M., Olmsted, R. A., Murphey-Corb, M., Purcell, R. H. & Johnson, P. R. An African primate lentivirus (SIVsmclosely related to HIV-2. *Nature* **339**, 389–392 (1989).

40. Hemelaar, J. The origin and diversity of the HIV-1 pandemic. *Trends Mol Med* **18**, 182–192 (2012).

41. Wertheim, J. O. & Worobey, M. Dating the age of the SIV lineages that gave rise to HIV-1 and HIV-2. *PLoS Comput Biol* **5**, e1000377 (2009).

42. Unaids. *Global HIV & AIDS statistics — Fact sheet*. (2022).

43. Robert Koch-Institut. *HIV/AIDS in Deutschland-Eckdaten der Schätzung**. (2022).

44. Samji, H. *et al.* Closing the Gap: Increases in Life Expectancy among Treated HIV-Positive Individuals in the United States and Canada. *PLoS One* **8**, e81355 (2013).

45. Jensen, B.-E. O. *et al.* In-depth virological and immunological characterization of HIV-1 cure after CCR5Δ32/Δ32 allogeneic hematopoietic stem cell transplantation. *Nat Med* **29**, 583–587 (2023).

46. Reardon, S. Third patient free of HIV after receiving virus-resistant cells. *Nature* **615**, 13–14 (2023).

47. Hsu, J. *et al.* HIV-1 remission and possible cure in a woman after haplo-cord blood transplant. *Cell* **186**, 1115-1126.e8 (2023).

48. Gupta, R. K. *et al.* HIV-1 remission following CCR5Δ32/Δ32 haematopoietic stem-cell transplantation. *Nature* **568**, 244–248 (2019).

49. A. Sáez-Cirión *et al.* Absence of viral rebound for 18 months without antiretrovirals after allogeneic hematopoietic stem cell transplantation with wild-type CCR5 donor cells to treat a biphenotypic sarcoma . *IAS 2023* Preprint at (2023).

50. MD, Peter M. Howley, David M. Knipe, Sean Whelan, Eric O. Freed Ph.D, J. L. C. *Fields Virology: RNA Viruses*. (Lippincott Williams & Wilkins, 2022).

51. Susanne Modrow, Dietrich Falke, Uwe Truyen, H. S. *Molekulare Virologie*. (Spektrum Akademischer Verlag, 2010).

52. German Advisory Committee Blood (Arbeitskreis Blut), S. ‘Assessment of P. T. by B. Human Immunodeficiency Virus (HIV). *Transfusion Medicine and Hemotherapy* **43**, 203 (2016).

53. Cohen, M. S., Hellmann, N., Levy, J. A., Decock, K. & Lange, J. The spread, treatment, and prevention of HIV-1: Evolution of a global pandemic. *Journal of Clinical Investigation* **118**, 1244–1254 (2008).

54. McLaren, P. J. & Fellay, J. HIV-1 and human genetic variation. *Nature Reviews Genetics 2021 22:10* **22**, 645–657 (2021).

55. Li, G. *et al.* An integrated map of HIV genome-wide variation from a population perspective. *Retrovirology* **12**, 18 (2015).

56. Brady, J. & Kashanchi, F. Tat gets the 'green' light on transcription initiation. *Retrovirology* **2**, 69 (2005).

57. Berkhout, B., Gatignol, A., Rabson, A. B. & Jeang, K. T. TAR-independent activation of the HIV-1 LTR: evidence that tat requires specific regions of the promoter. *Cell* **62**, 757–767 (1990).

58. Pumfery, A. *et al.* Chromatin remodeling and modification during HIV-1 Tat-activated transcription. *Curr HIV Res* **1**, 343–362 (2003).

59. Cato, A. C., Henderson, D. & Ponta, H. The hormone response element of the mouse mammary tumour virus DNA mediates the progestin and androgen induction of transcription in the proviral long terminal repeat region. *EMBO J* **6**, 363–368 (1987).

60. Malim, M. H., Hauber, J., Le, S. Y., Maizel, J. V. & Cullen, B. R. The HIV-1 rev trans-activator acts through a structured target sequence to activate nuclear export of unspliced viral mRNA. *Nature* **338**, 254–257 (1989).

61. Fornerod, M., Ohno, M., Yoshida, M. & Mattaj, I. W. CRM1 is an export receptor for leucine-rich nuclear export signals. *Cell* **90**, 1051–1060 (1997).

62. Mangeat, B. *et al.* Broad antiretroviral defence by human APOBEC3G through lethal editing of nascent reverse transcripts. *Nature* **424**, 99–103 (2003).

63. Desimmie, B. A. *et al.* Multiple APOBEC3 restriction factors for HIV-1 and one vif to rule them all. *J Mol Biol* **426**, 1220–1245 (2014).

64. Sheehy, A. M., Gaddis, N. C., Choi, J. D. & Malim, M. H. Isolation of a human gene that inhibits HIV-1 infection and is suppressed by the viral Vif protein. *Nature* **418**, 646–650 (2002).

65. Stupfler, B., Verriez, C., Gallois-Montbrun, S., Marquet, R. & Paillart, J. C. Degradation-Independent Inhibition of APOBEC3G by the HIV-1 Vif Protein. *Viruses* **13**, 617 (2021).

66. Tungaturthi, P. K. *et al.* Role of HIV-1 Vpr in AIDS pathogenesis: Relevance and implications of intravirion, intracellular and free Vpr. *Biomedicine and Pharmacotherapy* **57**, 20–24 (2003).

67. Le Rouzic, E. *et al.* HIV1 Vpr arrests the cell cycle by recruiting DCAF1/VprBP, a receptor of the Cul4-DDB1 ubiquitin ligase. *Cell Cycle* **6**, 182–188 (2007).

68. Cohen, E. A., Dehni, G., Sodroski, J. G. & Haseltine, W. A. Human immunodeficiency virus vpr product is a virion-associated regulatory protein. *J Virol* **64**, 3097–3099 (1990).

69. Goh, W. C. *et al.* HIV-1 Vpr increases viral expression by manipulation of the cell cycle: A mechanism for selection of Vpr in vivo. *Nat Med* **4**, 65–71 (1998).

70. Heinzinger, N. K. *et al.* The Vpr protein of human immunodeficiency virus type 1 influences nuclear localization of viral nucleic acids in nondividing host cells. *Proceedings of the National Academy of Sciences* **91**, 7311–7315 (1994).

71. Schubert, U. *et al.* CD4 glycoprotein degradation induced by human immunodeficiency virus type 1 Vpu protein requires the function of proteasomes and the ubiquitin-conjugating pathway. *J Virol* **72**, 2280–2288 (1998).

72. Neil, S. J. D., Zang, T. & Bieniasz, P. D. Tetherin inhibits retrovirus release and is antagonized by HIV-1 Vpu. *Nature* **451**, 425–430 (2008).

73. Malim, M. H. & Bieniasz, P. D. HIV restriction factors and mechanisms of evasion. *Cold Spring Harb Perspect Med* **2**, a006940 (2012).

74. Laguette, N. *et al.* SAMHD1 is the dendritic- and myeloid-cell-specific HIV-1 restriction factor counteracted by Vpx. *Nature* **474**, 654–657 (2011).

75. Hrecka, K. *et al.* Vpx relieves inhibition of HIV-1 infection of macrophages mediated by the SAMHD1 protein. *Nature* **474**, 658–661 (2011).

76. Buffalo, C. Z., Iwamoto, Y., Hurley, J. H. & Ren, X. How HIV Nef Proteins Hijack Membrane Traffic To Promote Infection. *J Virol* **93**, 10.1128/jvi.01322 (2019).

77. Life Cycle – Science of HIV. https://scienceofhiv.org/wp/life-cycle/#animation.

78. Wilen, C. B., Tilton, J. C. & Doms, R. W. HIV: Cell Binding and Entry. *Cold Spring Harb Perspect Med* **2**, a006866 (2012).

79. Sousa, R., Chung, Y. J., Rose, J. P. & Wang, B.-C. Crystal structure of bacteriophage T7 RNA polymerase at 3.3 Å resolution. *Nature* **364**, 593–599 (1993).

80. Butler, S. L., Johnson, E. P. & Bushman, F. D. Human Immunodeficiency Virus cDNA Metabolism: Notable Stability of Two-Long Terminal Repeat Circles. *J Virol* **76**, 3739–3747 (2002).

81. McDonald, D. *et al.* Visualization of the intracellular behavior of HIV in living cells. *J Cell Biol* **159**, 441 (2002).

82. Döhner, K., Nagel, C. H. & Sodeik, B. Viral stop-and-go along microtubules: taking a ride with dynein and kinesins. *Trends Microbiol* **13**, 320–327 (2005).

83. Guedán, A., Caroe, E. R., Barr, G. C. R. & Bishop, K. N. The Role of Capsid in HIV-1 Nuclear Entry. *Viruses 2021* **13**, 1425 (2021).

84. Dharan, A. & Campbell, E. M. Role of Microtubules and Microtubule-Associated Proteins in HIV-1 Infection. *J Virol* **92**, (2018).

85. Burdick, R. C. *et al.* HIV-1 uncoats in the nucleus near sites of integration. *Proc Natl Acad Sci U S A* **117**, 5486–5493 (2020).

86. Dharan, A., Bachmann, N., Talley, S., Zwikelmaier, V. & Campbell, E. M. Nuclear pore blockade reveals that HIV-1 completes reverse transcription and uncoating in the nucleus. *Nat Microbiol* **5**, 1088–1095 (2020).

87. Francis, A. C. & Melikyan, G. B. Single HIV-1 imaging reveals progression of infection through CA-dependent steps of docking at the nuclear pore, uncoating and nuclear transport. *Cell Host Microbe* **23**, 536 (2018).

88. Fassati, A. HIV infection of non-dividing cells: a divisive problem. *Retrovirology* **3**, 74 (2006).

89. Craigie, R. & Bushman, F. D. HIV DNA Integration. *Cold Spring Harb Perspect Med* **2**, a006890 (2012).

90. Siliciano, R. F. & Greene, W. C. HIV Latency. *Cold Spring Harb Perspect Med* **1**, a007096 (2011).

91. Nilson, K. A. & Price, D. H. The Role of RNA Polymerase II Elongation Control in HIV-1 Gene Expression, Replication, and Latency. *Genet Res Int* **2011**, e726901 (2011).

92. Nikolaitchik, O. A. *et al.* HIV-1 usurps transcription start site heterogeneity of host RNA polymerase II to maximize replication fitness. *Proc Natl Acad Sci U S A* **120**, e2305103120 (2023).

93. Barboric, M., Nissen, R. M., Kanazawa, S., Jabrane-Ferrat, N. & Peterlin, B. M. NF-kappaB binds P-TEFb to stimulate transcriptional elongation by RNA polymerase II. *Mol Cell* **8**, 327–337 (2001).

94. Martin Stoltzfus, C. Chapter 1. Regulation of HIV-1 alternative RNA splicing and its role in virus replication. *Adv Virus Res* **74**, 1–40 (2009).

95. Emery, A. & Swanstrom, R. HIV-1: To Splice or Not to Splice, That Is the Question. *Viruses* **13**, 181 (2021).

96. Freed, E. O. HIV-1 assembly, release and maturation. *Nat Rev Microbiol* **13**, 484 (2015).

97. Kuzembayeva, M., Dilley, K., Sardo, L. & Hu, W. S. Life of psi: How full-length HIV-1 RNAs become packaged genomes in the viral particles. *Virology* **454–455**, 362–370 (2014).

98. Ono, A. & Freed, E. O. Plasma membrane rafts play a critical role in HIV-1 assembly and release. *Proc Natl Acad Sci U S A* **98**, 13925–13930 (2001).

99. Sundquist, W. I. & Kräusslich, H.-G. HIV-1 Assembly, Budding, and Maturation. *Cold Spring Harb Perspect Med* **2**, a006924 (2012).

100. Kutluay, S. B. & Bieniasz, P. D. Analysis of the Initiating Events in HIV-1 Particle Assembly and Genome Packaging. *PLoS Pathog* **6**, e1001200- (2010).

101. Sumner, C. & Ono, A. Relationship between HIV-1 Gag Multimerization and Membrane Binding. *Viruses* **14**, 622 (2022).

102. Tang, C. *et al.* Entropic switch regulates myristate exposure in the HIV-1 matrix protein. *Proc Natl Acad Sci U S A* **101**, 517–522 (2004).

103. Resh, M. D. A myristoyl switch regulates membrane binding of HIV-1 Gag. *Proc Natl Acad Sci U S A* **101**, 417 (2004).

104. Massiah, M. A. *et al.* Comparison of the NMR and X-ray structures of the HIV-1 matrix protein: evidence for conformational changes during viral assembly. *Protein Sci* **5**, 2391–2398 (1996).

105. Hill, C. P., Worthylake, D., Bancroft, D. P., Christensen, A. M. & Sundquist, W. I. Crystal structures of the trimeric human immunodeficiency virus type 1 matrix protein: implications for membrane association and assembly. *Proc Natl Acad Sci U S A* **93**, 3099–3104 (1996).

106. Gheysen, D. *et al.* Assembly and release of HIV-1 precursor Pr55gag virus-like particles from recombinant baculovirus-infected insect cells. *Cell* **59**, 103–112 (1989).

107. Checkley, M. A., Luttge, B. G. & Freed, E. O. HIV-1 Envelope Glycoprotein Biosynthesis, Trafficking, and Incorporation. *J Mol Biol* **410**, 582 (2011).

108. Webb, J. A., Jones, C. P., Parent, L. J., Rouzina, I. & Musier-Forsyth, K. Distinct binding interactions of HIV-1 Gag to Psi and non-Psi RNAs: Implications for viral genomic RNA packaging. *RNA* **19**, 1078–1088 (2013).

109. Shubsda, M. F., Paoletti, A. C., Hudson, B. S. & Borer, P. N. Affinities of Packaging Domain Loops in HIV-1 RNA for the Nucleocapsid Protein. *Biochemistry* **41**, 5276–5282 (2002).

110. Morita, E. & Sundquist, W. I. Retrovirus budding. *Annu Rev Cell Dev Biol* **20**, 395–425 (2004).

111. Christian Hoffmann, J. K. R. *HIV 2022/2023*. (Medizin Fokus Verlag, 2022).

112. Pomerantz, R. J. HIV-1 reservoirs. *Clin Lab Med* **22**, 651–680 (2002).

113. Bandera, A., Gori, A., Clerici, M. & Sironi, M. Phylogenies in ART: HIV reservoirs, HIV latency and drug resistance. *Curr Opin Pharmacol* **48**, 24–32 (2019).

114. Lanman, T., Letendre, S., Ma, Q., Bang, A. & Ellis, R. CNS Neurotoxicity of Antiretrovirals. *J Neuroimmune Pharmacol* **16**, 130 (2021).

115. Trono, D. *et al.* HIV Persistence and the Prospect of Long-Term Drug-Free Remissions for HIV-Infected Individuals. *Science (1979)* **329**, 174–180 (2010).

116. Kessing, C. F. *et al.* In vivo suppression of HIV rebound by didehydro-Cortistatin A, a "block-and-lock" strategy for HIV-1 cure. *Cell Rep* **21**, 600 (2017).

117. Deeks, S. G. Shock and kill. *Nature* **487**, 439–440 (2012).

118. Boehm, D. *et al.* SMYD2-Mediated Histone Methylation Contributes to HIV-1 Latency. *Cell Host Microbe* **21**, 569–579 (2017).

119. Jadhav, S. & Nema, V. HIV-Associated Neurotoxicity: The Interplay of Host and Viral Proteins. *Mediators Inflamm* **2021**, 1267041 (2021).

120. Mahadevan, A. *et al.* Characterization of human immunodeficiency virus (HIV)-infected cells in infiltrates associated with CNS opportunistic infections in patients with HIV clade C infection. *J Neuropathol Exp Neurol* **66**, 799–808 (2007).

121. Zenebe, Y., Necho, M., Yimam, W. & Akele, B. Worldwide Occurrence of HIV-Associated Neurocognitive Disorders and Its Associated Factors: A Systematic Review and Meta-Analysis. *Front Psychiatry* **13**, 814362 (2022).

122. Saylor, D. *et al.* HIV-associated neurocognitive disorder — pathogenesis and prospects for treatment. *Nat Rev Neurol* **12**, 234–248 (2016).

123. Mekuriaw, B., Belayneh, Z., Teshome, W. & Akalu, Y. Prevalence and variability of HIV/AIDS-associated neurocognitive impairments in Africa: a systematic review and meta-analysis. *BMC Public Health* **23**, 997 (2023).

124. McArthur, J. C., Steiner, J., Sacktor, N. & Nath, A. Human immunodeficiency virus-associated neurocognitive disorders: Mind the gap. *Ann Neurol* **67**, 699–714 (2010).

125. Cassol, E., Alfano, M., Biswas, P. & Poli, G. Monocyte-derived macrophages and myeloid cell lines as targets of HIV-1 replication and persistence. *J Leukoc Biol* **80**, 1018–1030 (2006).

126. Chitrakar, A., Sanz, M., Maggirwar, S. B. & Soriano-Sarabia, N. HIV Latency in Myeloid Cells: Challenges for a Cure. *Pathogens* **11**, 611 (2022).

127. Smith, L. K., Kuhn, T. B., Chen, J. & Bamburg, J. R. HIV Associated Neurodegenerative Disorders: A New Perspective on the Role of Lipid Rafts in Gp120-Mediated Neurotoxicity. *Curr HIV Res* **16**, 258 (2018).

128. Akiyama, H. & Gummuluru, S. HIV-1 persistence and chronic induction of innate immune responses in macrophages. *Viruses* **12**, 711 (2020).

129. Davis, L. E. *et al.* Early viral brain invasion in iatrogenic human immunodeficiency virus infection. *Neurology* **42**, 1736–1739 (1992).

130. González-Scarano, F. & Martín-García, J. The neuropathogenesis of AIDS. *Nat Rev Immunol* **5**, 69–81 (2005).

131. Saylor, D. *et al.* HIV-associated neurocognitive disorder - Pathogenesis and prospects for treatment. *Nat Rev Neurol* **12**, 234–248 (2016).

132. Nath, A. & Rumbaugh, J. Developments in HIV neuropathogenesis. *Curr Pharm Des* **12**, 1023–1044 (2006).

133. Sanders-Beer, B. E. *et al.* Characterization of a monoclonal anti-capsid antibody that cross-reacts with three major primate lentivirus lineages. *Virology* **422**, 402–412 (2012).

134. Sunseri, N., O'Brien, M., Bhardwaj, N. & Landau, N. R. Human Immunodeficiency Virus Type 1 Modified To Package Simian Immunodeficiency Virus Vpx Efficiently Infects Macrophages and Dendritic Cells. *J Virol* **85**, 6263–6274 (2011).

135. Fu, S. *et al.* HIV-1 exploits the Fanconi anemia pathway for viral DNA integration. *Cell Rep* **39**, 110840 (2022).

136. Hofmann, H. *et al.* Inhibition of CUL4A Neddylation Causes a Reversible Block to SAMHD1-Mediated Restriction of HIV-1. *J Virol* **87**, 11741–11750 (2013).

137. Longo, P. A., Kavran, J. M., Kim, M.-S. & Leahy, D. J. Transient Mammalian Cell Transfection with Polyethylenimine (PEI). *Methods Enzymol* **529**, 227–240 (2013).

138. O'doherty, U., Swiggard, W. J. & Malim, M. H. Human Immunodeficiency Virus Type 1 Spinoculation Enhances Infection through Virus Binding. *J Virol* **74**, 10074–10080 (2000).

139. Chomczynski, P. A reagent for the single-step simultaneous isolation of RNA, DNA and proteins from cell and tissue samples. *Biotechniques* **15**, 532-534,536-537 (1993).

140. Lovatt, A. *et al.* High throughput detection of retrovirus-associated reverse transcriptase using an improved fluorescent product enhanced reverse transcriptase assay and its comparison to conventional detection methods. *J Virol Methods* **82**, 185–200 (1999).

141. Horie, M. *et al.* Endogenous non-retroviral RNA virus elements in mammalian genomes. *Nature* **463**, 84–87 (2010).

142. Malnati, M. S. *et al.* A universal real-time PCR assay for the quantification of group-M HIV-1 proviral load. *Nature Protocols 2008 3:7* **3**, 1240–1248 (2008).

143. Livak, K. J. & Schmittgen, T. D. Analysis of relative gene expression data using real-time quantitative PCR and the 2-ΔΔCT method. *Methods* **25**, 402–408 (2001).

144. Platt, E. J., Wehrly, K., Kuhmann, S. E., Chesebro, B. & Kabat, D. Effects of CCR5 and CD4 cell surface concentrations on infections by macrophagetropic isolates of human immunodeficiency virus type 1. *J. Virol.* **72**, 2855–2864 (1998).

145. Sanyal, A. *et al.* Novel assay reveals a large inducible replication competent HIV-1 reservoir in resting CD4(+) T cells. *Nat. Med.* **23**, 885–889 (2017).

146. Hofmann, H. *et al.* The Vpx Lentiviral Accessory Protein Targets SAMHD1 for Degradation in the Nucleus. *J Virol* **86**, 12552–12560 (2012).

147. Mattijssen, S. & Pruijn, G. J. M. Viperin, a key player in the antiviral response. *Microbes Infect* **14**, 419–426 (2012).

148. Wang, Y. *et al.* HIV-1 Vif suppresses antiviral immunity by targeting STING. *Cell Mol Immunol* **19**, 108–121 (2022).

149. Burleigh, K. *et al.* Human DNA-PK activates a STING-independent DNA sensing pathway. *Sci Immunol* **5**, 4219 (2020).

150. Gaidt, M. M. *et al.* Self-guarding of MORC3 enables virulence factor-triggered immunity. *Nature* **600**, 138–142 (2021).

151. Akiyama, H. *et al.* HIV-1 intron-containing RNA expression induces innate immune activation and T cell dysfunction. *Nat Commun* **9**, 3450 (2018).

152. McCauley, S. M. *et al.* Intron-containing RNA from the HIV-1 provirus activates type I interferon and inflammatory cytokines. *Nat Commun* **9**, 5305 (2018).

153. Gupta, S., Termini, J. M., Issac, B., Guirado, E. & Stone, G. W. Constitutively Active MAVS Inhibits HIV-1 Replication via Type I Interferon Secretion and Induction of HIV-1 Restriction Factors. *PLoS One* **11**, e0148929 (2016).

154. Sumner, R. P. *et al.* Disrupting HIV -1 capsid formation causes cGAS sensing of viral DNA. *EMBO J* **39**, e103958 (2020).

155. Rasaiyaah, J. *et al.* HIV-1 evades innate immune recognition through specific cofactor recruitment. *Nature* **503**, 402–405 (2013).

156. Nasr, N. *et al.* Mechanism of Interferon-Stimulated Gene Induction in HIV-1-Infected Macrophages. *J Virol* **91**, 10.1128/jvi.00744-17 (2017).

157. Tsuchiya, S. *et al.* Establishment and characterization of a human acute monocytic leukemia cell line (THP-1). *Int J Cancer* **26**, 171–176 (1980).

158. Auwerx, J. The human leukemia cell line, THP-1: A multifacetted model for the study of monocyte-macrophage differentiation. *Experientia* **47**, 22–31 (1991).

159. Chanput, W., Mes, J. J. & Wichers, H. J. THP-1 cell line: An in vitro cell model for immune modulation approach. *Int Immunopharmacol* **23**, 37–45 (2014).

160. Wang, Q. *et al.* CARD8 is an inflammasome sensor for HIV-1 protease activity. *Science (1979)* **371**, (2021).

161. Ralph, P., Moore, M. A. S. & Nilsson, K. Lysozyme synthesis by established human and murine histiocytic lymphoma cell lines. *J Exp Med* **143**, 1528–1533 (1976).

162. Koren, H. S., Anderson, S. J. & Larrick, J. W. In vitro activation of a human macrophage-like cell line. *Nature* **279**, 328–331 (1979).

163. García, A. *et al.* Differential effect on U937 cell differentiation by targeting transcriptional factors implicated in tissue-or stage-specific induced integrin expression. *Exp Hematol* **27**, 353–364 (1999).

164. Decalf, J. *et al.* Sensing of HIV-1 Entry Triggers a Type I Interferon Response in Human Primary Macrophages. *J Virol* **91**, e00147-17 (2017).

165. Malim, M. L.-T., Biihnlein, S., Hauber, J. & Cullen, B. R. Functional Dissection of the HIV-1 Rev Trans-Activator-Derivation of a Trans-Dominant Repressor of Rev Function. *Cell* **58**, 205–214 (1989).

166. Freed, E. O., Orenstein, J. M., Buckler-White, A. J. & Martin, M. A. Single amino acid changes in the human immunodeficiency virus type 1 matrix protein block virus particle production. *J Virol* **68**, 5311 (1994).

167. Adamson, C. S. & Jones, I. M. The molecular basis of HIV capsid assembly - Five years of progress. *Rev Med Virol* **14**, 107–121 (2004).

168. Deeks, S. G., Tracy, R. & Douek, D. C. Systemic Effects of Inflammation on Health during Chronic HIV Infection. *Immunity* **39**, 633–645 (2013).

169. Doyle, T., Goujon, C. & Malim, M. H. HIV-1 and interferons: Who's interfering with whom? *Nat Rev Microbiol* **13**, 403–413 (2015).

170. Altfeld, M. & Gale, M. Innate immunity against HIV-1 infection. *Nat Immunol* **16**, 554–562 (2015).

171. Germain, R. N. Antigen processing and CD4+ T cell depletion in AIDS. *Cell* **54**, 441–444 (1988).

172. Chun, T. W. *et al.* Quantification of latent tissue reservoirs and total body viral load in HIV-1 infection. *Nature* **387**, 183–188 (1997).

173. Finzi, D. *et al.* Latent infection of CD4+ T cells provides a mechanism for lifelong persistence of HIV-1, even in patients on effective combination therapy. *Nat Med* **5**, 512–517 (1999).

174. Siliciano, J. D. *et al.* Long-term follow-up studies confirm the stability of the latent reservoir for HIV-1 in resting CD4+ T cells. *Nat Med* **9**, 727–728 (2003).

175. Harman, A. N. *et al.* HIV Blocks Interferon Induction in Human Dendritic Cells and Macrophages by Dysregulation of TBK1. *J Virol* **89**, 6575–6584 (2015).

176. Akiyama, H. *et al.* Expression of HIV-1 Intron-Containing RNA in Microglia Induces Inflammatory Responses. *J Virol* **95**, 10.1128/jvi.01386-20 (2021).

177. Chan, P. & Brew, B. J. HIV associated neurocognitive disorders in the modern antiviral treatment era: prevalence, characteristics, biomarkers, and effects of treatment. *Curr HIV/AIDS Rep* **11**, 317–324 (2014).

178. Cingöz, O. & Goff, S. P. HIV-1 is a poor inducer of innate immune responses. *mBio* **10**, 10.1128/mbio.02834-18 (2019).

179. Herzner, A. M. *et al.* Sequence-specific activation of the DNA sensor cGAS by Y-form DNA structures as found in primary HIV-1 cDNA. *Nature Immunology 2015 16:10* **16**, 1025–1033 (2015).

180. Giese, S. & Marsh, M. Tetherin Can Restrict Cell-Free and Cell-Cell Transmission of HIV from Primary Macrophages to T Cells. *PLoS Pathog* **10**, e1004189 (2014).

181. Magnani, M. *et al.* Drug-loaded red blood cell-mediated clearance of HIV-1 macrophage reservoir by selective inhibition of STAT1 expression. *J Leukoc Biol* **74**, 764–771 (2003).

182. Lahaye, X. *et al.* NONO Detects the Nuclear HIV Capsid to Promote cGAS-Mediated Innate Immune Activation. *Cell* **175**, 488-501.e22 (2018).

183. Gao, D. *et al.* Cyclic GMP-AMP synthase is an innate immune sensor of HIV and other retroviruses. *Science (1979)* **341**, 903–906 (2013).

184. Yoh, S. M. *et al.* PQBP1 Is a Proximal Sensor of the cGAS-Dependent Innate Response to HIV-1. *Cell* **161**, 1293–1305 (2015).

185. Manel, N. *et al.* A cryptic sensor for HIV-1 activates antiviral innate immunity in dendritic cells. *Nature* **467**, 214–217 (2010).

186. Nasr, N. *et al.* HIV-1 infection of human macrophages directly induces viperin which inhibits viral production. *Blood* **120**, 778–788 (2012).

187. Brown, J. N., Kohler, J. J., Coberley, C. R., Sleasman, J. W. & Goodenow, M. M. HIV-1 Activates Macrophages Independent of Toll-Like Receptors. *PLoS One* **3**, e3664- (2008).

188. Hiscott, J., Kwon, H. & Génin, P. Hostile takeovers: viral appropriation of the NF-kB pathway. *J Clin Invest* **107**, 143–151 (2001).

189. Sultana, T. *et al.* Multiple Pathways To Avoid Beta Interferon Sensitivity of HIV-1 by Mutations in Capsid. *J Virol* **93**, (2019).

190. Forshey, B. M., von Schwedler, U., Sundquist, W. I. & Aiken, C. Formation of a Human Immunodeficiency Virus Type 1 Core of Optimal Stability Is Crucial for Viral Replication. *J Virol* **76**, 5667–5677 (2002).

191. von Schwedler, U. K., Stray, K. M., Garrus, J. E. & Sundquist, W. I. Functional Surfaces of the Human Immunodeficiency Virus Type 1 Capsid Protein. *J Virol* **77**, 5439–5450 (2003).

192. Lee, K. E. *et al.* Flexible Use of Nuclear Import Pathways by HIV-1. *Cell Host Microbe* **7**, 221 (2010).

193. Yang, R. *et al.* Second-site suppressors of HIV-1 capsid mutations: restoration of intracellular activities without correction of intrinsic capsid stability defects. *Retrovirology* **9**, 30 (2012).

194. Oo Chang Tomoyuki Suzuki Hitoshi Suzuki Hiroshi Takaku, M. HIV-1 Gag-Virus-Like Particles Induce Natural Killer Cell Immune Responses via Activation and Maturation of Dendritic Cells. *J Innate Immun* **4**, 187–200 (2012).

195. Cingöz, O., Arnow, N. D., Puig Torrents, M. & Bannert, N. Vpx enhances innate immune responses independently of SAMHD1 during HIV-1 infection. *Retrovirology* **18**, 4 (2021).

196. Chen, S., So, E. C., Strome, S. E. & Zhang, X. Impact of Detachment Methods on M2 Macrophage Phenotype and Function. *J Immunol Methods* **426**, 56–61 (2015).

197. Pocock, G. M., Becker, J. T., Swanson, C. M., Ahlquist, P. & Sherer, N. M. HIV-1 and M-PMV RNA Nuclear Export Elements Program Viral Genomes for Distinct Cytoplasmic Trafficking Behaviors. *PLoS Pathog* **12**, 1–30 (2016).

198. Lee, P. P. & Linial, M. L. Efficient particle formation can occur if the matrix domain of human immunodeficiency virus type 1 Gag is substituted by a myristylation signal. *J Virol* **68**, 6644 (1994).

199. Reil, H., Bukovsky, A. A., Gelderblom, H. R. & Gö Ttlinger, H. G. Efficient HIV-1 replication can occur in the absence of the viral matrix protein. *EMBO J* **17**, 2699–2708 (1998).

200. Liu, S. *et al.* Phosphorylation of innate immune adaptor proteins MAVS, STING, and TRIF induces IRF3 activation. *Science (1979)* **347**, (2015).

201. Zhu, Y. *et al.* Heme Oxygenase 2 Binds Myristate to Regulate Retrovirus Assembly and TLR4 Signaling. *Cell Host Microbe* **21**, 220–230 (2017).

202. Schildberger, A., Rossmanith, E., Eichhorn, T., Strassl, K. & Weber, V. Monocytes, peripheral blood mononuclear cells, and THP-1 cells exhibit different cytokine expression patterns following stimulation with lipopolysaccharide. *Mediators Inflamm* **2013**, (2013).

203. Solis, M. *et al.* RIG-I-Mediated Antiviral Signaling Is Inhibited in HIV-1 Infection by a Protease-Mediated Sequestration of RIG-I. *J Virol* **85**, 1224–1236 (2011).

204. Dragin, L. *et al.* Evidence that HIV-1 restriction factor SAMHD1 facilitates differentiation of myeloid THP-1 cells. *Virol J* **12**, 201 (2015).

205. Stuck, M. *et al.* HIV-1 infection causes depletion of monocytic cells through a non-canonical cell death pathway. *bioRxiv* 2022.12.20.521186 (2022) doi:10.1101/2022.12.20.521186.

206. Espada, C. E. *et al.* SAMHD1 impairs type I interferon induction through the MAVS, IKKε, and IRF7 signaling axis during viral infection. *J Biol Chem* **299**, 104925 (2023).

207. Chen, S. *et al.* SAMHD1 suppresses innate immune responses to viral infections and inflammatory stimuli by inhibiting the NF-κB and interferon pathways. *Proc Natl Acad Sci U S A* **115**, E3798–E3807 (2018).

208. Holm, C. K. *et al.* Influenza A virus targets a cGAS-independent STING pathway that controls enveloped RNA viruses. *Nat Commun* **7**, 10680 (2016).

209. Rihn, S. J. *et al.* The Envelope Gene of Transmitted HIV-1 Resists a Late Interferon Gamma-Induced Block. *J Virol* **91**, 10.1128/jvi.02254-16 (2017).

210. Zhao, D. C., Yan, T., Li, L., You, S. & Zhang, C. Respiratory syncytial virus inhibits interferon-α-inducible signaling in macrophage-like U937 cells. *Journal of Infection* **54**, 393–398 (2007).

211. Guerrero-Arguero, I., Høj, T. R., Tass, E. S., Berges, B. K. & Robison, R. A. A comparison of Chikungunya virus infection, progression, and cytokine profiles in human PMA-differentiated U937 and murine RAW264.7 monocyte derived macrophages. *PLoS One* **15**, e0230328- (2020).

Appendix

Supplementary Figures

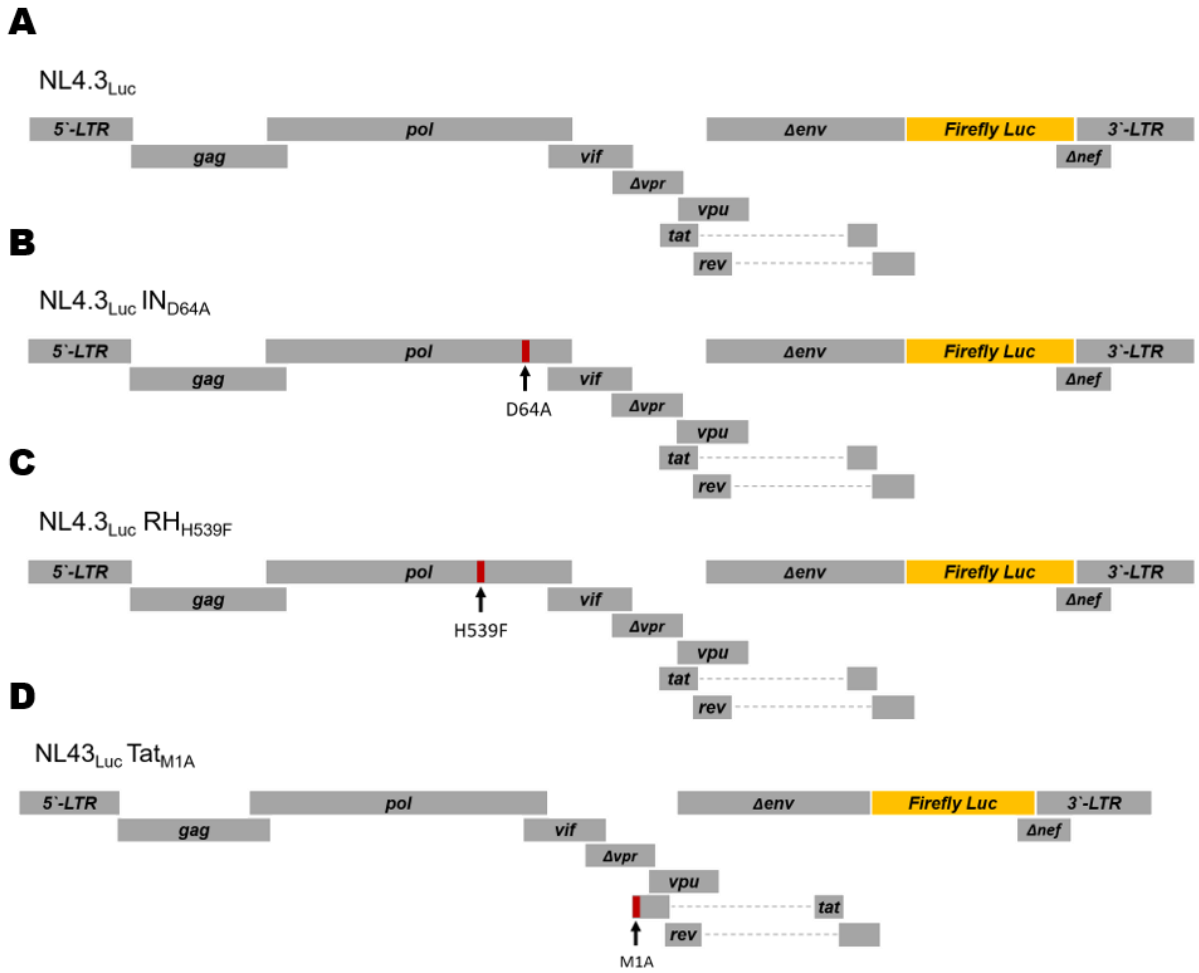

Figure 24: Mutants Specifically Created for the HIV-1 Luciferase Reporter System

Schematic figures illustrate the generated viral genome mutants using the **(A)** $NL4.3_{Luc}$ vector. Six mutants were generated, with three mutants in just $NL4.3_{Luc}$ vector system: **(B)** IN_{D64A}, designed to produce a IN deficient protein. **(C)** RH_{H539F}, engineered to result in a ribonuclease H-deficient domain of the RT. **(D)** Tat_{M1A}, do not express Tat protein.

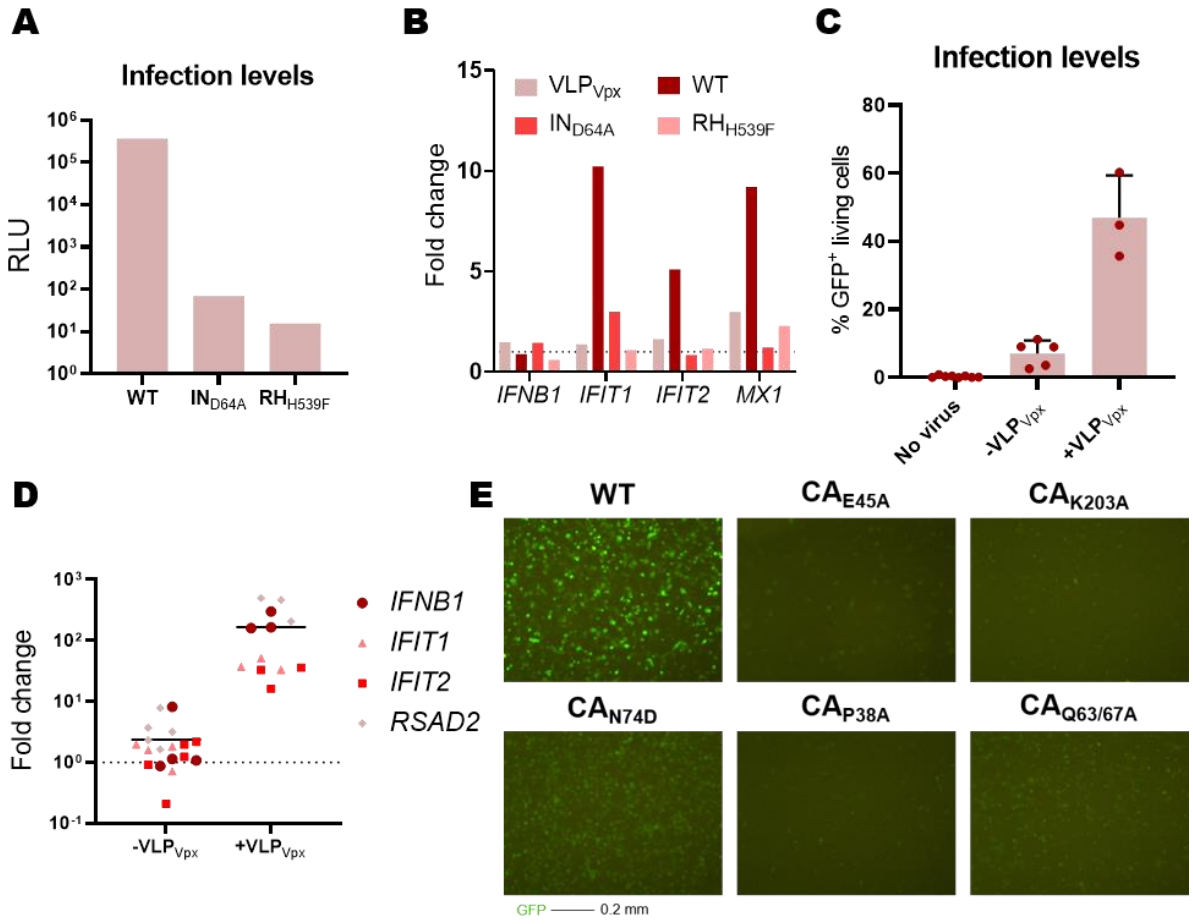

Figure 25: Additional Supporting MDM Figures

(A) Indication of infectious levels by relative light units (RLU) of MDMs (*n*=1) infected with NL4.3$_{Luc}$ WT, IN$_{D64A}$ or RH$_{H539F}$ (MOI=2). Cells were harvested 72 hpi, lysed with passive lysis buffer, and analyzed by luciferase assay. **(B)** MDMs (*n*=1) were infected with the viruses mentioned in (A), and cells were also treated with VLPs containing Vpx (VLP$_{Vpx}$) as a control. Cells were harvested at time points as indicated. The gene expression of *IFNB1*, *IFIT1*, *IFIT2*, and *MX1* was measured using RT-qPCR and the fold change is shown (uninfected). **(C)** Infection levels of MDMs from blood donors (*n*=3-8) infected with NL4.3$_{GFP}$ Δgag/pol with or without VLP$_{Vpx}$ (MOI=3 and 6). Cells were harvested 72 hpi and analyzed by FACS. The percentage of live/dead cells was determined by FVD-660 staining. **(D)** Comparison of ISGs fold change levels (uninfected) of those infected MDMs (C). **(E)** Representative fluorescence images of GFP (green) signals from MDMs infected with NL4.3$_{GFP}$ and CA-mutants (MOI=3). A scale bar of 0.2 mm is provided under the images **(C)** The means ± SEM or **(C)** The means ± SD or **(D)** grand means are shown and each symbol represented **(C)** donor from an experiment **(D)** or a measured expression of a gene.

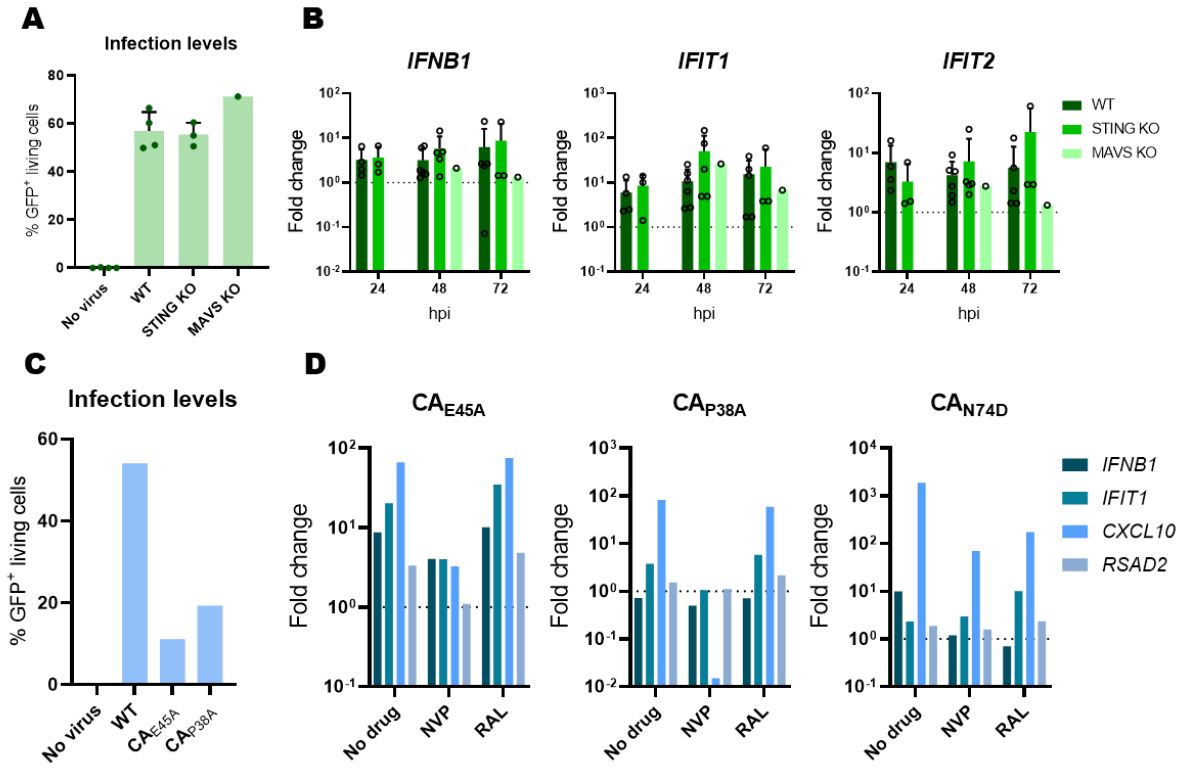

Figure 26: Macrophage-Like Cell Lines Exhibit Different Innate Immune Phenotypes Against HIV-1 Compared to MDMs

(A) Infectious levels of differentiated THP-1 WT (*n*=3), STING KO (*n*=3) and MAVS KO (*n*=1) cells infected with $NL4.3_{GFP}$ (MOI=1.5). After 72 hpi, cells were harvested, and the levels of GFP^+ cells were analyzed using FACS **(B)** Comparison of ISGs fold change levels (uninfected) of those (B) infected THP-1 cells relative to uninfected cells. **(C)** Infection levels of differentiated U937 (*n*=1) infected with $NL43_{GFP}$ WT or defective-CA (E45A, P38A, N74D; MOI=3) in addition with VLP_{Vpx}. Cells were harvest 72 hpi and analyzed by FACS. **(D)** Comparison of ISGs fold change levels of those (C) infected U937 cells relative to uninfected cells. **(A, C)** The percentage of live/dead cells was determined by FVD-660 staining. **(A, B)** The means ± SD are shown and each symbol represents an independent experiment.

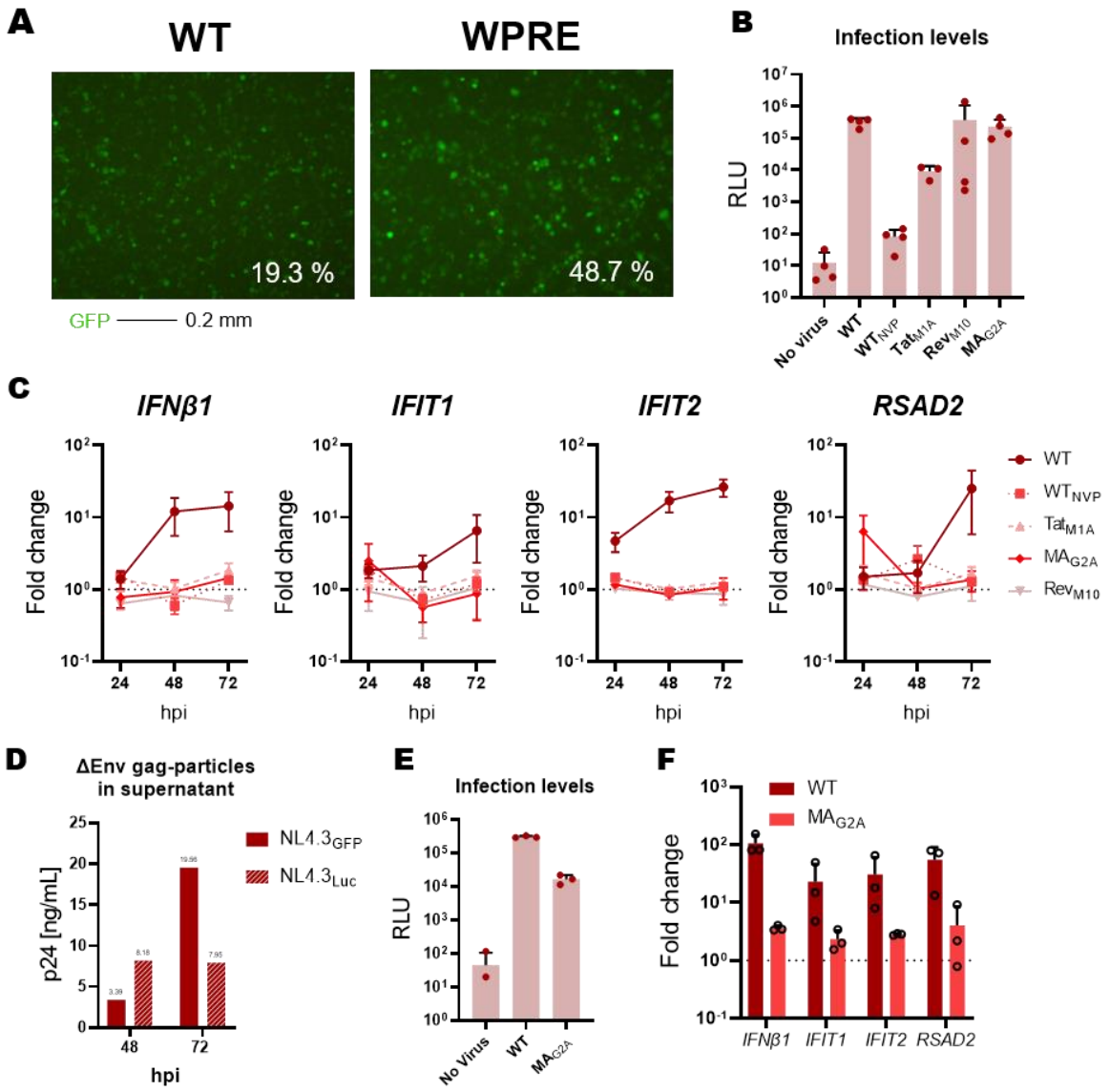

Figure 27: Sensing of NL4.3 Luciferase Reporter Virus in MDMs Induced Gag Myristoylation Dependent Late-Stage Innate Immune Response

(A) Fluorescence images of GFP (green) signals from MDMs infected with $NL4.3_{GFP}$ and $WPRE_{GFP}$ (MOI=6). A scale bar of 0.2 mm is provided under the images, and the percentage of GFP^+ living cells measured from the FACS analysis is indicated. **(B)** Infection levels of MDMs from different donors (*n*=3-4) infected with $NL4.3_{Luc}$ WT, Tat_{M1A}, Rev_{M10}, and MA_{G2A}, virus, or left uninfected as control (MOI=3). After 72 hpi, cells were harvested, lysed with passive lysis buffer, and analyzed by luciferase assay **(C)** MDMs were infected with the viruses mentioned in (B), and were also treated with NVP (10 µM) as a control. Cells were harvested at specific time points as indicated. The expression of ISGs, including *IFNB1*, *IFIT1*, *IFIT2*, and *RSAD2*, was measured using RT-qPCR and fold change is shown (uninfected). **(D)** Measured p24 amounts of the supernatant of infected MDMs with $NL4.3_{GFP}$ or $NL4.3_{Luc}$ (MOI=3) collected at time points as indicated. **(E)** Indication of infectious levels by relative light units (RLU) of MDMs (*n*=3) infected with $NL4.3_{Luc}$ WT and MA_{G2A} (MOI=6). Cells were harvested 72 hpi, lysed with passive lysis buffer, and analyzed by luciferase assay. **(F)** Comparison of fold change in ISG expression levels 72 hpi in those (E) infected MDMs relative to uninfected cells. **(B, C, E, F)** Dot plots display the means ± SEM, while bar graphs show the means ± SD, with each symbol representing an independent well.